The Relevancy between Visual Cortex and Motor Cortex and Its Spatio-Temporal Neural Dynamics

李, 照軒

KYUSHU UNIVERSITY

DOCTORAL THESIS

The Relevancy between Visual Cortex and Motor Cortex and Its Spatio-Temporal Neural Dynamics

---

Author:

Zhaoxuan LI

Supervisor:

Professor Keiji IRAMINA

A thesis submitted in fulfillment of the requirements

for the Doctor degree

in the Graduate School of Systems Life Sciences

Kyushu University, Fukuoka, Japan

November 27, 2022

KYUSHU UNIVERSITY

Abstract

Graduate School of Systems Life Sciences

The Relevancy between Visual Cortex and Motor Cortex and Its Spatio-Temporal Neural Dynamics

by Zhaoxuan LI

Although the cerebral cortex has been divided into different regions according to their function in cognitive process, many researches in past decades have demonstrated that the neurons in a region do not just work locally; on the contrary, the correlation between neurons from different function regions, which can be observed as functional connectivity, happens frequently. In this thesis, we studied about the cerebral activity when normal healthy people were presented with visual stimulus, and the relevancy between occipital lobe and the other cortical areas, and revealed its features in both time and space.

Firstly, previous studies have reported that a series of sensory–motor-related cortical areas are affected when a healthy human is presented with images of tools. Obviously, these images caused a relevancy between the neurons here and at occipital lobe. This phenomenon has been explained as seeing familiar tools launching a memory-retrieval process to provide a basis for using the tools. Consequently, we postulated that this theory may also be applicable if images of tools were replaced with images of daily objects if they are graspable (i.e., manipulable). Therefore, we designed and ran experiments with human volunteers (participants) who were visually presented with

images of three different daily objects and recorded their electroencephalography (EEG) synchronously. Additionally, images of these objects being grasped by human hands were presented to the participants. Dynamic functional connectivity between the visual cortex and all the other areas of the brain was estimated to find which of them were influenced by visual stimuli. Our results showed that manipulable objects caused a series of cerebral activity at several motor-sensory-related regions, corresponding with the two pathway of visual object recognition. Moreover, many evidence indicated that looking at images of interactions did not induct similar activity as seeing the same object alone, and so did images of hand. In addition, we also investigated the ability of using phase synchrony to track the two pathways of visual information.

With the findings in above research, we noticed the potential of estimating phase locking value to measure how much a cerebral region participated in current cognitive process. Therefore, we tried to apply it to solve a problem in the field of neurorobotics—make machines be able to distinguish brain's activity when someone is imagining a movement from actually making a movement, and seeing a movement made by others. To collect data for training and evaluating a machine learning model, another brand new EEG experiment was created and run on 17 healthy volunteers. Based on the support vector machine (SVM), we proposed a data-driven method to searching for cerebral regions that were to the benefit of above classification. Consequently, the system we built achieved an average accuracy which has been significantly greater than random probability, and there is still room for improvement. In the meantime, several substantial differences of cerebral region activation were discovered by the approach of analyzing features selected by three classifiers. Results showed that when someone is watching, imagining, and executing a movement, the Broca's area, motor cortex, the Wernicke's area, and visual cortex performed differently. Finally, although the development of machine learning has been tremendous in recent years, its benefits have barely been brought to the studies in the field of cognitive neuroscience. This thesis proposed a

viable methodology to cover this shortage preliminarily.

In the final part, we shared several un-mentioned questions and possible future directions. Firstly, the role of that ERS when saw interactions is not clear; it might suggested the difference between non-tool manipulable objects and tools, which is the expectation of a third-party. Secondly, all of the findings here are obtained by studying right-handed volunteers, which lead to a shortage on inferring the lateralization; same experiment can be run on more left-handed participants in the future. Moreover, participation of visual cortex was observed during movement imagination; its purpose and function is worthy to be studied. All these topics are worthy for a further study.

Acknowledgements

Foremost, I would like to express my sincere gratitude to my supervisor, Professor Keiji Iramina, who has continuously supported my PhD study and research, for the best research conditions, the warmest care, and the wisest advices. He also provided me with opportunities to experience the cutting-edge topics in multiple fields, to present my research on international conference, and to working at my own pace. Moreover, Prof. Iramina also helped me with application of scholarships to keep me away from finance problem. His kindness and encouragement motived my enthusiasm to finish my PhD.

In addition, I would like to thank all my fellows in Iramina Lab. Every one of them helped me more or less. Particularly, De Bi helped me with making experiment materials, and Yuliang Cheng did a lot to recruit volunteers for my research. Jingwei Tang played as a reliable partner during our cooperation and brought much happiness to my life. Ageno and Sanuki helped me a lot with the administrative affairs. The company from my fellows gave me the power to keep a positive attitude during the epidemic of COVID-19.

Next, I would to thank my family, who have always left a leeway for me. Parents' support gave me the confidence and the heart of no fear. My fiancée, Chenyi Mei, has always been the one who provides me with consolations during these years. Their words and deeds made me who I am.

Finally, thanks to Kyushu University, and Japan Science and Technology Agency, for providing me with the infrastructure and funding to live a comfortable life.

Contents

Chapter 1

General Introduction

1.0 Structure and Topics

This thesis consists of four parts. The first part talks about the background of our study in a general way, including instructions of related theories and demonstrations of basic data processing method we used in researches. The second and third parts are two researches we mainly focused on during my doctoral study. The final part is a general summary of our findings and conclusions, and a discussion about possible directions in the future.

The first research we shared is about exploring the spatial and temporal features during visually recognizing different targets. A general opinion is that when normal human sees a familiar graspable object in view, neurons near postcentral gyrus (somatosensory cortex) fires to get prepared for a potentially coming interaction with the target object. During the preparing, these neurons have to decide the posture to contact with that object. However, we were curious about what if a proper posture is already given. For exploring this topic, we asked volunteers to recognize objects presented to them, and also shows images of grasping those objects with proper postures, and recorded their EEG data.

The other research is about making machines be able to distinguish human's brain

activity when someone is seeing, imagining, and executing movements. This research used our findings in last one that quantify the degree that an area participated in current cognition task by measuring the functional connectivity between it and other areas. In this way, the spatial information can be integrated into features for pattern recognition.

1.1 Two pathway from visual cortex

Visual cortex is defined as a cerebral region which receives and processes the nerve impulse from optic nerve, and locates at occipital lobe. The optical information in the environment is collected by retina and coded into nerve impulse, then transmitted to visual cortex, where those optical information is presented to brain in the form of visual sense. Thereby, human sees. Note that, seeing is different with understanding. People cannot understand the things in sight if above information flow ends at visual cortex, although they are still able to see them clearly. This phenomenon is called as visual agnosia. Patients with visual agnosia can normally see the objects in their view, but meet difficulties in recognizing those things when only rely on their eyes.

By studying the patients with above agnosia, scientists have proposed a widely accepted model to describe the output of visual cortex: two pathways at dorsal and ventral side (Milner & Goodale, 2006; Milner & Goodale, 2008). As a general speaking, the dorsal stream transmits information from occipital lobe to frontal lobe. The function of dorsal stream is believed to be concerned with establishing an egocentric coordinate system in real-world scale and planning the movement to reach the target object. Therefore the system supported by dorsal stream is called the “vision for action”. On the other hand, ventral pathway transmits information from occipital lobe to temporal lobe. The function of ventral pathway is related to understand the representation of the target object in a relative scale, and the description of relationship with surroundings. It is actually the perceptive information, so the system mediated by ventral stream is also

called the “vision for perception”.

Just as most entities that consist of multiple sub-systems, the dorsal stream vision system is not totally separated with the ventral stream. Milner described their relationship as that the ventral stream determine the proper posture (or gesture) to interactive with the target object, and the dorsal stream maps the determined posture into real-world scale, including the process of transforming the relative information into the egocentric coordinate system.

1.2 Purposed movement

Making movements is a gifted ability of almost every animal. It includes voluntary movement, such as move your hand to approach the cup when you are thirsty; and involuntary movement, or reflex, such as the knee jerk reflex. A significant difference is involuntary movement does not need the participation of central nervous system. In other words, making a voluntary movement needs brain to give orders for controlling muscles (see Figure 1.1) (Nicholls & Nicholls, 2001).

Voluntary movement usually have a purpose: adjusting body to a certain position. For example, when you want to drink a cup of coffee, you have to move your arm and hand to a certain position by which you would be able to approach the cup. We call this a purposed movement, which is actually a complicated operation consists of two stages. Firstly, you need to know where the cup is. This stage usually need the participation of eyes, to recognize the cup on the table. Secondly, planning a route to reach the cup, which is almost an automatic procedure and be finished unconsciously. This stage contained an inferior step—decide the posture (or gesture) to contact with the cup. Possibly, make a precise movement to let index finger pass through the handle ring and cooperate with thumb to hold it. Besides, when you actually execute the movement, visual monitoring is usually needed.

Above example reflects a fact that a series of neuron activity are behind a simple purposed movement. These neurons mostly located in several cerebral cortices, which have different functions with each other. In above example, neurons in visual cortex receive information from optic nerves and transmit it via both the dorsal and ventral streams, and finally motor cortex execute the movement. During the process, somatosensory cortex helps to know where our body parts are. Consequently, at least the occipital lobe, temporal lobe, and parietal lobe are involved in the visual recognition procedure before actually make a movement. Obviously, a purposed movement is completed by the joint effort of many different cortices.

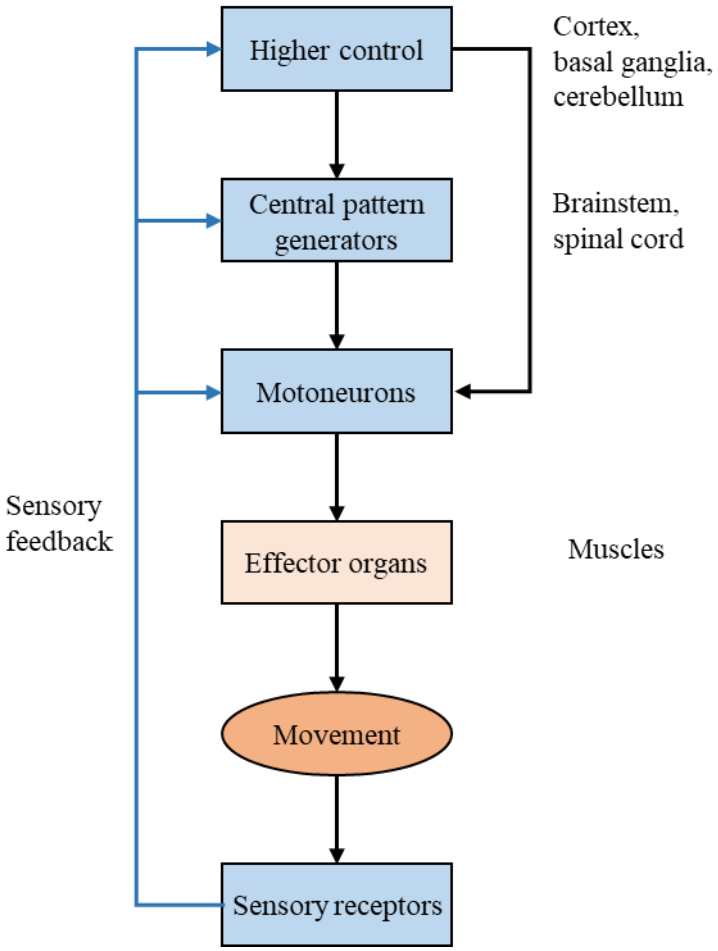

Figure 1.1 General scheme for motor system organization. Movement is finished by muscles controlled by motoneurons which receive orders from the upper structure. Brainstem and spinal cord constitute the central pattern generators that transmit nerve

impulse from higher control to motoneurons, but not all of the orders have to go through this procedure. Generally, the higher control includes cortex, basal ganglia, and cerebellum. Movement will lead to an activation of sensory receptors, and these receptors will feedback to every level of motor control to help with guiding and monitoring the executing of movement.

1.3 Cooperation among cortices

Integrating information for decision making usually happens in daily life. For example, prior studies have defined driving as a complex combination includes a series of cognitive procedures (Weiler et al., 2000). Drivers use their eyes to observe surroundings, based on which they decide to push the accelerator or turn the steering. In the meantime, they have to recall the map in memory or get lost. This simple example includes the use of vision, motor ability, and memory, which is the result of a cooperation among visual cortex, motor cortex, somatosensory cortex, and prefrontal cortex (Groeger, 2013). Another study precisely indicated five cortical regions that associated with driving via fMRI as shown in Figure 1.2.

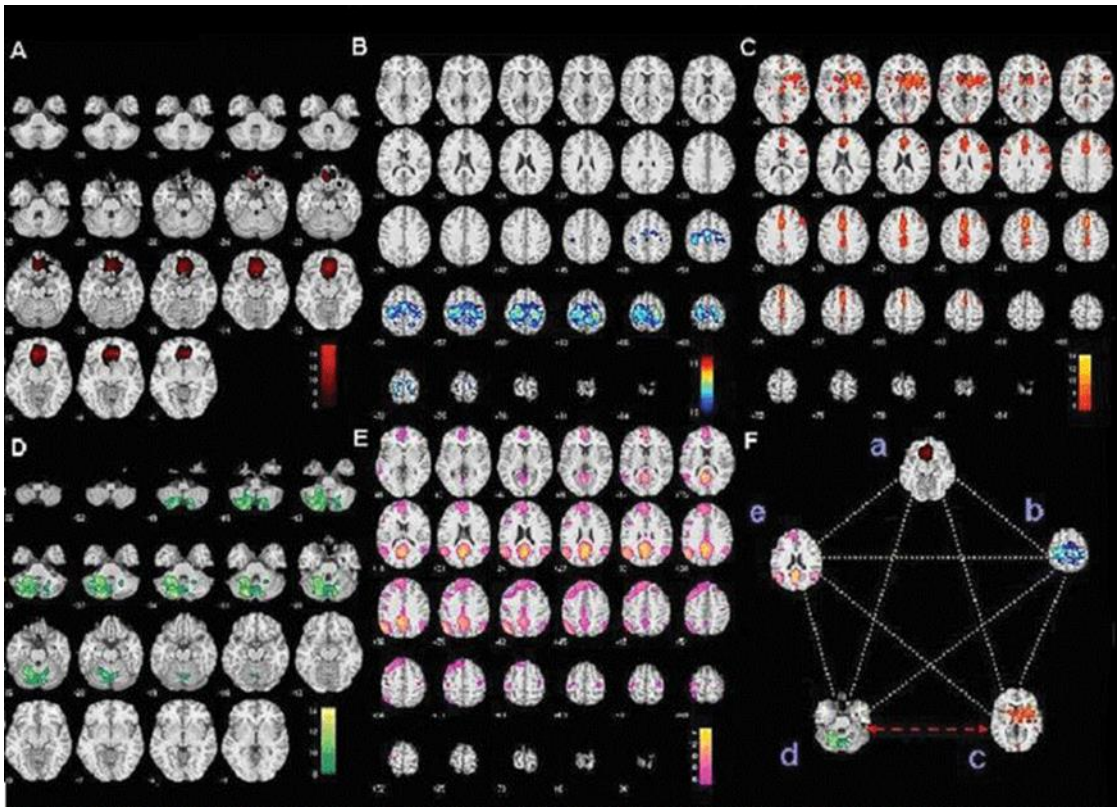

Figure 1.2 Brain circuits associated with driving. (A—E) Axial slices of where the five circuits locate. (F) Functional connectivity among them during driving simulation (Rzepecki-Smith et al., 2010).

To be specific, external information would be collected by sensory organs (eyes, ears, skin, and so on) and transmitted to brain, where several cortices work together to understand the situation, and sometimes give out an order for the other part of body to execute as a result. The perception that integrates more than 2 different sensory modalities is called as a crossmodal perception. Crossmodal perception is always accompanied with a synchronous activity between corresponding neurons, which can be observed by several neuroimaging techniques.

1.4 Neuroimaging

Like the other imaging techniques, neuroimaging aims to let us be able to see the neurons (which generally means the neurons in brain). Based on the content that the image shows, it can be divided into 2 classes: structural imaging, which shows the

anatomy of cerebral cortex, and functional imaging, which reflects the firing of neurons and usually used for studying brain function. Figure 1.3 shows an example from a prior study to describe the difference between structural and functional imaging.

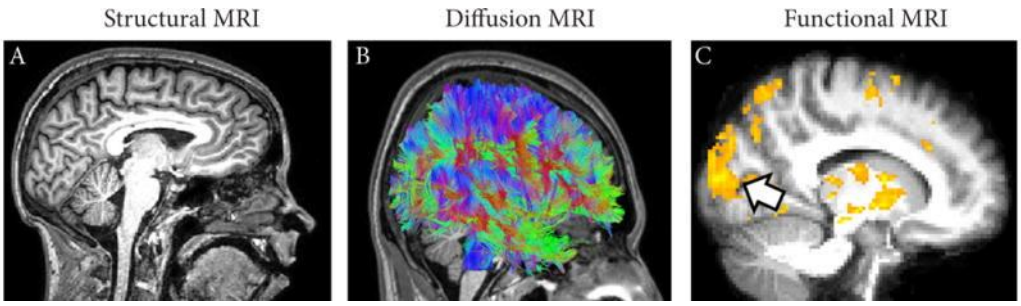

Figure 1.3 (A) Structural imaging, which presents the anatomical look of body tissues. (B) Diffusion imaging reveals the orientation of white matter fibers which lay under the gray matter. (C) Functional neuroimaging suggests the activation of neuron groups when individuals are processing on a specific task (Hirsch et al., 2015).

Firing neurons is actually proceeding a series of biochemical reactions, during which the energy and oxygen are consumed and results in the potential flip of the inside and outside of nerve cells. Based on these phenomena, scientists have created several non-invasive methods to image the activity of neurons (see Table 1). These methods have been proved to be reliable and admitted by a large number of neurosciences, cognitive science, and psychology studies. As the oldest non-invasive functional neuroimaging technique, EEG is the mostly used one since its economy, almost non-limits on subjects and environment, and the ability to record instantaneous cerebral activities.

Table 1.1 Compare of different functional neuroimaging approaches.

Name	Principle	Features			
		Temporal resolution	Spatial resolution	Cost	Special Requirements
EEG	Bioelectricity	Highest	Lowest	Lowest	None
MEG	Bioelectricity	High	Low	High	Magnetic shield room
fMRI	BOLD*	Middle	Highest	High	Metal-free room
fNIRS	BOLD*	Middle	Middle	Low	None
PET	Radiation	Middle	High	High	Radiation shield room

*: Blood oxygen level dependent. A firing neuron consumes energy and oxygen outside the cytomembrane, which will lead to a rapidly decrease of them around the activated

neuron. In order to meet the demand of that neuron, much more sugar and oxygen will be delivered to the firing neuron then by blood, which finally lead to a change of relative of oxyhemoglobin (HbO) and deoxyhemoglobin (HbR) near the activated neuron. FNIRS measures the HbO and HbR via the absorption of near-infrared light (specifically, HbO and HbR have different absorption coefficients on both sides of the 810nm light), while fMRI measures them based on their magnetic performance (specifically, HbR is paramagnetic while HbO is diamagnetic).

1.5 EEG

EEG records the electrical activity on the scalp which caused by electrophysiological activities of thousands or millions of neurons at similar spatial location, via several electrodes (generally from a few to as many as 256) and an amplifier. Neurons' electrical activity have to go through the skull before the scalp electrodes are able to record the slight change, which lead to a distortion due to the effect of volume conduction and finally caused the poor spatial resolution. Although there have been a lot of methods (either with or without hardware supporting) proposed to be useful for analyzing the source of electrical signal recorded by electrodes since last century (Domingo Pascual-Marqui, 1999) till recent years (Asadzadeh et al., 2020), the reliability is still controversial.

Anyway, in order to describe the location of electrodes on scalp, the 10—20 system was created (see Figure 1.4 A). The original 10—20 system defined locations of electrodes by the distance between 2 neighboring electrodes which was either 10% or 20% of the total front-back or left-right distance of the skull. This location system provided 19 channels (i.e. place 19 electrodes on scalp) for EEG recording (Klem et al., 1958). With a further demand for recording EEG with more electrodes to collect more details, an improvement was made to allow a layout of up to 69 electrodes (Figure 1.4 B) by replacing the 20% with 10% in the definition of 10—20 system, which is called as 10—10 system (Chatrian et al., 1985). Moreover, there has been location system with higher resolution known as 10—5 system (Figure 1.4 C), based on similar principle

(Oostenveld & Praamstra, 2001). However, it is doubted that whether a single increase in the number of electrodes pays off because the poor spatial resolution associated with EEG, especially when more electrodes means consuming much more time in the preparation phase before experiment, which may let subject feel exhausted even before the start of experiment.

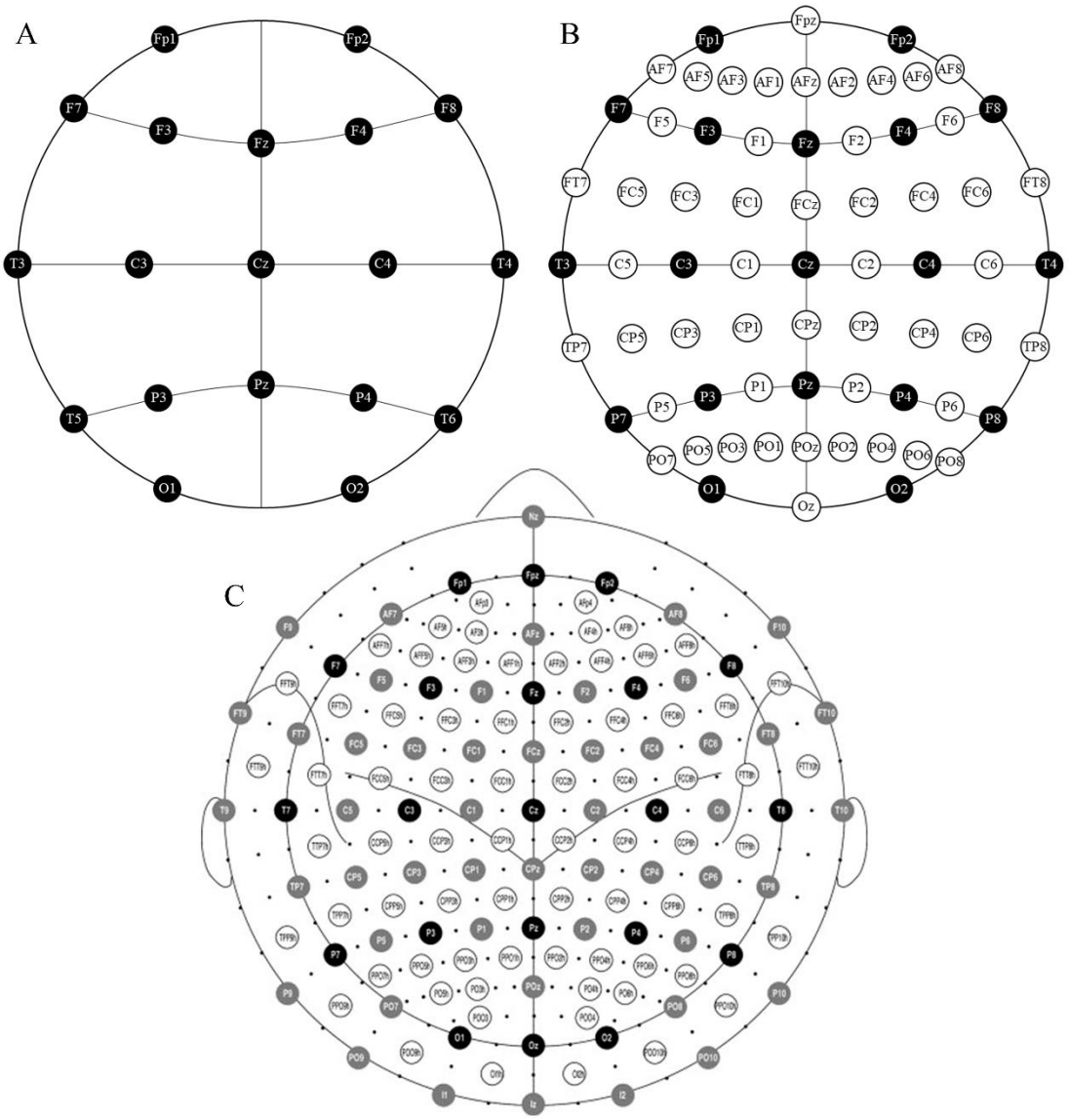

Figure 1.4 (A) Original 10—20 system with 19 EEG channels. (B) A 10—10 system with 69 EEG channels, which is generated by adding electrodes into the empty space. Sometimes this system would be extended to make accommodate for more channels by creating an extra layer. (C) A 10—5 system provides locations for from 128 to 345 electrodes (Oostenveld & Praamstra, 2001).

Although a single neuron's electrophysiological activity generally happens on the scale of tens of millivolt, with the attenuation before the potential change reaches scalp, the firing of millions of neurons finally results in a weak change of EEG on the scale of tens of microvolts. Moreover, slight movements also change the potential of surface of the skin, which always have a greater amplitude than the one caused by cerebral cortices. Based on the above reasons, the SNR of EEG is extremely low. Thus, a difference amplifier would be used for reduce the effect from common-mode signal via two inputs of EEG electrodes and reference electrodes respectively. In other words, what is recorded by an EEG device is the difference between potential changes detected on scalp and the reference potential detected at a position that almost be not affected by cerebral activity (i.e. a theoretical zero-potential point). However, it is still necessary to preprocess the recorded signals before trying to analyze.

1.6 Basic preprocesses of raw EEG data

In most cases, an analog filter has been applied during EEG recording to reduce the noise that definitely not belongs to the frequency band of detectable scalp electrophysiological activity. However, it does not mean that all the rest of them is worthy to be analyzed. Based on the topic of study, a digital band-pass filter is usually applied as the first step of preprocess. Figure 1.5 shows a segment of EEG signal before and after band-pass filter.

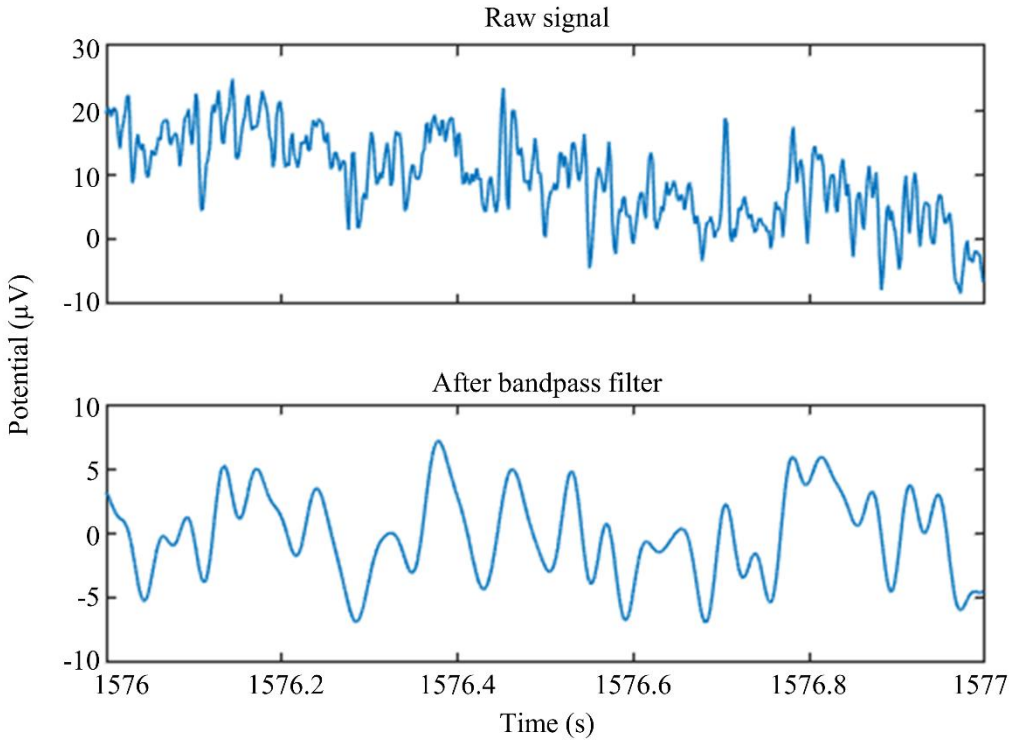

Figure 1.5 Using a 1—30 Hz band-pass filter to remove the frequency components that not belongs to the brain activity that the current study is focusing on.

The next step is re-reference, which has become more popular in recent years. During EEG recording, the data actually reflects the difference between potentials recorded at scalp and at reference spot (which is earlobe generally). In other words, for an EEG electrode e, one sample it recorded EEG_e is:

$$EEG_e = U_e - Ref$$

where U_e is the potential on scalp, and Ref is the one at reference spot. However, the reference spot is just a theoretical zero potential spot, which means the potential there actually changes along time. In order to erase the effect from reference spot, the recorded EEG data would be re-referenced to common average reference, by:

$$EEG_e{}' = EEG_e - EEG_{avg}$$

where EEG_{avg} represents the mean value of all EEG electrodes at one sample, and $EEG_e{}'$ is the new EEG data that would be analyzed in future step. In this way, the reference potential does not participate in the calculation anymore, so its variation would not affect the EEG. To be specific, the process can be descripted as:

$$EEG_e{}' = EEG_e - \frac{\sum_{n=1}^{N} EEG_n}{N}$$
$$= U_e - Ref - \frac{\sum_{n=1}^{N}(U_n - Ref)}{N}$$
$$= U_e - Ref - \frac{\sum_{n=1}^{N} U_n}{N} + Ref$$
$$= U_e - \overline{U_n}$$

however, average potential of human scalp should be zero, so $\overline{U_n} = 0$, and $EEG_e{}' = U_e$.

Another essential operation is to remove ocular artifacts. During EEG recording, movement of eyes will cause distortions of EEG, even if subjects are asked try not to blink in trials. Due to the greater potential of EOG, electrodes near eyes will be affected obviously (see Figure 1.6). Thus, scientists have proposed many approaches to reduce the distortion. The mostly used method is ICA, which considers this problem as a blind source separation question.

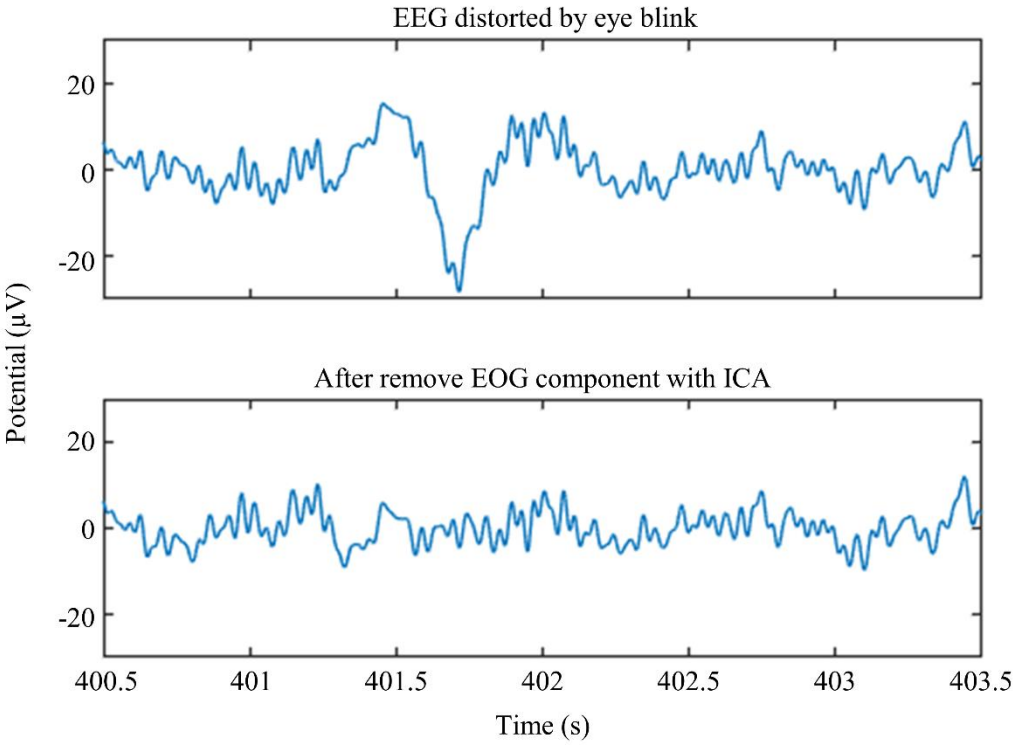

Figure 1.6 A segment of EEG signal recorded at O1 position was affected by a blink happened at 401.5—402 seconds. ICA successfully corrected this distortion with almost no effect on the rest of the EEG signal.

After above procedures, the EEG recordings are ready to be cut into epochs for following analysis. Epochs containing drastic potential changes are usually caused by accidental events (e.g. unexpected head movements) during experiment and considered as wrong data and will be abandoned as a general operation.

1.7 Time and Frequency

For each channel, EEG is recorded as a series of values that changes along time. This kind of data is considered as time series. Analyzing its variation in both time domain and frequency domain usually tells its characteristics.

1.7.1 Fourier Transform

In order to see how a time series looks like in frequency domain, a useful tool is the Fourier Transform. When apply this method with a computer, it turns to be the Discrete Fourier Transform due to the fact that computer can only treat discrete data in a limited length. Figure 1.7 gives time series data which are generated by put two periodical signals together, and shows the result of doing DFT on them (via FFT which is a faster algorithm of DFT). From this example, it is found that although the frequency components are exposed in the result, the sequence of them is not told. In the other word, the DFT is not able to reflect the change of frequency across time.

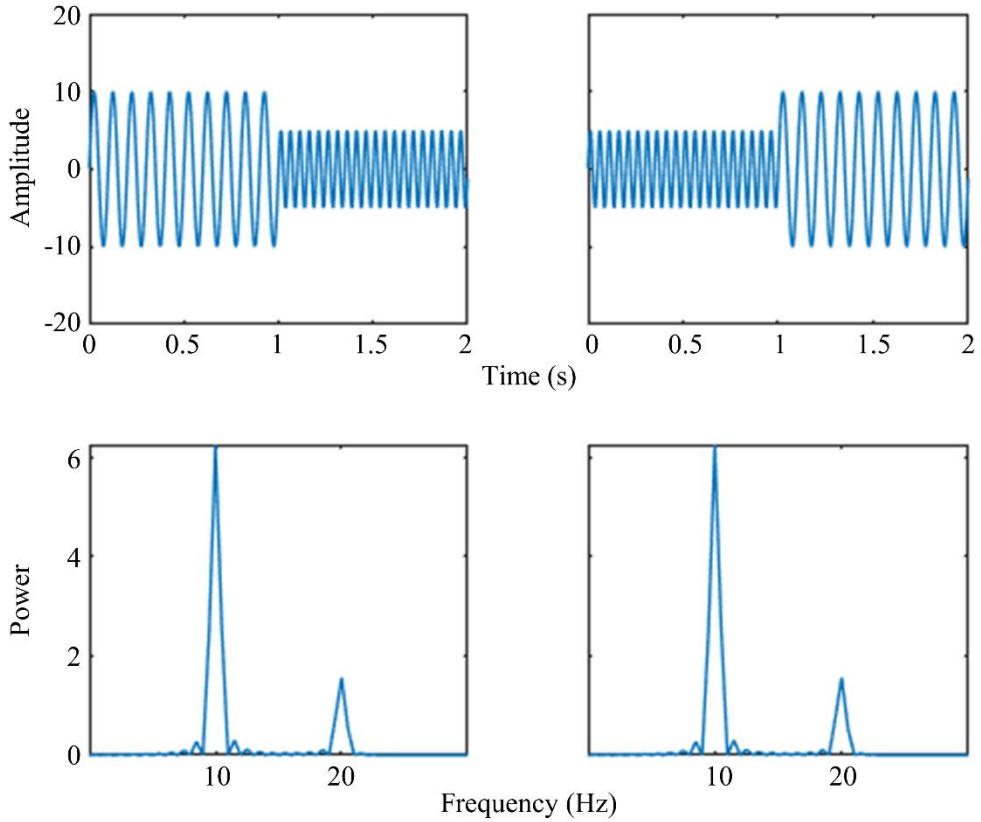

Figure 1.7 Generate two sinusoidal signals $X_1 = 10\sin(10 \times 2\pi)$ and $X_2 = 5\sin(20 \times 2\pi)$, then connect them with different order to form two new signals Y_1 and Y_2. DFT of the two new signals are totally same because DFT cannot reveal the sequence of frequency components.

1.7.2 Short-time Fourier transform

A doable solution for the above problem is cutting the signal into short time segments and then do DFT on every one of them to get the frequency variation. Analyze the signals in Figure 1.7 by STFT, frequency variation is successfully observed (see Figure 1.8). However, it would lead to another distortion problem when it is necessary to observe a low frequency band due to the generalized uncertainty principle: lower frequency component needs longer time series. Thus, a short time series leads to worse estimation of the spectrum of low frequency component. In the meantime, high frequency component can still be distinguished even with a shorter time series, which means that the time resolution of high frequency component would be improved by apply DFT on shorter time series. Ideally, a shorter time window is expected when

analyze high frequency component while a longer one when analyze low frequency component.

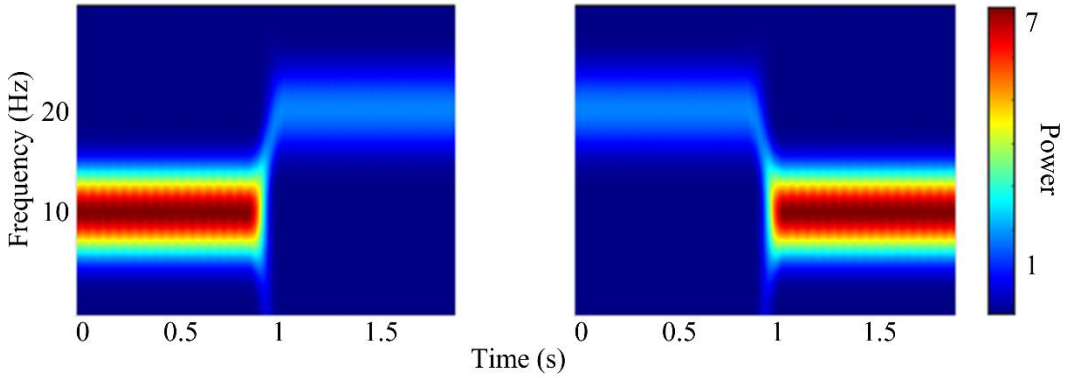

Figure 1.8 STFT results of Y_1 and Y_2. A slide hamming window with length of 0.2 second was applied to reduce frequency leak and keep temporal resolution at an acceptable level. In this situation, the frequency resolution would be decreased to 5 Hz.

1.7.3 Wavelet transform

Wavelet can extract signal's frequency and energy by making a convolution with the signal. Changing the scale of a certain wavelet would generate a wavelet family with many wavelets of which the length and frequency are inverse. Then, convolute every one of them with the time series and the time-frequency characteristics would be exposed as shown in Figure 1.9. Moreover, there has been researches reported that Morlet wavelet is useful in EEG study (Roach & Mathalon, 2008).

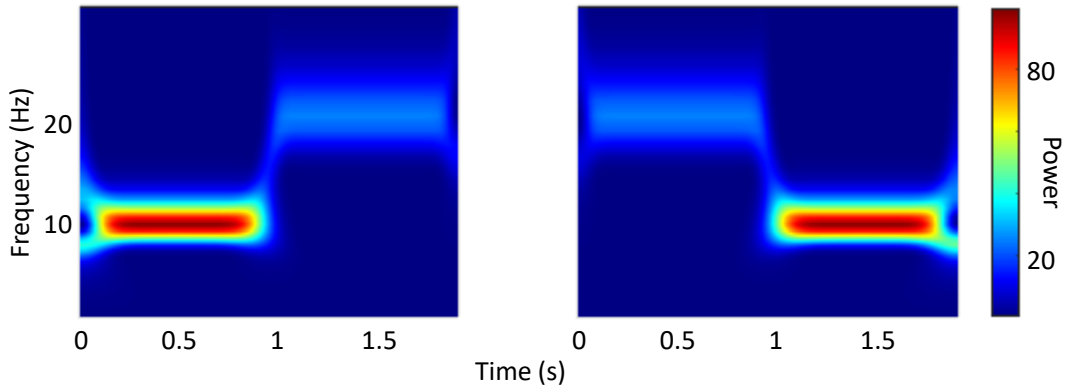

Figure 1.9 Using wavelet transform to balance the temporal and frequency resolution. Obviously, the frequency band is narrower than the result of STFT. Note that the boundary effect will lead to a widening of frequency range and also the decreasing of power estimation, especially in low frequency because low frequency band is estimated by wavelets with larger scale. An often-used solution is to extent the data symmetrically before wavelet transform.

1.7.4 ERD, ERS and ERSP

Brain never stops its activity, which means the time-frequency features always exist whatever a stimulus is given or not. Therefore, the emphasis of time-frequency analysis is to answer "what is changed after apply the stimulus?" The variation of EEG energy is usually used to represent the changes of cerebral activity after subjects are given stimulus and considered as the variation is caused by the event that stimulus is given to subject. In order to quantify this variation, it is necessary to calculate the energy of EEG before and after stimulus onset. The energy many changes differently according to the frequency component, so the first step is to calculate the time-frequency spectrum. Then, for a certain frequency f, calculate the energy of sample n:

$$E_{n,f} = \sqrt{U_{n,f}{}^2}$$

and the average energy before stimulus onset can be calculated as:

$$E_{0,f} = \frac{\sum_{n=1}^{N} E_{n,f}}{N}$$

where N is the number of samples in the range of baseline period, and $U_{n,f}$ means the potential recorded. Now the energy data is ready and the nest step is to evaluate how

much does the energy changed by:

$$P_{n,f} = 10 \times \log_{10} \frac{E_{n,f}}{E_{0,f}}$$

where $P_{n,f}$ represents the difference between $E_{n,f}$ and $E_{0,f}$ in dB. In this way, we can know how the stimulus affects brain's activity at a certain frequency component. If the energy is decreased after stimulus onset, it is called as an ERD phenomenon (Figure 1.10 A). Inversely, if the energy is increased, it is called as an ERS phenomenon. Extend this concept to all of the frequency components, a spectrum that reflects the difference between each sample and energy baseline is generated, which is called as ERSP (Figure 1.10 B). The role of analyzing ERSP will be discussed with a truly example later in Chapter 2.

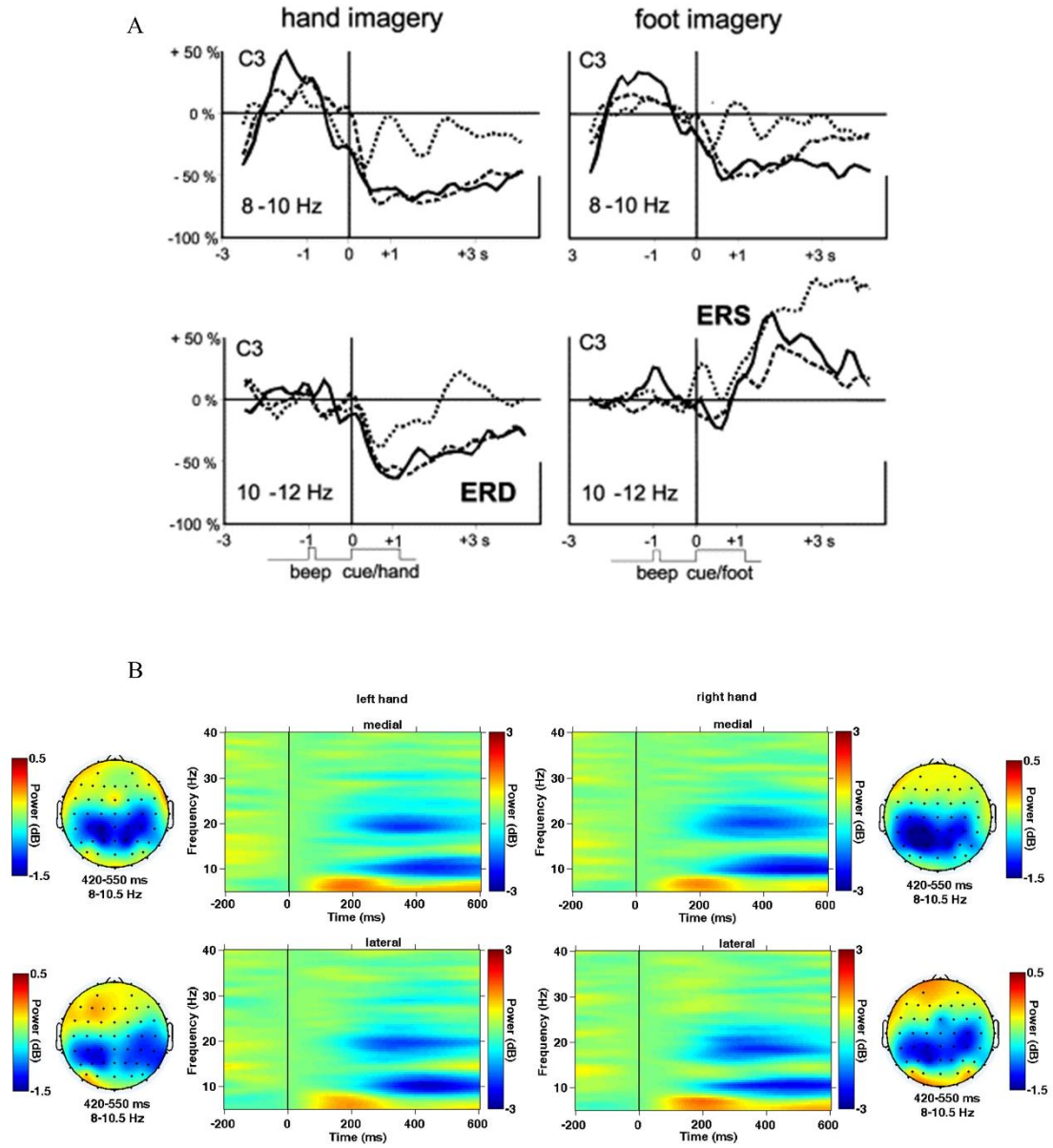

Figure 1.10 Examples of ERD and ERS phenomena, and ERSP figures. (A) After subjects began imagining a movement of right hand, the alpha band (8—12 Hz) power of EEG recorded at C3 was decreased. While, when it turned to be foot, the power of 10—12 Hz was enhanced (Neuper & Pfurtscheller, 2001). These phenomena are called ERD and ERS respectively. In the past, they are usually quantified by the change as a percentage of baseline. However, ERS in percentage might be an extremely great number if the baseline is close enough to zero. Therefore, later studies preferred to describe it after logarithmic transformation. (B) ERSP when subjects were trying to recognize both the left and right hands with different orientations (Chen et al., 2013). Investigation of ERSP allows observing both frequency and temporal changes at the same time. Note that power is shown in dB.

1.8 Network and Connectivity

In the past days, most of the cognitive science studies focused on locating the neuron groups that are in charge of specific cognitive functions. This research strategy is based on a hypothesis that functions are undertaken by modules, which means cognitive functions corresponding to function regions is separated and independent with each other. In this way, another control group is necessary for comparing with the experiment group and so that it is possible to highlight the region that is concerned with current cognition process.

Many studies have supported above hypothesis that activities from different regions are able to be considered as performing independently. However, as mentioned in 1.2, sometimes cortices with different functions would work as a team. A part of complicated cognitive functions need participation of multi regions and can only be finished by integrate their specialties. Thus, in order to study about how human cognizes more comprehensively, more and more scientists have proposed to not only focus on cognitive function locating but also cooperation and integration between different function regions.

The latter one studies the relevancy and interaction between two or more regions in cerebral cortices, which means it brings a network formed by activities recorded at different locations of brain.

Network is based on a series of connections. These connections are generally classified into three classes by the observed object: structural connectivity, effective connectivity, and functional connectivity. Structural connectivity studies the physical connection among anatomic structures and tissues in brain. Effective connectivity is defined as the effect that a neuron subsystem imposed on another neuron subsystem, and aims to discover the causality among neurons. Functional connectivity considers the temporal

relevancy between neurons located at different spatial regions, which reflects the coordination among neuron modules with different functions during cognition process.

In the situation mentioned in section 1.2, the neuron groups located in one cortex will communicate with other neuron groups belongs to another cortex, and this process still relies on the activation of neurons to transmit information. Therefore, scientists considered that approaches from information theory can be useful in analyzing functional connectivity in cerebral cortex. However, due to the volume conductor effect, the EEG signal recorded at scalp is a result of field effect which does not reflect the actual position that electric activity happened, so a functional connectivity between two cortices is an estimation.

1.8.1 Functional connectivity

Functional connectivity reflects the relevance between signals recorded from two different locations. Approaches for estimating functional connectivity are mainly based on statistics, causality, and mutual information. Table 1.2 shows a list of methods that used to estimate functional connectivity.

Table 1.2 Methods for estimating functional connectivity.

Method	Directed	Principle
Corr	NO	Common variation on amplitudes
DTF	YES	Causal influence
MI	NO	Amount of information
PS	NO	Tendency to keep a relative phase angle
TE	YES	Amount of directed transfer of information

In general, these methods can be classified into two classes: directed and undirected estimation. However, directed estimations like DTF usually require a long signal length to reach a reliable result. This leads to a problem when study on a cognitive process which would be completed rapidly. Therefore, undirected functional connectivity estimation methods still play irreplaceable roles in cognitive neurosciences. One of

them is the phase synchronization, which is able to analyze functional connectivity with the same temporal resolution as sampling rate.

1.8.2 Phase Synchronization

A directed evidence to prove that brain processes information in a network way is that coherence appeared between EEG recorded at two far parted cerebral regions. Phase synchronization assumes two related signals could performs a synchronization phenomenon (i.e. coherence) even if they have no correlation on their amplitudes which means linear methods such as correlation is not able to reveal it.

Based on the dimension that phase synchronization is calculated, it is divided into 2 kinds of indicator: PLV and PLI. PLV quantifies the average functional connectivity during a continuous time series, while PLI reflect the variation of functional connectivity along samples by examining the stability of phase synchronization among different trials.

The first step of estimating phase synchronization is to obtain the phases of a time series, which can be finished by using Hilbert Transform to a time-domain signal. Figure 1.11 shows how the Hilbert Transform helps with compute the instantaneous phase. Then, for an estimation of phase synchronization between two channels, the next step is to calculate their phase difference at every sample pair. PLV and PLI are both estimated by the average distribution of phase difference on a unit circle, while the direction of taking the average is not the same as shown in Figure 1.12.

In order to test the method before apply it to analyze EEG, a simulation of using phase synchronization to estimation the relationship between concerned and non-concerned signal is demonstrated.

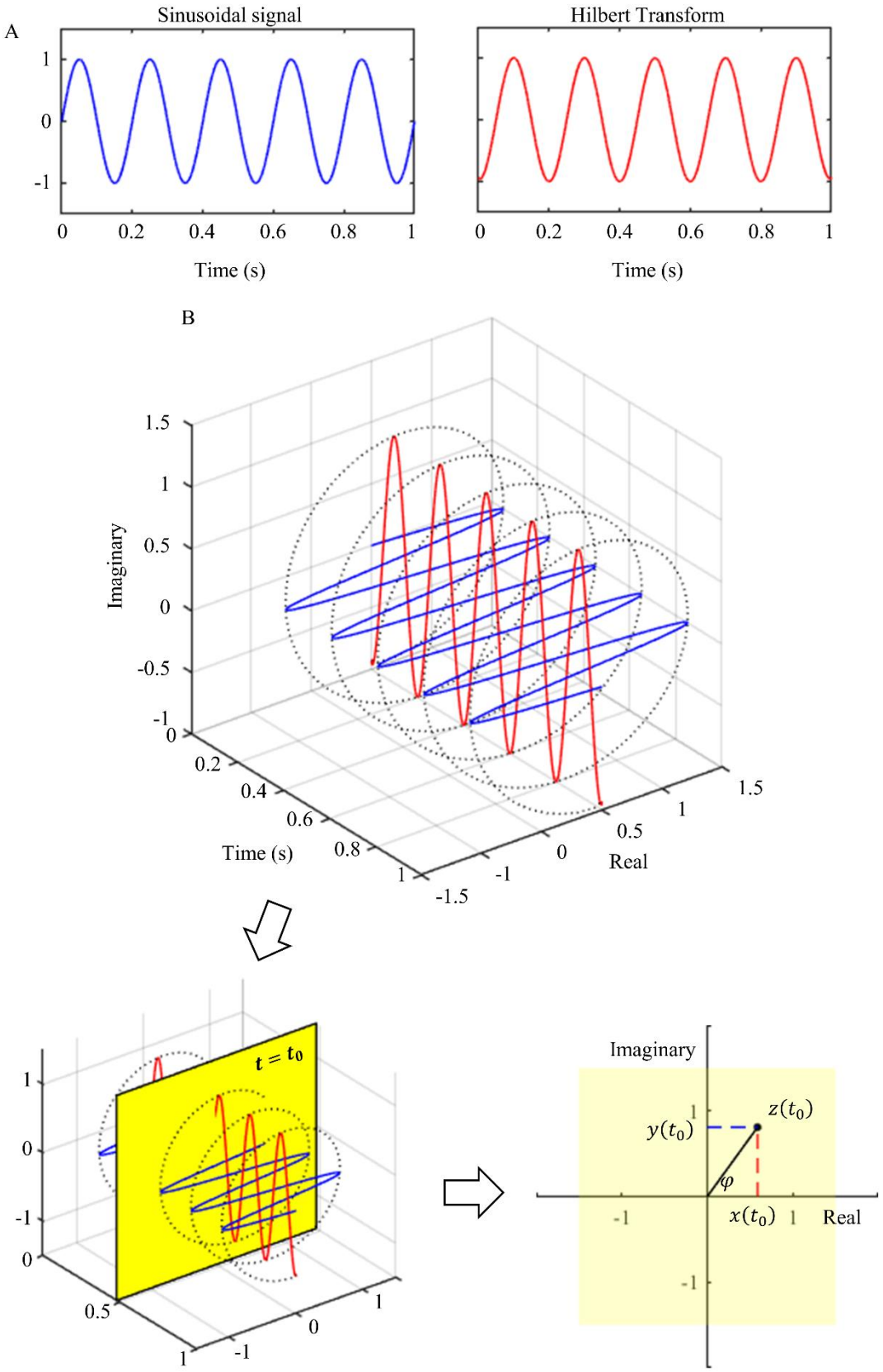

Figure 1.11 Hilbert Transform adds a delay of 90° on the phase of all the frequency components of a given signal. For example, the first second of a sinusoidal signal

$x(t) = sin(2\pi \cdot 5 \cdot t)$ is given in the left figure of (A). The right one shows the result of its Hilbert Transform $y(t) = hilbert(x)$. Construct the signal $z(t) = x(t) + iy(t)$ and show it in (B). At a specific time $t = t_0$, the position of $z(t_0)$ can be indicated as a point in the complex plane. In this way, the phase of $x(t_0)$ can be calculated as $\varphi(t_0) = \tan^{-1}\frac{y(t_0)}{x(t_0)}$.

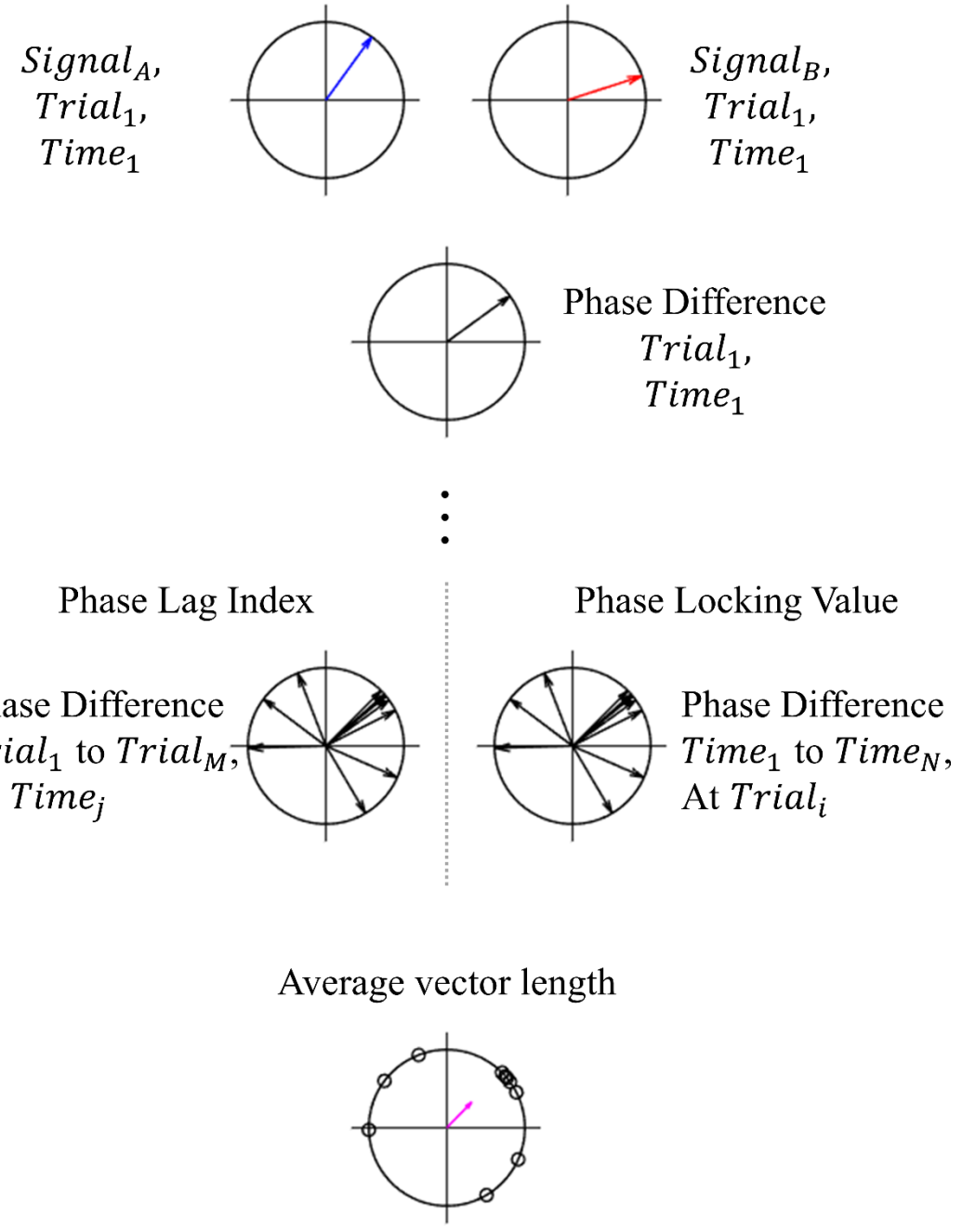

Figure 1.12 Method for estimating PLI and PLV between two signals. After phases are exposed, phases at corresponding time and trial are subtracted to obtain their phase difference. For estimation of PLI, place the unit vectors belonging to all of the trials at

current time together at a unit circle. For estimation of PLV, it turns to be placing the ones from all the sample points at current trial. Finally, the average vector length is the indicator of phase synchronization. Therefore, PLI is able to analyze the variation of functional connectivity along time, while PLV is estimated with a single trial and suitable for analyzing the difference of functional connectivity among trials.

1.8.3 Simulation

Prior studies have demonstrated several different approaches about how to generate functional connected and non-connected data for testing the performance of all kinds of estimation methods in simulation (Glomb et al., 2017; Monti et al., 2015). However, they were not specially aiming at phase-concerned features in signals. Fortunately, a recent study proposed a novel method for generating phase synchronized and non-synchronized simulation data for evaluating all kinds of phase-based functional connectivity estimation methods (Basti et al., 2022). In this section, similar approach would be used for generating simulation data.

The core feature of a generated signal has to be modulated phase variation while its amplitude is randomly distributed.

Firstly, the frequency bands for generating signals was determined. Since this study aimed to analyze EEG signals, it was defined based on the general demarcation of EEG bands, which is delta (1—3 Hz), theta (4—7 Hz), alpha (8—13 Hz), and beta (14—30 Hz). For two signals of a certain band, they were generated as the sum of a series of sinusoids with frequencies from current band in steps of 0.01 Hz. Hereby, amplitudes and phases of each frequency component are randomly distributed from a uniform distribution from 0 to 50 and $-\pi$ to π respectively. After passing through an autoregressive filter, two signals without coupling of phases $S_1(t)$ and $S_2(t)$ were generated. To obtain phase synchronized signals, calculate instantaneous phase of $S_1(t)$ through its analytic signal computed by Hilbert transform, and then re-construct

$S_2(t)$ as below:

$$S_2'(t) = A_2(t) \cdot \sin(\varphi_1(t) + \Delta\theta)$$

where $A_2(t)$ is the instantaneous amplitude of the original $S_2(t)$, and $\varphi_1(t)$ is the instantaneous phase of $S_1(t)$. $\Delta\theta$ is a randomly chosen value in the range of $[-\pi, \pi]$ to represent the constant phase difference between two coupling signals. As a demonstration of above procedures, Figure 1.13 gives examples of analyzing PLV and PLI between two generated signals. From these examples, it is obvious that PLI has an advantage that cannot be neglected: reveal connectivity that would be finished during a short time window.

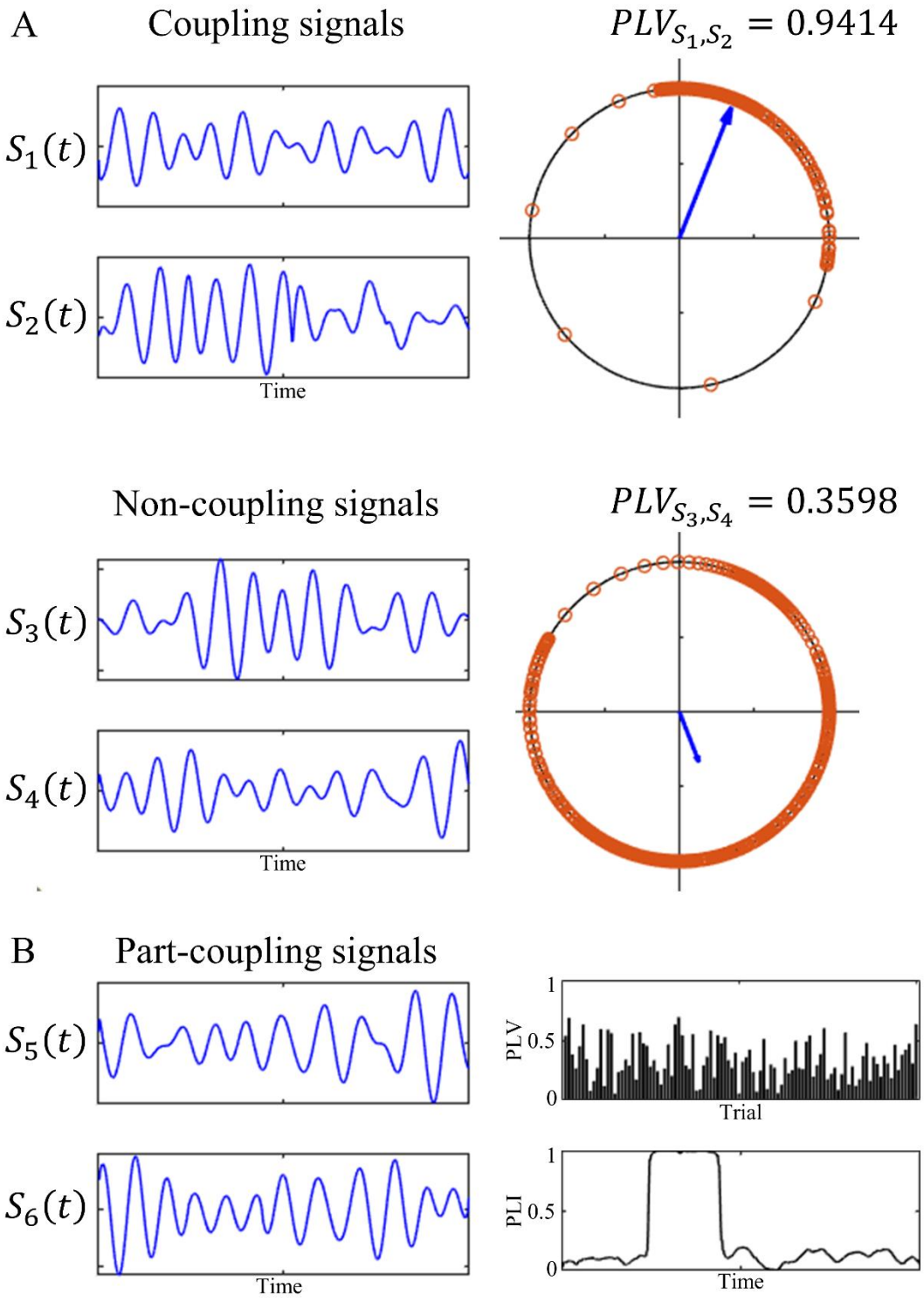

Figure 1.13 (A) $S_1(t)$ and $S_2(t)$ are a pair of phase-synchronized signals. By calculating their PLV with the method mentioned in 1.7.2, it is found that their phase difference at each moment almost always stays in the range of $[0, \frac{\pi}{2}]$, and resulted in a PLV close to 1. $S_3(t)$ and $S_4(t)$ are with randomly distributed phases, which caused random distribution of phase differences as well, and resulted in a very low PLV. (B)

However, there is still another situation that two signals are partly coupled (as the $S_5(t)$ and $S_6(t)$); their phase synchrony only happened at a certain period of the cognition process. This kind of coupling phenomenon can be observed by averaging phases across trials. It results in another shape of PLV, and some researchers proposed calling it phase locking index (PLI).

1.9 Summary

In this chapter, we introduced basic theory of the neural mechanism of motor, and the methods to observe the cerebral activity via EEG. In the latter part, we emphasized the features of EEG and introduced a reliable method to reveal the co-operation processes between two different functional regions. In the next chapter, the above was applied into a study about the visual perception and motor-related neural activities.

Chapter 2

Spatio-Temporal Neural Dynamics of Visual Recognizing Manipulable Objects and Interactions

Abstract: Previous studies have reported that a series of sensory–motor-related cortical areas are affected when a healthy human is presented with images of tools. This phenomenon has been explained as that familiar tools launching a memory-retrieval process to provide a basis for using the tools. Consequently, we postulated that this theory may also be applicable if images of tools were replaced with images of daily objects if they are graspable (i.e., manipulable). Therefore, we designed and ran experiments with human volunteers (participants) who were visually presented with images of three different daily objects and recorded their electroencephalography (EEG) synchronously. Additionally, images of these objects being grasped by human hands were presented to the participants. Dynamic functional connectivity between the visual cortex and all the other areas of the brain was estimated to find which of them were influenced by visual stimuli. Our results showed that manipulable objects caused a series of cerebral activity at several motor-sensory-related regions, corresponding with the two pathway of visual object recognition. Moreover, many evidence indicated that looking at images of interactions did not induct similar activity as seeing the same object alone, and so did images of hand.

2.1 Introduction

Tools play a special role among the objects that people usually come in contact with in daily life. Neuroscientists have found confirmatory evidence that using tools can lead to a lasting, discernible change on the perception of someone's own body (Cardinali et al., 2009). Furthermore, looking at a tool can also initiate a series of changes in cerebral activity. Many previous studies demonstrated that observing tools resulted in a left hemisphere advantage, while this did not occur with other objects (Chao & Martin, 2000; Garcea et al., 2012; Verma & Brysbaert, 2011). The most popular explanation for the neural mechanism behind this phenomenon is that tools have the property of "manipulability" and their appearance suggests an associated action or movement (McNair & Harris, 2012; Ni et al., 2019). In other words, it is reasonable to consider that the tool-associated cerebral activity is concerned with a motor to interact with the presented object. However, in past decades, most studies paid attention on comparing seeing manipulable objects with seeing other objects (such as a chair or plane that could not be grasped by hand), but few focused on the difference and relation between seeing the object and seeing interacting with them. Therefore, we decided to investigate the cognitive process when normal human are shown with images of manipulable objects, and then try to figure out what is changed when they are shown with images representing interactions with these objects.

As mentioned above, the first purpose of this study is to search for the representative characteristic of cerebral cortex activity after normal humans are presented with 1) images of manipulable objects, and 2) images of interactions (with those objects). In the meantime, due to the "hand" that contained in the images of interactions, the activity when shown with images of hand has to be studied as well. Furthermore, a condition that shows a combination of hand and object but without the motor of interaction is designed to reveal the unique component belongs to the motor of interaction.

In this study, we collected electroencephalography (EEG) data when volunteered participants were executing visual presentation tasks. By analyzing event-related potentials (ERPs), the functional connectivity, and time-frequency features, the characteristics of each condition is demonstrated. Furthermore, we also discussed possible explanations for several unexpected results.

2.2 Materials and methods

2.2.1 Experiments

Materials: Our hypothesis requires that the objects used as the stimuli need to be manipulable but are not tools. Additionally, a previous visual–somatosensory cross-modal study reported that objects from different categories may not lead to the same neural activity. Therefore, we chose only three objects that often appear in daily life, are easy to hold by hand, and do not have immediate associations with each other. Meanwhile, this design allowed us to use the same stimuli a number of times before participants felt tired. When creating the condition of "seeing an object being grasped" (i.e., participants saw an interaction with an object), to control the variables as much as possible, the conception of an interaction was analyzed first. An interaction includes three elements: subject, object, and a solution to draw a relation between them. Therefore, two more kinds of stimuli were added between "object" and "interaction": in our design, we used a normal human hand as a subject; orange, bottle, and smart phone as objects; and hand grasping as the solution, which is one of the most common forms of manipulability in our daily life. Figure 2.1 (a) shows the images used as visual stimuli in the experiment.

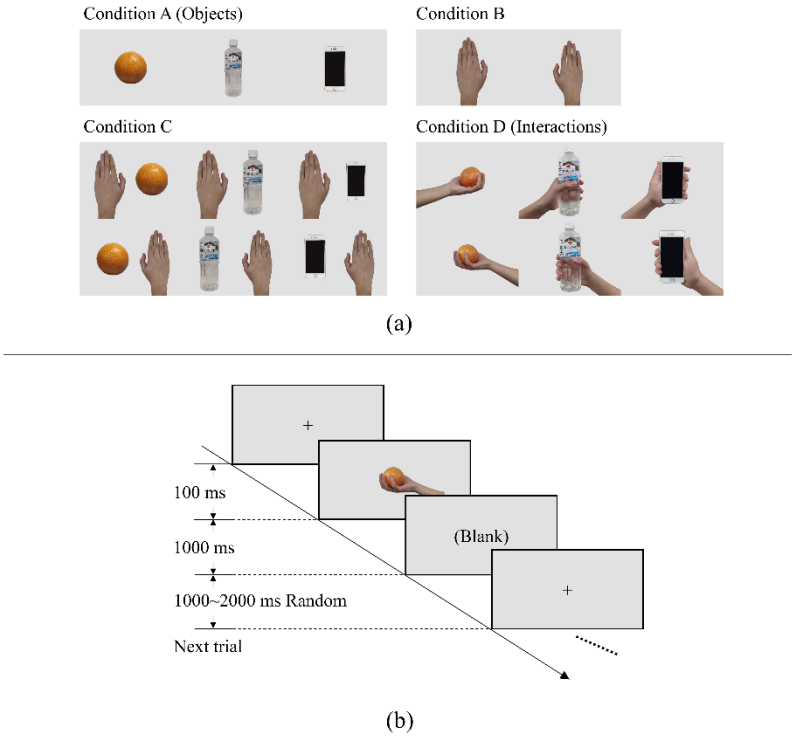

Figure 2.1 (a) Four kinds of images used in our experiment. Condition A presented participants with images of an orange, bottle, and smart phone (three objects). Condition B presented images of hands. Condition C combined the three objects and hands within the images. Condition D showed whole actions of hands grabbing objects (interactions). (**b**) Workflow of the trial. The images after the cross were randomly chosen from images corresponding to the current session (e.g., orange session, bottle session, and phone session).

Participants: A total of 20 healthy humans (including 8 females; mean age 24.05 years, range 22–27 years) with normal or corrected-to-normal vision participated in this experiment. This study was reviewed and approved by the Department of Informatics, Faculty of Information Science and Electrical Engineering, Kyushu University (admission No. 2021-13), and every participant signed the informed consent form voluntarily before the experiment began. As all volunteers were right-handed, in this paper, we do not discuss the situation containing the left hand as a stimulus.

Stimulus presentation: Visual stimuli were presented to participants on a 17-inch LCD display. The resolution and refresh rate were set at 1280 × 720 pixels and 60 Hz,

respectively. The distance between the eyes and display was in the range of 90–100 cm. Two runs were executed for each participant, and each run included three sessions with different topics: orange session, bottle session, and smart phone session. At the beginning of each run, the sequence of the three sessions was decided randomly. In 140 trials for each session, images containing the chosen object (five images from conditions A, C, and D) and subject (two images from condition B) were shown randomly and repetitively (20 times each image) after a fixed cross sign at the center of the screen and then back to a black screen, shown after 1 s, as depicted in Figure 1b. An interval with a duration of 1000–2000 ms was randomly placed between two trials.

EEG recording. A multi-channel EEG recording device (EEG-1100; Nihon Kohden Cooperation, Tokyo, Japan) was used for recording EEG with a sampling rate of 500 Hz. Electrodes were set based on the extended international 10–20 system with an electrode cap (M64 montage without FT9, FT10, TP9, and TP10, EASYCAP GmbH, Herrsching, Germany). Electrodes were connected to a 64-channel amplifier, including one channel for reference in the left earlobe, two channels for horizontal and vertical electrooculogram (EOG) respectively, and 61 channels for EEG. Ground was set between the eyebrows.

2.2.2 Data Analysis

EEG data processing: Data from nineteen participants were included for analyses; data for one were excluded due to an unexpected technical malfunction. The recorded data were re-referenced to a common average, and then sent through a zero-phase-shift frequency domain band-pass filter with the cut-off frequency set at 1 and 30 Hz. Next, the Independent Component Analysis (ICA) completed by the Algorithm for Multiple Unknown Signals Extraction was used to remove EOG artifacts (Tong et al., 1991). Trials with potentials over 100 μV were seen as ab-normal and abandoned. Finally, over 97.5% of trials of each condition remained for further analysis. The data recorded from

200 ms before stimulus onset (as the baseline) to the end of a trial were extracted as an epoch.

Statistical test based on Monte Carlo method: Most of the statistical analysis revealed that the data were not normally distributed; there-fore, we chose one-tailed nonparametric test methods for this research. Many researches have proven that the permutation test is reliable for testing neural signals (Groppe et al., 2011; Maris & Oostenveld, 2007). In this research, the workflow can be described as follows:

a. For two independent sample sets, $sampA$ and $sampB$, where H_0: $\overline{sampA} \leq \overline{sampB}$, v_0 was calculated as follows:

$$v_0 = \overline{sampA} - \overline{sampB}, \quad (1)$$

where H_0 is the null hypothesis and v_0 is the test statistic.

b. $sampA$ and $sampB$ were put into the same group. Then, the elements of this group were randomly divided into two sub-groups: $sampA_1$ and $sampB_1$, which had the same size. The new statistic of test v_1 was calculated as follows:

$$v_1 = \overline{sampA_1} - \overline{sampB_1}, \quad (2)$$

c. Step b was repeated 10,000 times to obtain $v_1, v_2, \dots, v_{10000}$;

d. The $v_1, v_2, \dots, v_{10000}$ values were sorted in ascending manner, and the sequence number of the first value that was greater than v_0 was identified as the "$location$". The *p*-value of the statistic test was calculated as follows:

$$p = 1 - \frac{location}{10000}, \quad (3)$$

Similarly, when it comes to a paired test, we used the bootstrap resampling approach to obtain the confidence interval of the difference between the paired samples. The bootstrap statistical method is also a nonparametric approach with proven validity and has been approved in many studies (Darvas et al., 2004; Delorme & Makeig, 2004; Graimann et al., 2002). The procedures are shown below:

1. For two paired sample sets, $sampC$ and $sampD$, where H_0: $\overline{sampC} \leq$

$\overline{sampD}$, we constructed a paired sample set $sampP$, as follows:

$$sampP = sampC - sampD, \quad (4)$$

2. Resampling was performed from $sampP$ with a replacement to generate a new sample set, $sampP_1$; then, its mean value A_1 was calculated as follows:

$$A_1 = \overline{sampP_1}, \quad (5)$$

3. The last step was repeated to obtain $A_2, A_3, \ldots, A_{10000}$, which were then sorted in ascending manner, and then, the index of the first value that was greater than zero was identified as the $index$. The p-value of this test was calculated as follows:

$$p' = \frac{index}{10000}, \quad (6)$$

Functional connectivity and effective phase-locking value (ePLV): We estimated the phase-locking values (PLVs) to measure the connectivity between the data recorded near the occipital lobe (a fusion of EEG recorded from electrodes Oz, O1, O2, POz, PO3, and PO4) and all the other electrodes (Catrambone et al., 2019). The result of the Hilbert Transform (HT) of each epoch was used to generate analytic signals for computing the instantaneous phase at each moment. The PLV between regions i and j at time t is estimated as follows:

$$PLV_{i,j,t} = \sqrt{\begin{matrix}\left[\frac{1}{n}\sum_{k=1}^{n} cos\left(\theta_{i,k,t} - \theta_{j,k,t}\right)\right]^2 \\ + \left[\frac{1}{n}\sum_{k=1}^{n} sin\left(\theta_{i,k,t} - \theta_{j,k,t}\right)\right]^2\end{matrix}}, \quad (7)$$

where n is the number of epochs and θ is the phase in radians obtained from HT (Lachaux et al., 1999). For each subject, one PLV time series was estimated. However, these values do not always mean that there is a relationship between the two regions because even noise signals would have a PLV between 0 and 1. To know which of them are significantly different from the baseline (effective PLV, ePLV), estimated PLVs were submitted to a bootstrap-resampling-based, paired statistical test program to eliminate false positives by testing with the PLVs during baseline. This program works in two steps: (i) for each participant, the PLVs during the baseline period (i.e., before the

stimulus was given) were resampled to extract the mean value according to central-limit theorem, and then (ii) paired tests between PLVs at each moment and the mean value were conducted. The workflow can be described as follows:

For each PLV time series,

1. Values during the baseline period were extracted and were put into the baseline vector;
2. Resampling was performed from $baseline$ with a replacement to obtain a new vector $baseline'$ with the same size;
3. The mean $baseline'$ across time was calculated;
4. Steps 2–3 were repeated 10,000 times and then a grand mean value of the results in step 3 was obtained.

After the above procedures were executed on every PLV time series, a mean value vector was generated as the $baseline$, which was used as a sample set of the control group in the following paired test. Finally, we could determine which of the PLVs represented a meaningful functional connectivity and could be considered as ePLVs.

Event-related spectral perturbation (ERSP): Every epoch was conducted with continuous Morlet wavelet transform to unfold their frequency dimension via the Wavelet Toolbox in MATLAB (MathWorks, Natick, MA, USA). ERSP reflects the energy changes in EEG after providing a stimulus, which is defined as the ratio of power at the current time and baseline mean (Makeig, 1993). For each epoch, ERSP at time i of a specific frequency component j can be calculated as follows:

$$ERSP_{i,j} = 10 \times \log_{10} \frac{u_{i,j}}{baseline_j}, \quad (8)$$

where $u_{i,j}$ is the absolute value of potential at time i and frequency j, and $baseline_j$ is the average of the one at frequency j before the stimulus was presented. To highlight the source of ERSP variation at the sensor level, a finite difference-based spatial Laplacian transformation was conducted via Brainstorm (Carvalhaes & De Barros,

2015; Nunez & Westdorp, 1994; Pernier et al., 1988). This procedure used the ERSP data to replace the potential data in the algorithm (Oostenveld et al., 2011).

2.3 Results

2.3.1 Functional Connectivity

It is noticed that functional connectivity estimated by EEG filtered at different bands is totally inconsistent (Pockett et al., 2009). Therefore, the preprocessed EEG epochs were filtered into four different bands (delta: 1–3 Hz, theta: 4–7 Hz, alpha: 8–13 Hz, and beta: 14–30 Hz); next, the PLVs between EEG recorded at the occipital lobe and other locations were then calculated and the ePLVs were then screened out. The number of ePLVs varied over time. The topography shown in Figure 2.2 displays the distribution of ePLVs calculated with data from the four frequency bands at different moments. These moments were selected to show as many connections as possible.

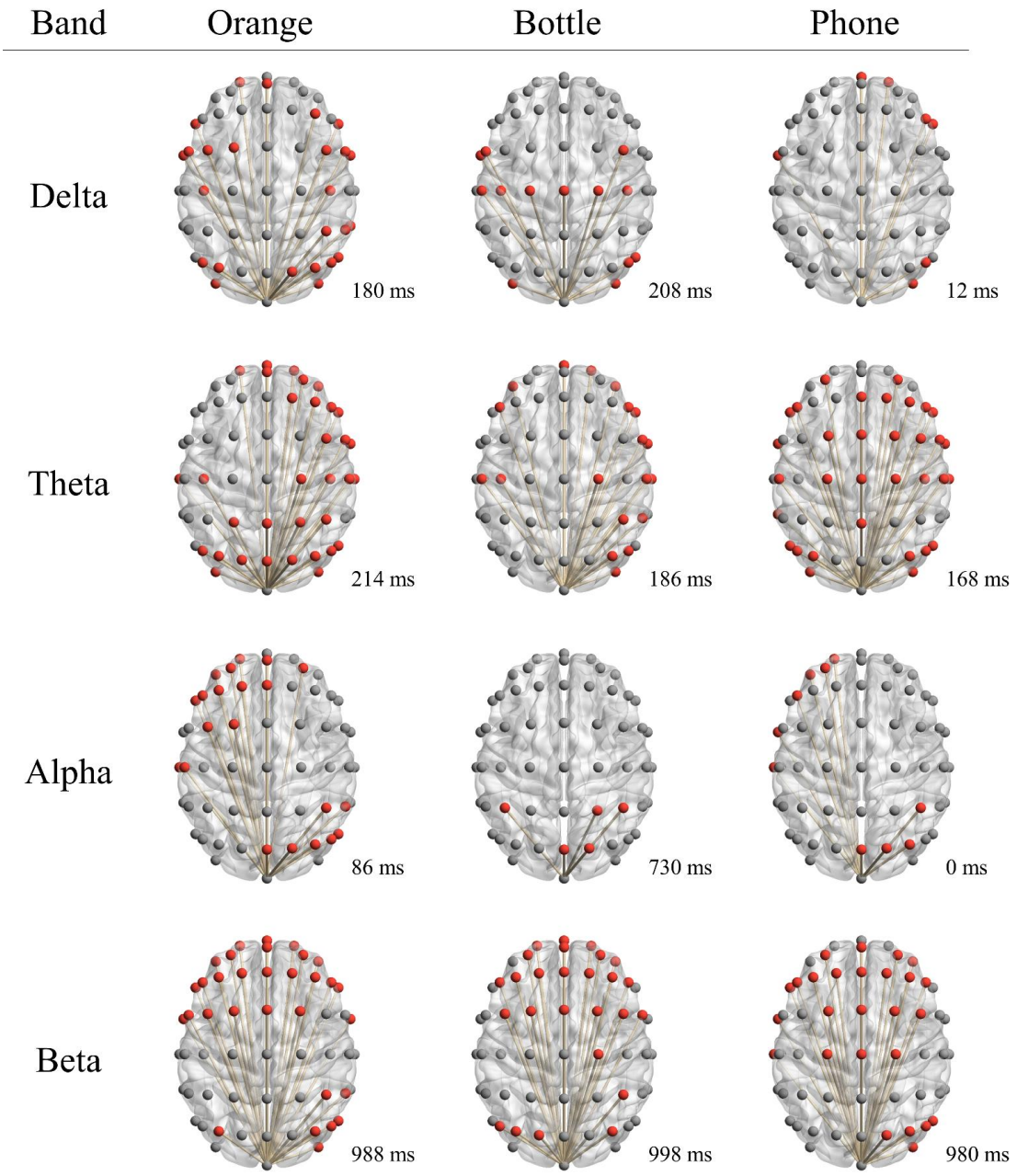

Figure 2.2 Functional connectivity between visual cortex and other regions when participants were shown with images from condition A. Colored electrode indicates that connectivity between that region and the occipital lobe actually exists. Time is determined based on the principle of showing the connections as many as possible.

At the delta and alpha bands, the number of ePLVs was fewer than that of the other bands; furthermore, across the three objects, there was a noteworthy change in the moment that the maximum number of connections appeared. By contrast, the ePLVs estimated at the theta band and the beta band were more credible because of the number

of observed connections, especially their stability across time and objects. Results from beta band suggested that, regions connected with occipital lobe were mainly the central frontal area and the right angular gyrus, but a further analysis in time domain showed that beta band PLVs did not changed a lot than baseline (see Figure 2.3). This false positive suggested beta band is not good at representing the cerebral activity connected with current task. In theta band, it was noticed that the right frontal area (RF), bilateral central sulcus (L/RCS), right temporal lobe (RT), and right angular gyrus (RAG) did establish functional connectivity with occipital lobe. Obvious increase of PLV was noticed at about 200 ms after stimulus onset (as shown in Figure 2.4). Compared with others, theta band showed a unique advantage on measuring functional connectivity by estimating PLV, and consist with the opinion that the theta band has advantages in observing functional connectivity (Fellrath et al., 2016; Murias et al., 2007; Sauseng et al., 2005).

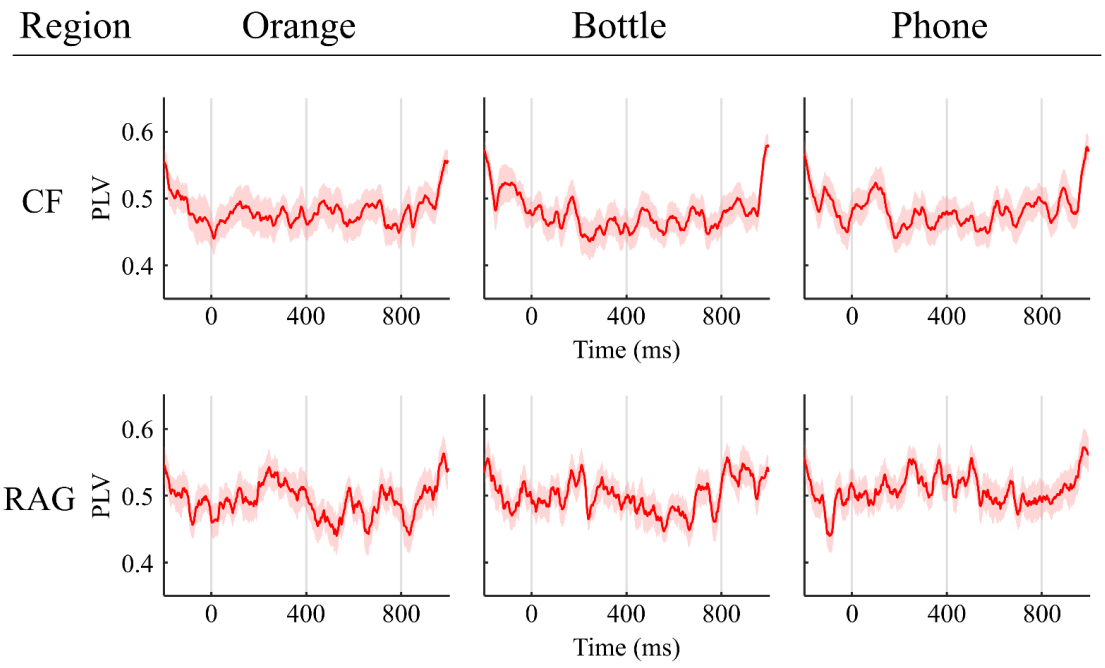

Figure 2.3 Variation of PLV along time at central frontal (CF) and right angular gyrus (RAG) in condition A. Red line means average value across subjects, and shaded area means standard error ($N = 19$). Obvious increase could only be observed near the end (after 900 ms) and in a narrow time band. It is possibly a false positive due to the Gibbs phenomenon when apply Hilbert Transform on a wide-band signal. Beside this, most of the values were at the same level with baseline.

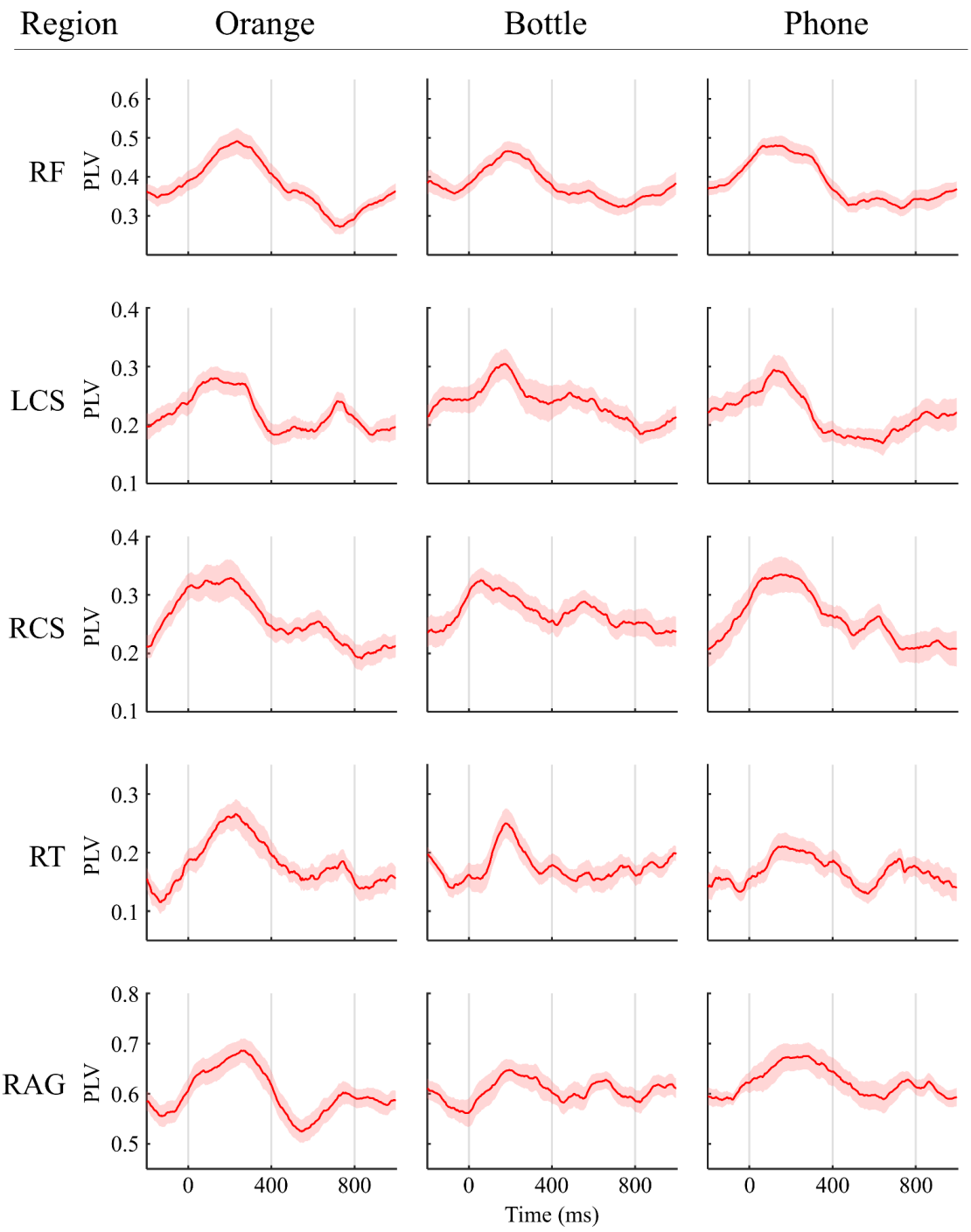

Figure 2.4 Variation of PLV along time at central frontal (CF) and right angular gyrus (RAG) in condition A. Red line means average value across subjects, and shaded area means standard error (N=19). All of the curves increased significantly in the interval of 0 to 400 ms after stimulus onset, and peaked at about 200 ms. Baseline level varies in different areas, but not related with the Euclidean distance to occipital lobe.

Distribution of occipital-lobe-connected ePLVs of each condition was shown in Figure 2.5. Results suggested more regions joint the process when a hand is included in visual stimulus. These new-appeared regions are mainly left frontal lobe and left temporal-parietal junction (including left angular gyrus, LAG).

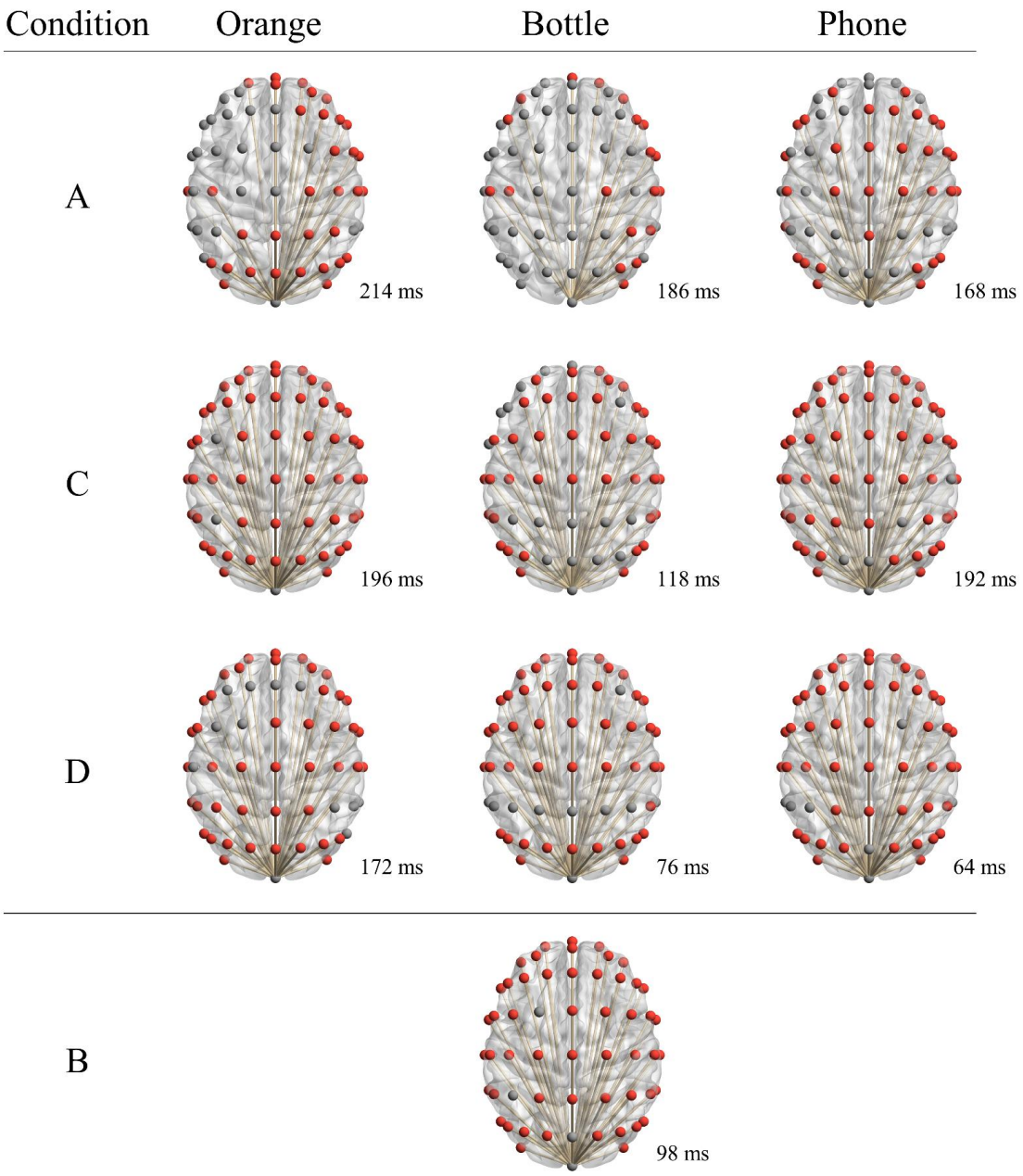

Figure 2.5 Distribution of ePLVs in each condition. Each colored electrode means there is a connection between that electrode and occipital lobe, at the moment indicated on the bottom-right corner of each topography. Larger area participated in condition C and D than only seeing objects. The moment that most connections were observed is earlier

in condition D.

Additionally, the moment that a maximum connection number was reached showed a regular pattern: condition D is the earliest, then condition C follows, and condition A is the latest.

In summary, the topography demonstrated that functional connectivity between the occipital lobe and regions of RF, L/RCS, RT, and RAG were established similarly when participants saw images either the three conditions. To make it more intuitive, the PLV-over-time plot of the regions mentioned above is shown in Figure 2.6. On the contrary, the difference is embodied in the area covered by electrodes F5, F7, FC5, and FT7, which is believed to be Broca's area (BA) (Fadiga et al., 2009; Fadiga & Craighero, 2006; Fazio et al., 2009; Rizzolatti et al., 1996) and the left angular gyrus (LAG). Same as before, we demonstrated these differences in the plot of PLV over time in Figure 2.7. The results of paired test suggested that these differences are significant.

Additionally, we noticed that the distribution of PLVs when participants were shown with images of hand is similar with condition C and D. This phenomenon revealed that human brain treats hand differently with objects. Figure 2.8 was drawn to figure out the relation and difference between them. Although they both established functional connectivity between occipital lobe and right temporal lobe, it was stronger when seeing objects.

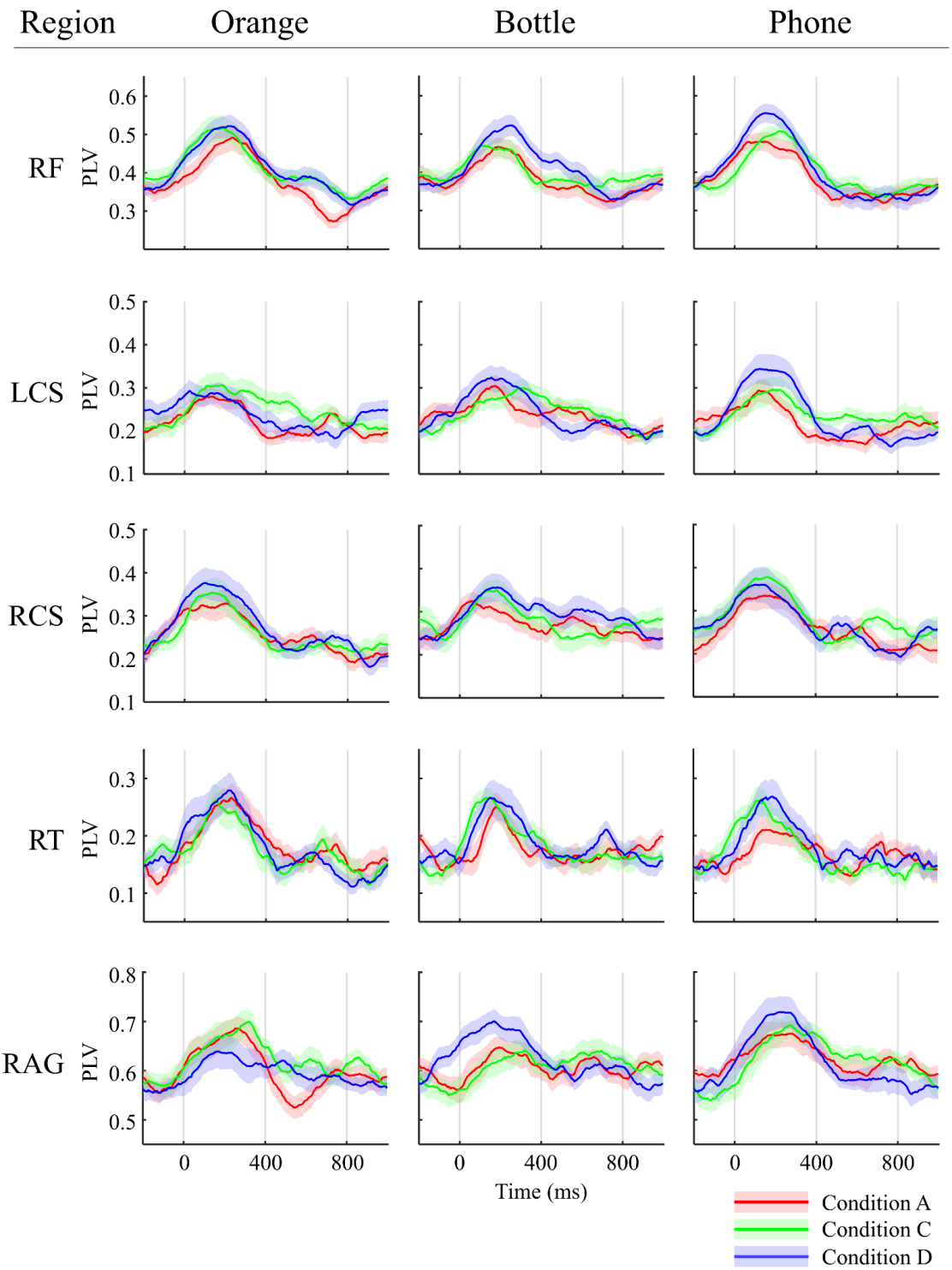

Figure 2.6 PLVs over time. Red line shows phase locking values (of theta band) when participants were shown images in condition A; green line when condition C; blue line when condition D. Shaded areas are standard error. Besides the sporadic unstable difference between condition A and D, PLVs among the three conditions varied similarly at these regions. The green curve seems to consist with either the red or blue curve of the same plot randomly, or part of the red curve followed by part of the blue one (e.g. RAG-Orange plot).

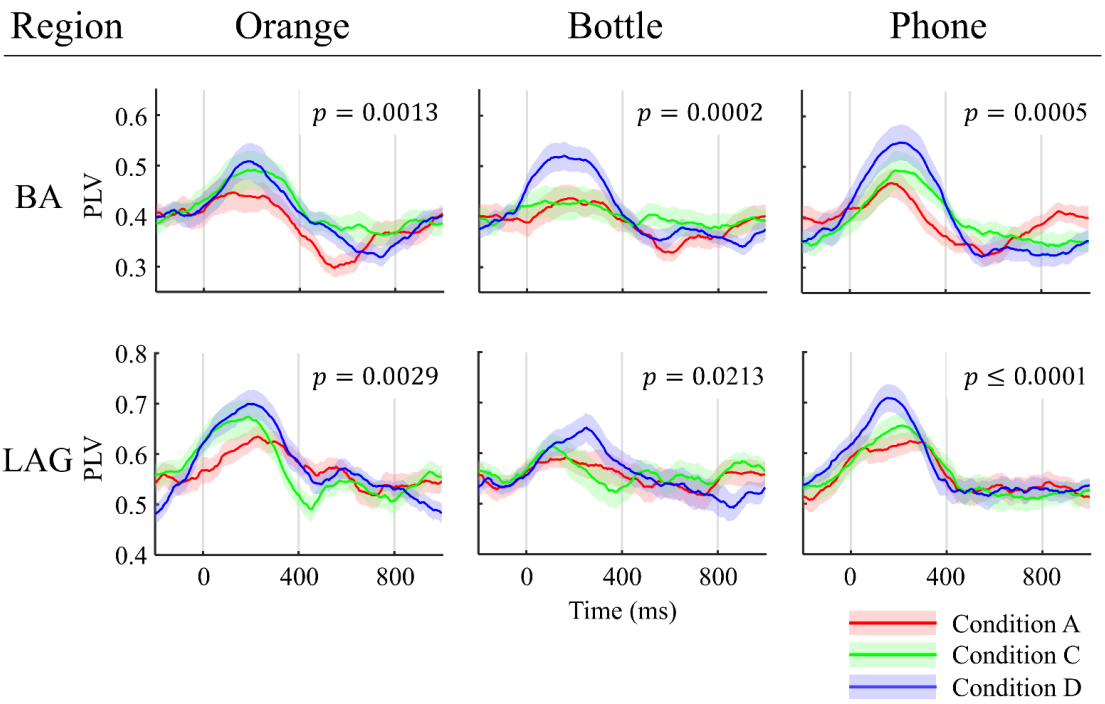

Figure 2.7 Red line shows phase locking values (of theta band) when participants were shown images in condition A; green line when condition C; blue line when condition D. Shaded areas are standard error. Significant difference was noticed between seeing objects and seeing interactions at 200 ms after presenting the stimulus to participants ($\alpha = 0.05$). Green curve tends to between the red and blue curve.

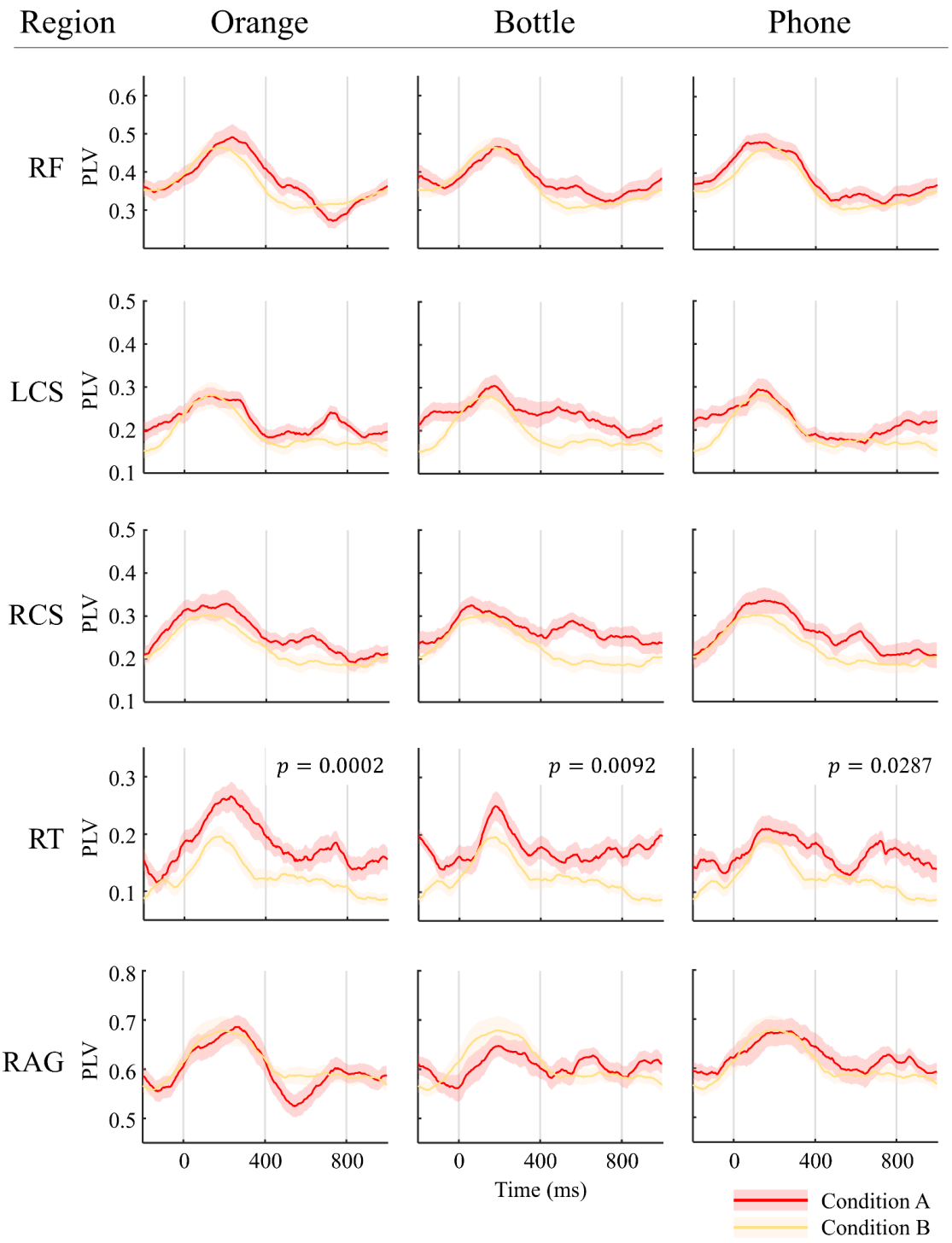

Figure 2.8 Comparison between seeing object and hand. Red curve shows the PLV-time plot of condition A, and yellow curve shows that of condition B. Shaded area means standard error. In these regions, right temporal area performed specially—significant difference of average PLV during 0—400 ms was noticed. Right temporal cortex connected with occipital lobe stronger when seeing objects than when seeing hand.

Many visual object recognition related studies has proved that temporal lobe contributes to object recognition process (“vision for perception”, Mishkin et al., 1983). Therefore, we also measured the functional connectivity between temporal lobe and the other regions, as shown in Figure 2.9. These regions are mainly the frontal lobe and contralateral parietal lobe. The right hemisphere of temporal lobe (T8) seemed to be more essential than its left part in all the four conditions. Therefore, we compared the PLVs between right temporal lobe and left parietal lobe (LP), and the result suggested a stronger connection when seeing interactions (see Figure 2.10).

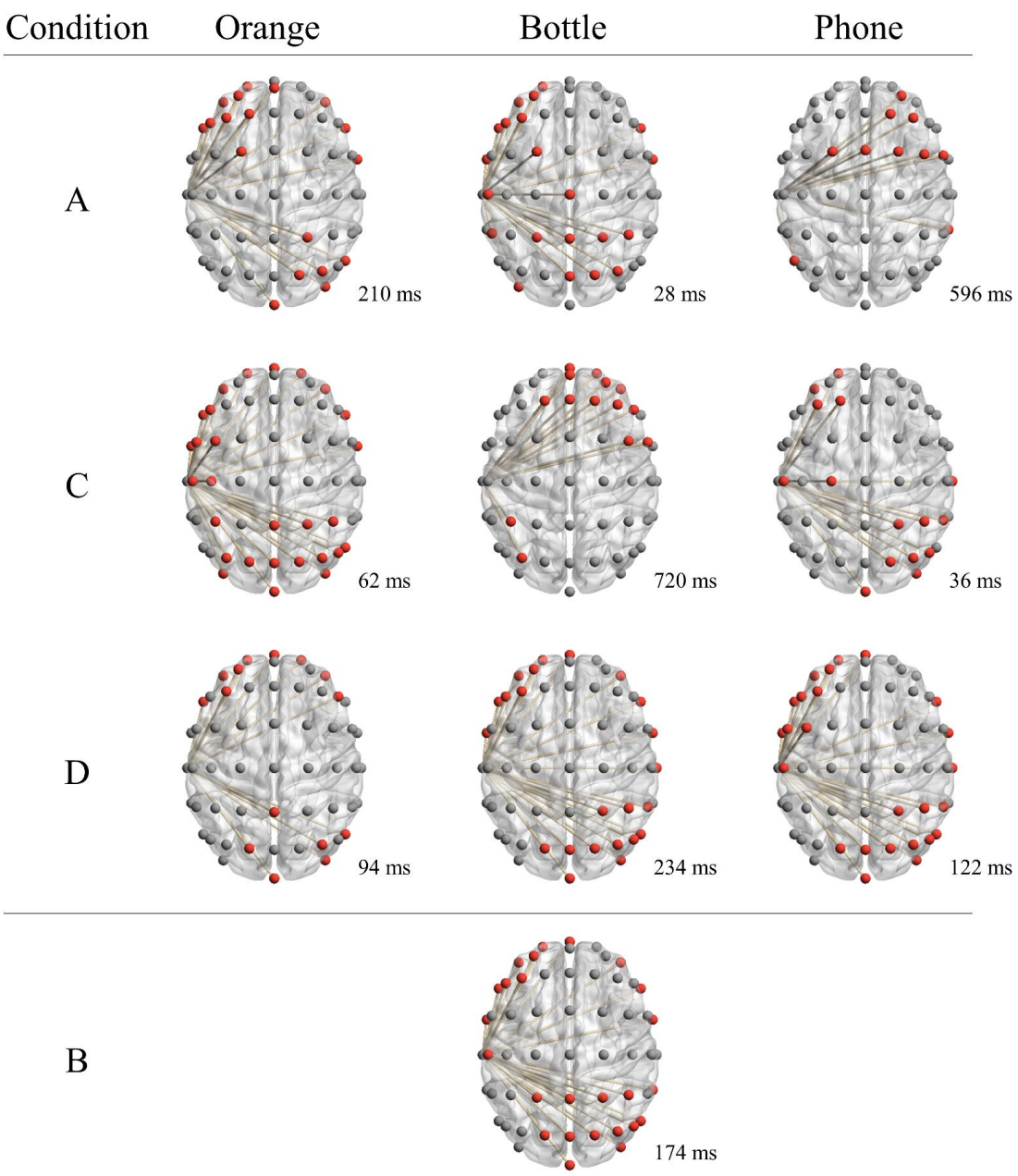
Condition
Orange
Bottle
Phone
A
210 ms
28 ms
596 ms
C
62 ms
720 ms
36 ms
D
94 ms
234 ms
122 ms
B
174 ms

(A)

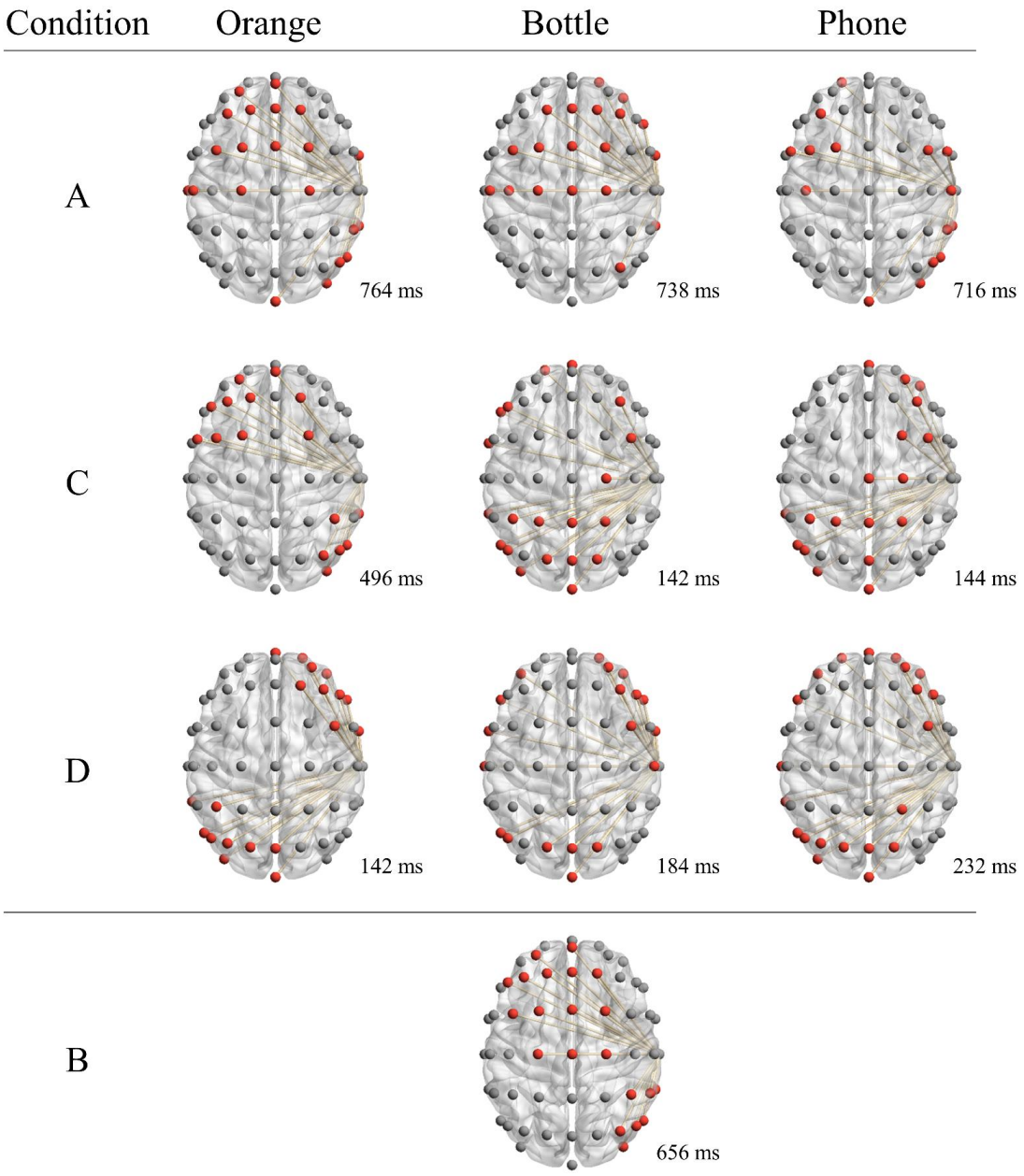

(B)

Figure 2.9 Effective PLVs between (A) left temporal lobe and other regions, and between (B) right temporal lobe and other regions. A notable feature was that temporal lobe connected to contralateral parietal lobe when participants saw interactions, and this phenomenon was not obvious when seeing objects, especially for right hemisphere—no ePLV between right temporal lobe and left parietal lobe was observed when seeing only objects. The time that most ePLVs appeared in (A) varied more dramatically than (B), which may suggested right temporal lobe was modulated more than the left part.

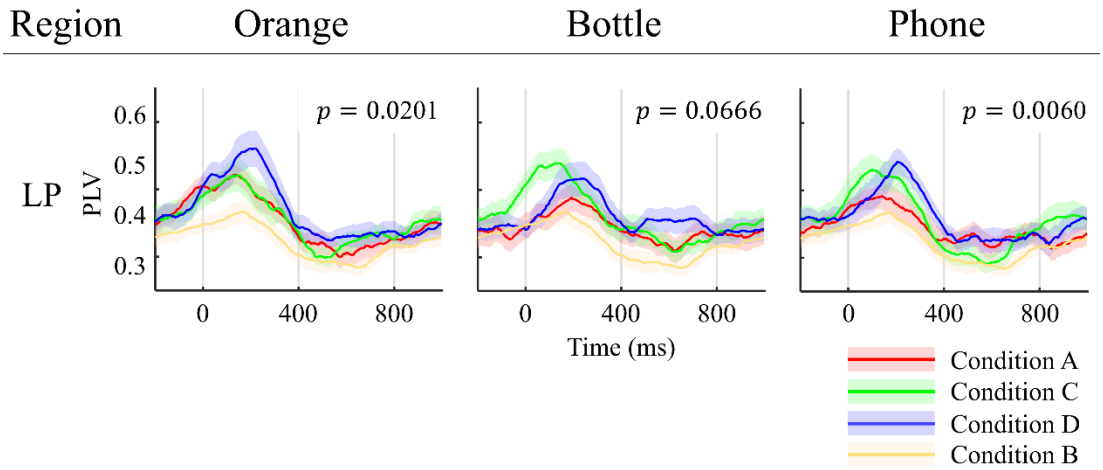

Figure 2.10 PLV-time plot of the PLVs between right temporal lobe and left parietal lobe. Difference between condition A and D was noticed at about 230 ms.

2.3.2 Power Variations

As mentioned in the Introduction, we were expecting to find some motor-related EEG features when participants looked at non-tool objects. Thus, our attention was turned to power changes in the mu rhythm (Caldara et al., 2004; Jeannerod, 1994; Pfurtscheller & Neuper, 1997), and clear event-related desynchronization (ERD) was noticed with both "seeing objects" and "seeing interactions", as shown in Figure 2.11a. The topography was drawn with EEG data filtered at 8–13 Hz and then was Laplacian spatial filtered to highlight the changes. ERD was mainly observed at the region of the bilateral postcentral gyrus, which may suggest the participation of the primary somatosensory cortex (Oostenveld & Praamstra, 2001). Among all three objects, the most obvious ERD occurred at the area covered by electrodes C5, CP3, and CP5 in the left hemisphere (LS), as well as the corresponding position in the right hemisphere (RS). Figure 2.11b revealed its dynamic changes over time. Although all of these plots performed clear ERD at the end, there was obvious event-related synchronization (ERS) observed during the process when participants saw objects being grasped. This ERS was widespread from 100 to 200 ms, especially in LS.

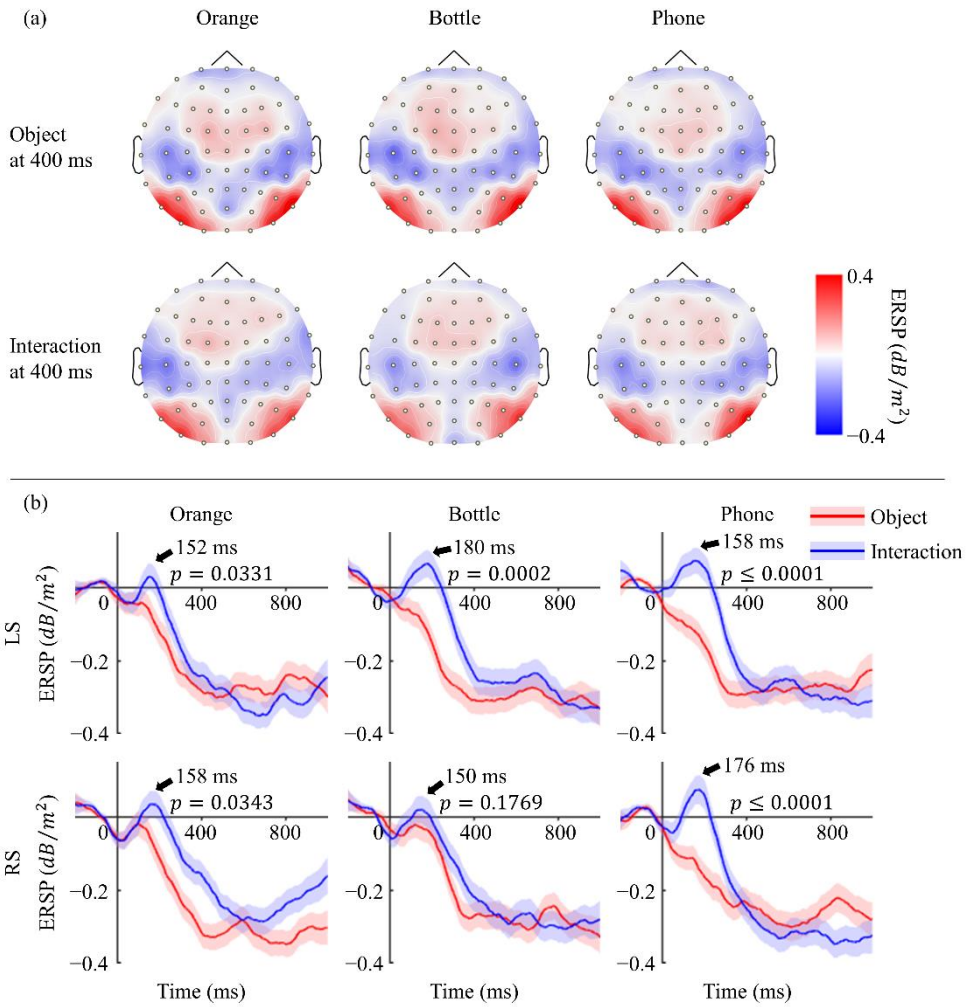

Figure 2.11 (**a**) Topography of ERSP at 400 ms. Mu rhythm ERD distributed at bilateral posterior central gyrus with a little left advantage and performed similarly in all six situations. (**b**) ERSP over time. Red line shows ERSP when participants were shown objects, while the blue line shows ERSP when they were shown objects being grasped by human hands. Shaded areas are standard error. A clear ERS was observed only when seeing interactions, and its peak time is indicated with an arrow. The significance of ERS was confirmed by a permutation test on the ERSP value in the two conditions at the corresponding time ($\alpha = 0.05$).

Undoubtedly, the difference in power change in the somatosensory cortex is due to the difference in visual stimuli, which means that the ERS may be caused by the hand contained within the image or the combination of a hand and the object. Fortunately, we have collected EEG data from when participants were shown only a hand and both a hand and an object. By comparing the topography in Figure 2.12a, we found that they

showed ERS in the left somatosensory cortex for both conditions, although the values were not completely the same. This suggests that the hand seen in the visual stimuli partly contributed to the ERS. We also analyzed the data from condition C and interestingly found that it was different from that of the other three kinds of stimulus. It seems that participants recognized the hand and object in each image as two entities. We found that, at about 200 ms after visual stimulus onset, a positive event-related potential (ERP) component appeared at both the PO7 and PO8 electrodes but with a right hemisphere asymmetry. The plot in Figure 2.12b shows the ERP difference between the PO7 and PO8 electrodes. Evidently, two clear peaks were observed in condition C, while only one was observed in the other two conditions. A further test with a one-way ANOVA-based multiple comparison suggested that the lateralization phenomenon in condition C was significantly different from the others ($p < 0.05$).

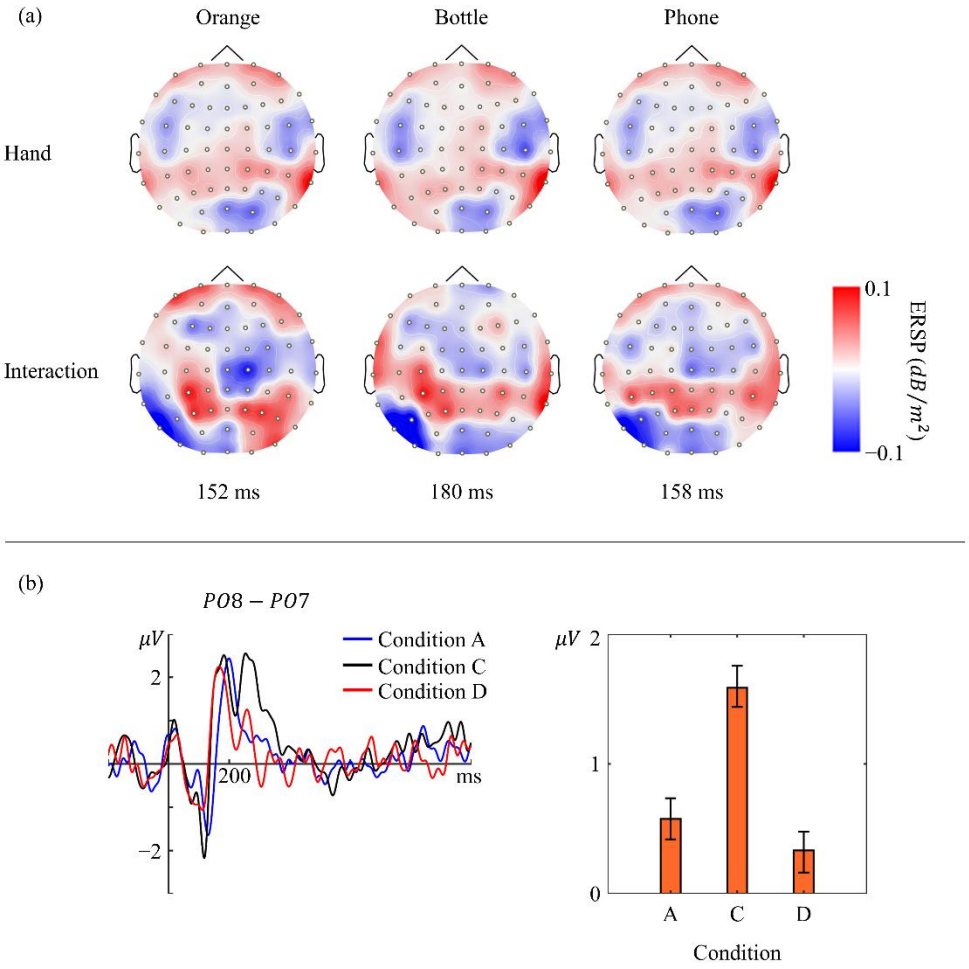

Figure 2.12 (**a**) Topography of 8–13 Hz ERSP when seeing human right hand and seeing interactions using the right hand at 152, 180, and 158 ms. ERS at LS is weaker when only images of a hand are presented to participants. (**b**) Plot shows a grand averaged ERP difference between electrodes PO7 and PO8. A remarkable second peak (black line) appeared when participants were presented with images in condition C. The bar graph on the right shows mean and standard error of the difference data in the range from 246 to 300 ms.

2.3.3 ERPs

Event-related potentials (ERPs) were observed via EEGLAB, and the result from Orange series stimulus were shown in Figure 2.13 as an example (Delorme & Makeig, 2004). High SNR ERPs can only be observed at occipital lobe. In occipital lobe, three components were found, which sourced at PO7 and PO8 electrodes. But there was no difference among the four conditions. We then paid attention to temporal lobe, because it is a part of the ventral stream in visual object recognition. Finally the statistic test proved that the FT8 electrode performed differently when participants were shown with images in condition C ($p = 0.0015$). Moreover, we also expected that the ERPs in Broca's area might be different since there is no cue to launch the MNS, but still no significant difference among them.

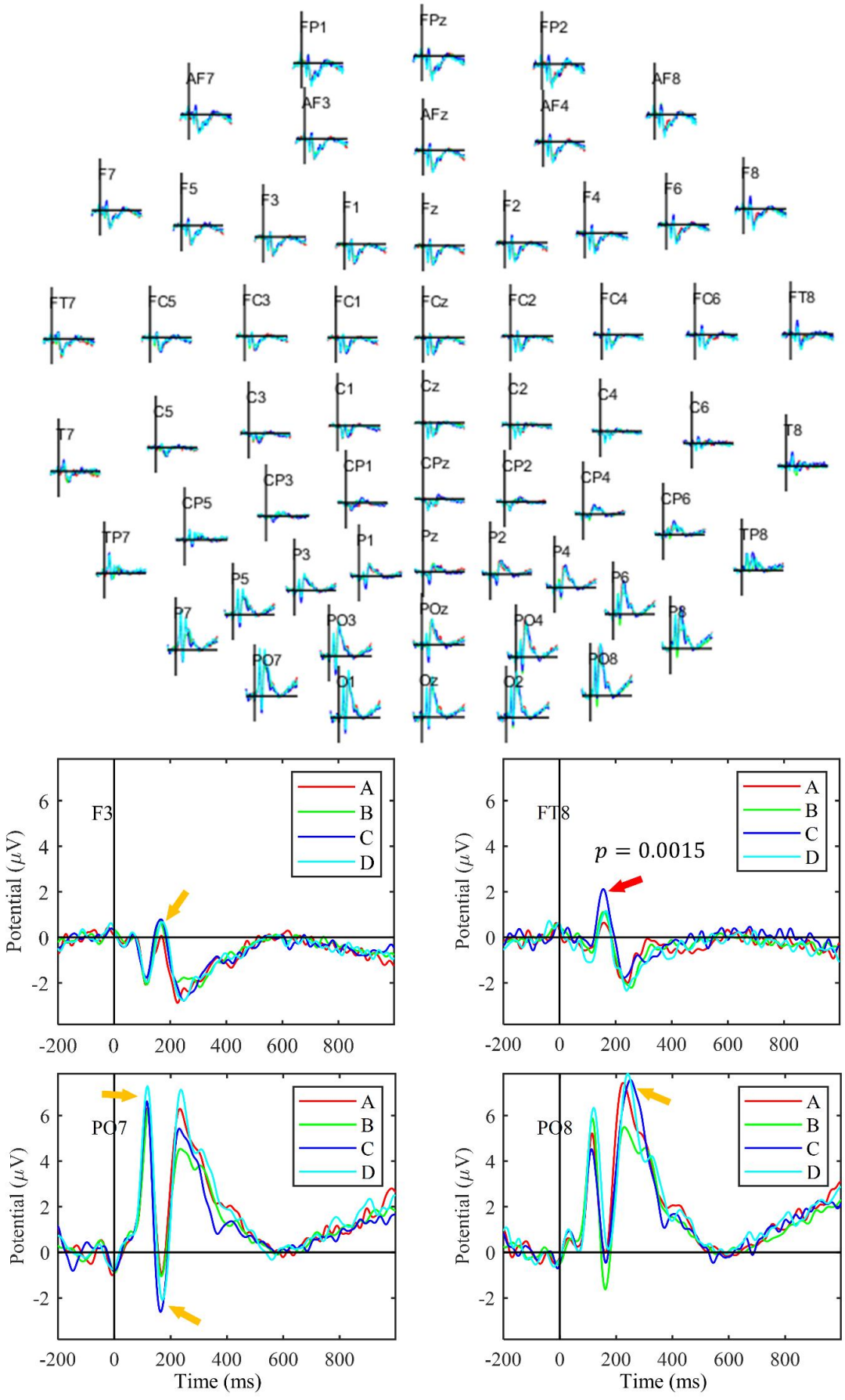
FP1
FPz
FP2
AF7
AF3
AFz
AF4
AF8
F7
F5
F3
F1
Fz
F2
F4
F6
F8
FT7
FC5
FC3
FC1
FCz
FC2
FC4
FC6
FT8
T7
C5
C3
C1
Cz
C2
C4
C6
T8
CP5
CP3
CP1
CPz
CP2
CP4
CP6
TP7
TP8
P5
P3
P1
Pz
P2
P4
P6
P7
P8
PO7
PO3
POz
PO4
PO8
O1
Oz
O2
F3
FT8
$p = 0.0015$
PO7
PO8
A
B
C
D
Potential (μV)
Time (ms)
-200
0
200
400
600
800
6
4
2
0
-2

Figure 2.13 Grand average ERPs of Orange series ($N = 19$). Sources of components were located by searching maximum value at sensor level. The P1 and N1 components sourced at electrode PO7, while the P2 component sourced at PO8. No significant difference was found by ANOVA multi-comparison. Due to the existence of ventral stream, we then paid attention to temporal lobe, and the potential of condition C at FT8 showed a significant difference with condition A and D ($p = 0.0015$). Additionally, we looked into Broca's area (F3), but no significant different appeared ($p = 0.2403$).

2.4 Discussion

ERP analysis was not effective enough in this study. ERP technique relies on the phase-locking phenomenon during cognition process. Those well-locked components would be remained while the others would be erased during averaging procedure. This characteristic makes it can only reveal the evoked process, but not the induced process. In our experiment, visual evoked potentials were exposed successfully, but the other regions were not. It suggested that the processes happened in other regions more tended to be induced ones. In visual cortex, difference between PO7 and PO8 electrode exposed the particularity of condition C—two entities in view. This evidence proved the number of entities was perceived at visual cortex. In addition to this point, no more difference was found. However, in temporal lobe, ERP of condition C was highlighted. Considered with the function of ventral stream of visual object recognition, it is reasonable to infer that temporal lobe launch the process for evaluation relationship between the two entities, while no such need in other conditions.

Functional connectivity between occipital lobe and temporal lobe performed differently when saw object and when saw human hand. A possible explanation is that perception of a human hand does not need that much resources as perception of artificial objects. However, the regions that were involved in recognition of hand was more than that of objects. All the signs indicated that human hand is special in visual perception.

Another very interesting result is from the observation of functional connectivity

between temporal lobe and left parietal lobe. When showing participants the images that already contained a proper posture to grasp the target object with right hand, that connection get stronger than only present them with images of objects. The ventral stream of visual cortex output was changed. In condition C, this cross-hemisphere information sharing phenomenon was not observed as obvious as in condition D. Therefore, the contralateral communication between temporal lobe and parietal lobe may be a marker of the concept “interact” or “contact”. This is worthy to investigate in the future.

Many studies considered that the particularity of tools is derived from the action applied to use them, which they come naturally with (Creem-Regehr & Lee, 2005). Therefore, we suspected that the presentation of a manipulable object may cause a similar cerebral activity to that which occurs upon seeing an interaction with that object. However, our experimental results rejected this inference with the additional functional connectivity between the occipital lobe and BA as well as between the occipital lobe and LAG when participants were shown images of objects being grasped. Although the controversy about its location is still on-going, a large majority of scholars believe that the mirror neuro system (MNS) exists near Broca’s area (or BA44), the inferior parietal lobule (near the LAG), and the superior temporal sulcus (Cerri et al., 2015; Gallese et al., 1996; Papitto et al., 2020; Rizzolatti & Craighero, 2004). Hence, connectivity observed at BA and LAG can be reasonably regarded as activity of the MNS evoked by seeing the action of grasping objects. This may explain the different distributions of functional connectivity for seeing objects vs. seeing interactions with objects; nevertheless, ERS in the somatosensory cortex, which can only be noticed in the latter case, still exists. All of this evidence led us to the conclusion that the changes observed in the cerebral cortex after seeing objects being grasped were not the same as those that occurred after seeing only objects.

In summary, this study investigated the functional connectivity related with visual cortex, and related with temporal cortex, after healthy participants saw daily objects that are manipulable. We figured out the spatial and temporal features of seeing manipulable objects. Next, we assessed whether seeing a manipulable object led to a similar mu rhythm change to seeing an interaction with the same object; however, the evidence rejected our hypothesis: additional activation of Broca's area and the left angular gyrus, and early alpha band ERS in the somatosensory cortex were only observed when participants saw interactions. Finally, we found that the connection between temporal lobe and parietal lobe might be related with the cue of interaction in vision.

2.5 Summary

In this chapter, the PLV calculated across trials (or PLI, in some definitions) revealed which regions participated in the post-process after normal human saw a manipulable object. However, in consideration of application, this kind of multi-trial based algorithm is not suitable in actual using. Therefore, in the next chapter, another study about classifying human's EEG when seeing other's movement, imagining a certain movement, and actually executing a movement through the approach of calculating PLV in a single trial will be introduced.

Chapter 3

Classify EEG Signal among Movement Observation, Imagination, and Execution

Abstract: It has been found that the functional connectivity is useful in recognize the cerebral regions that take part in a specific cognitive process. In this research, we tried to use this method to study which areas participated in the movement observation, imagination, and execution process. A total of 17 healthy volunteered participants provided their electrophysiological data in the experiments. Then, a series of methods based on Support Vector Machine (SVM) were used to search for effective features from electroencephalograph (EEG) to distinguish those processes from each other. Consequently, an average classification accuracy of 44.0% was achieved via both the phase locking value features and power variation features. Moreover, during the classification, it was confirmed that the Broca's area, motor cortex, the Wernicke's area, and visual cortex participated in these processes. Additionally, we proposed to pay more attention on the late component of EEG in doing researches because their importance were exposed in this study.

3.1 Introduction

In previous study, it has been noticed that a huge range at cerebral cortex participated in the cognitive process after the images showing an interaction movement were presented to normal human volunteers. Not only the visual cortex, but the activated neurons also included the (pre-)motor cortex, somatosensory cortex, and the region

believed to be related to the mirror neuron system as well (as shown in Figure 2.2). Therefore, the reason why these neurons engaged in this process can be speculated as: 1) the observation of movement just lead to their firing; or, 2) the observation of movement caused an involuntary imagination of that movement, which then caused the activations; or, 3) the volunteers tried to execute the observed movement. In order to figure out which of them were the actual reason, a novel EEG experiment were conducted in this study.

Moreover, as is well known, imagination of movements causes electrophysiological activities at similar neural circuit as when execute the same movement actually. Based on this principle, scientists have invented the motor-imagining brain-computer interface (MI-BCI) and applied it into many occasions in different fields. Similarly, the discovery of mirror neuron system also uncovered an acknowledged theory that human are intendent to imitate in the meantime seeing other people making a movement. However, these phenomena come to be a problem when we try to make machines understand when someone is trying to make a movement and when someone just saw other's movement, because theoretically they induce similar neural activities (Sté Phanie Cochin et al., 1999).

Hence, this study focused on the topic of distinguishing the EEG signal recorded when volunteered participants were taking these tasks: movement observation, imagination, and execution. In the following sections, a whole sketch was provided to show how we studied the topic with a data-driven thinking, and particularly using the feature selection method to figure out the spatio-temporal activity of cerebral cortex.

3.2 Materials and methods

3.2.1 Experiment

Materials: A total of 20 gestures were determined as stimulus. Movies that show moving right hand from an open palm to pose these gestures and finally back to an open palm were created by Unity (San Francisco, CA, US). Figure 3.1 shows static images of these gestures, and the processes contained in the movie is shown in Figure 3.2. In the beginning of a trial, one of the short movie was chosen randomly and shown to participants. Then, the screen back to empty and participants were asked to recall the movement shown in the movie. Finally, a progress bar was presented and participants were asked to finish the gesture shown in that movie before the progress bar was at its end. These three procedures in a trial were named as “observation phase”, “imagination phase”, and “execution phase” (see Figure 3.3). During the experiment, a camera was set against participant’s right hand and take photos during execution phase, in order to check whether participants finished the target gesture successfully. The gesture of a trial was chosen randomly from those 20 gestures mentioned above. 30 trials were run for each participant.

Figure 3.1 The 20 gestures used in experiments. They were determined based on the principle of hard to be named in case participants easily memorized them through semantic coding.

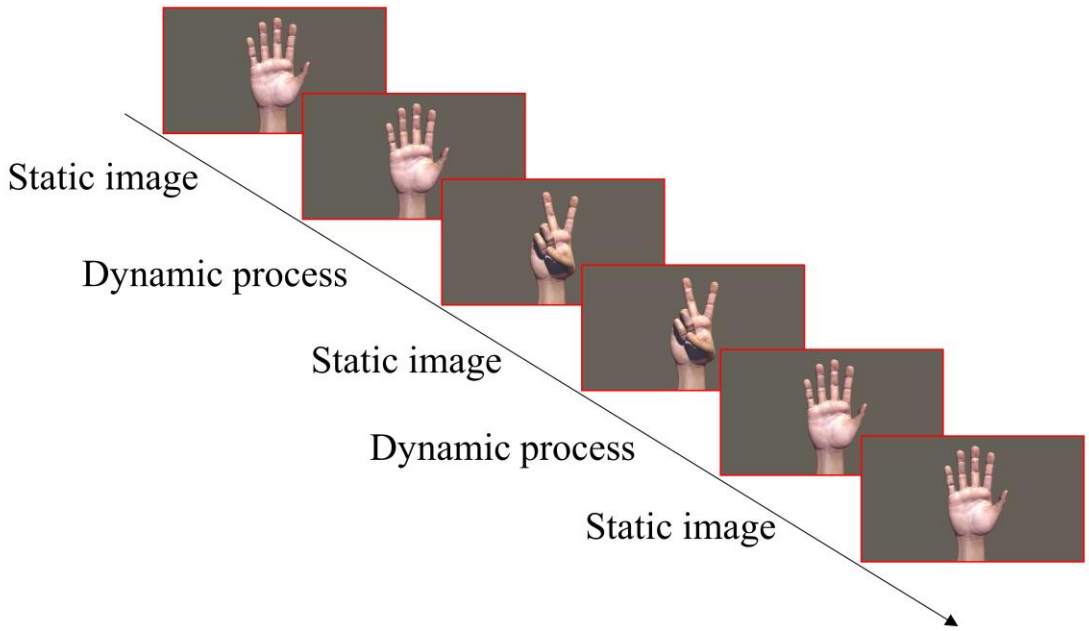

Figure 3.2 The construction of the movie shown to participants during the observation phase. In the first 0.5 s of the video, the scene kept showing an open palm; then the palm turned to move until it showed a gesture (the target gesture) listed in Figure 3.1 in the next 0.5 s, and it kept at the gesture for another 0.5 s. Finally, it back to the open palm in 1 s with reverse procedures.

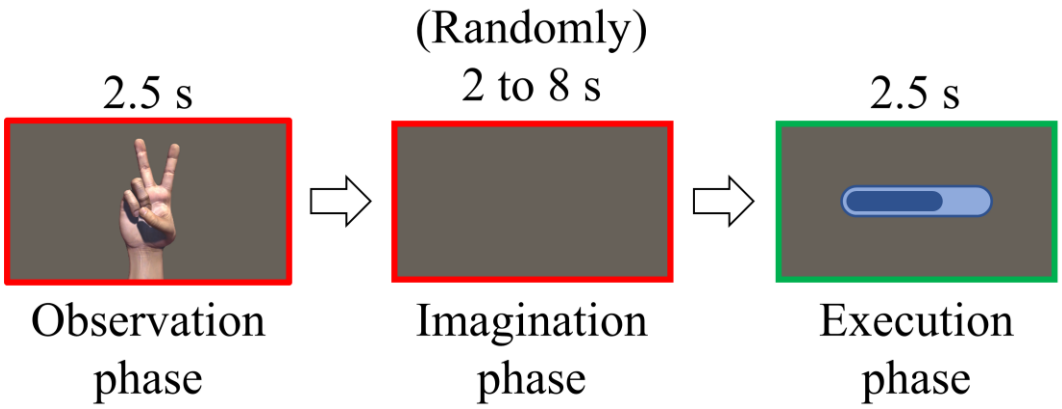

Figure 3.3 Three phases in a trial. Participants were asked not to make any movement with their right hand when the border color was red, and imitate the presented gesture shown at observation phase as soon as the border color turned to green. They had 2.5 s to finish the movement and keep the gesture till the end of process bar. A camera would take a photo at the end so that we can confirm whether participants made the correct gesture during analysis.

Participants: A total of 17 healthy humans (including one female; mean age 23.05 years, range 22–27 years) with normal or corrected-to-normal vision participated in this experiment. This study was reviewed and approved by the Department of Informatics, Faculty of Information Science and Electrical Engineering, Kyushu University (admission No. 2021-13), and every participant signed the informed consent form voluntarily before the experiment began. As 16 volunteers were right-handed as they own reported, in this paper, we shows results from right-handed volunteers if we do not indicate specially. During experiment, participants were ask to set on a comfortable chair and put right arm at a certain place where can be captured by the camera, as shown in Figure 3.4.

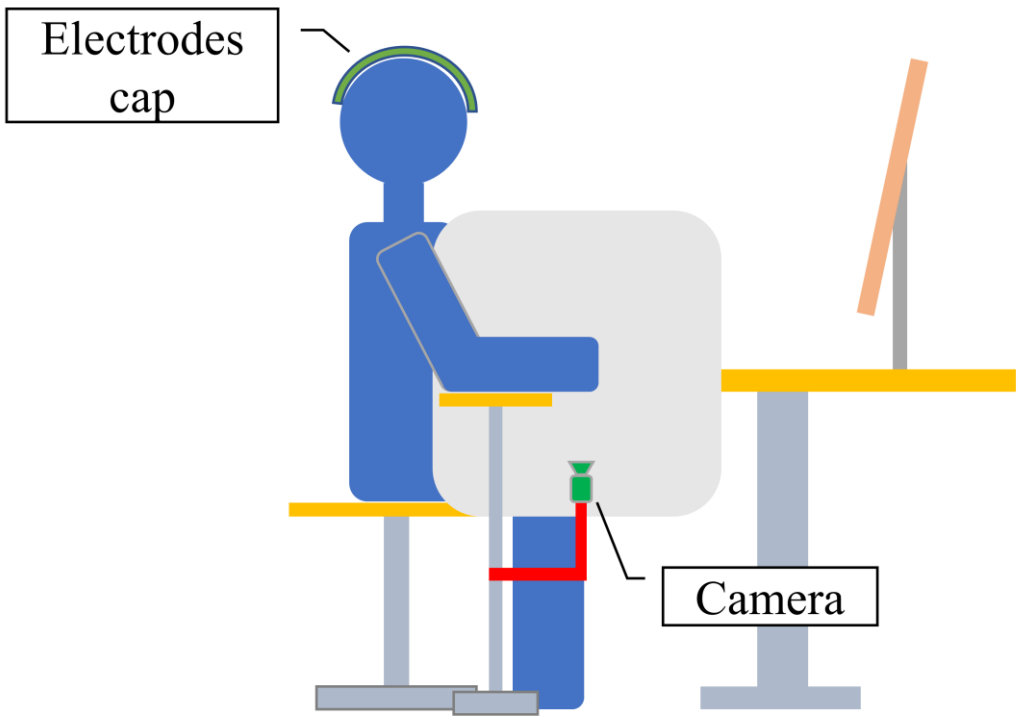

Figure 3.4 Image of the experiment environment. A white foam board was set at the location of the light grey rounded rectangle to block out the sight of participant from seeing their own right hand, in case they observed the movement of their own hand during execution phase.

Stimulus presentation: The stimulus presentation program was created with PsychoPy (Jonathan Peirce et al., 2019), and stimulus were presented to participants via a 15.6-

inch LED display. The resolution and refresh rate were set at 1920 × 1080 pixels and 60 Hz, respectively. The distance between the eyes and display was in the range of 60–80 cm.

EEG recording: A multi-channel EEG recording device (Polymate V; Miyuki Giken Co., Ltd, Tokyo, Japan) was used for recording EEG with a sampling rate of 500 Hz. Electrodes were set based on the international 10–20 system with an electrode cap (19 channels;). Ground was set between the eyebrows.

3.2.2 Data Analysis

A whole framework of the data processing procedures is shown in Figure 3.5. Before analysis, we manually confirmed that all the participants posed correct gesture in execution phase. Moreover, data from 8 random-chosen participants was used for training the machine learning model and the others for evaluation.

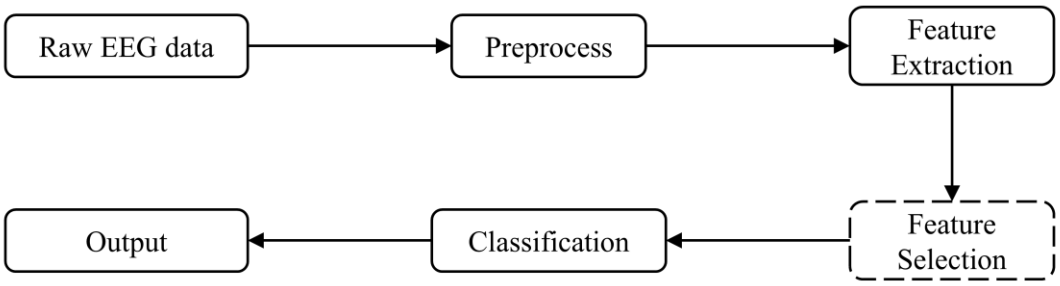

Figure 3.5 A whole framework of the data processing procedures. Note that the Feature Selection will only be done during training the models for the classifiers; in evaluation, the feature selection solution generated during training would be applied to the end of feature extraction procedure and then the classification would be run with only the determined features.

EEG data preprocess: We used the EEGLAB toolbox for preprocessing the recorded EEG data (Delorme & Makeig, 2004). These data were firstly re-referenced to a common average, and then filtered into 1 to 30 Hz. Here, we set an abnormal value

threshold at 100 μV and a whole trial will be excluded from the following analysis if it contained any value over the threshold. Then, ICA were carried out for the rest of data to remove EOG components included in them. Finally, the EEG data belongs to the period of baseline, observation phase, imagination phase, and execution phase were extracted respectively.

Feature extraction: Based on the findings in Chapter 2, we proposed to use two kinds of features included in EEG data: phase locking value (PLV) and event-related (de-)synchronization (ERD/S). The procedures for extracting PLV features from each trial are described as below:

1. Filter the signals into theta band (i.e. 4—7 Hz),
2. Calculate the analytic signals of the above signals via Hilbert transform,
3. For each signal, calculate its phase angle at each moment,
4. Calculate PLV between signals from each two channels:

$$PLV_{u_1,u_2} = \sqrt{\begin{matrix}\left[\frac{1}{n}\sum_{t=t_0}^{T} cos\left(\theta_{u_1,t} - \theta_{u_2,t}\right)\right]^2 \\ + \left[\frac{1}{n}\sum_{t=t_0}^{T} sin\left(\theta_{u_1,t} - \theta_{u_2,t}\right)\right]^2\end{matrix}},$$

   where $\theta_{u_1,t}$ means phase angle at moment t of signal u_1, and $\theta_{u_2,t}$ means those of signal u_2. t_0 and T means the start and end of the interval for calculation.

5. For each channel, calculate its average PLV between itself and all the others,

$$feature_{c,1} = \frac{1}{N-1}\left(\sum_{p=1}^{c-1} PLV_{c,p} + \sum_{q=c+1}^{N} PLV_{c,q}\right)$$

Therefore, 19 features were extracted after above procedures. Similarly, the ERD/S features of each trial could be easily extracted by:

1. Execute wavelet transform on data from each channel via the Wavelet Toolbox in MATLAB (MathWorks, Natick, MA, USA) and acquire the power variation on both time and frequency.
2. Calculate the variation of power in alpha band (8—13 Hz) compared with baseline,

$$P_{c,t} = 10 \times \log_{10} \frac{u_{c,t}}{baseline_c},$$

where $u_{c,t}$ is the absolute value of potential at channel c and time t, and $baseline_c$ is the average of the one at channel c before the stimulus was presented.

3. For each channel, we got a feature value by calculate the average during a determined interval,

$$feature_{c,2} = \frac{1}{T} \sum_{k=t_0}^{t} P_{c,k},$$

where t_0 and t mean the start and end of the interval, and $T = t - t_0$.

Till now, another 19 features were extracted. Finally, for each trial we got a 38-dimension feature vector.

Feature selection: A selection method named as Sequential Forward Floating Selection (SFFS) was used for a wrapper based feature selector. It traverse the combination of features included in input feature vector and find out which one gives best performance. The workflow of SFFS is described as:

1. Take a feature from the feature vector $FEATURE$ and put it into a subset $feature$.
2. Classify the samples with the subset, and its accuracy is $accuracy$
3. Take a new feature from $FEATURE$ and add it into the subset $feature$.
4. Classify the samples with the subset, and its accuracy is $new\_accuracy$.
5. Compare the $new\_accuracy$ with $accuracy$, if $new\_accuracy < accuracy$, remove the last feature and jump to step 3; otherwise, give $accuracy$ the value of $new\_accuracy$, and go to step 6.
6. Classify the samples without the first feature in $feature$, and its accuracy is $new\_accuracy$. If all of the features in $feature$ have been evaluated, jump to step 3.
7. Compare the $new\_accuracy$ with $accuracy$, if $new\_accuracy < accuracy$, move the first feature in $feature$ to the end, and jump to step 6; otherwise, remove the first feature in $feature$, and give $accuracy$ the value of $new\_accuracy$,

and go to step 6.

After the above steps, a feature subset that with best performance for classification is generated. A graphical description of the procedures of SFFS is given in Figure 3.6.

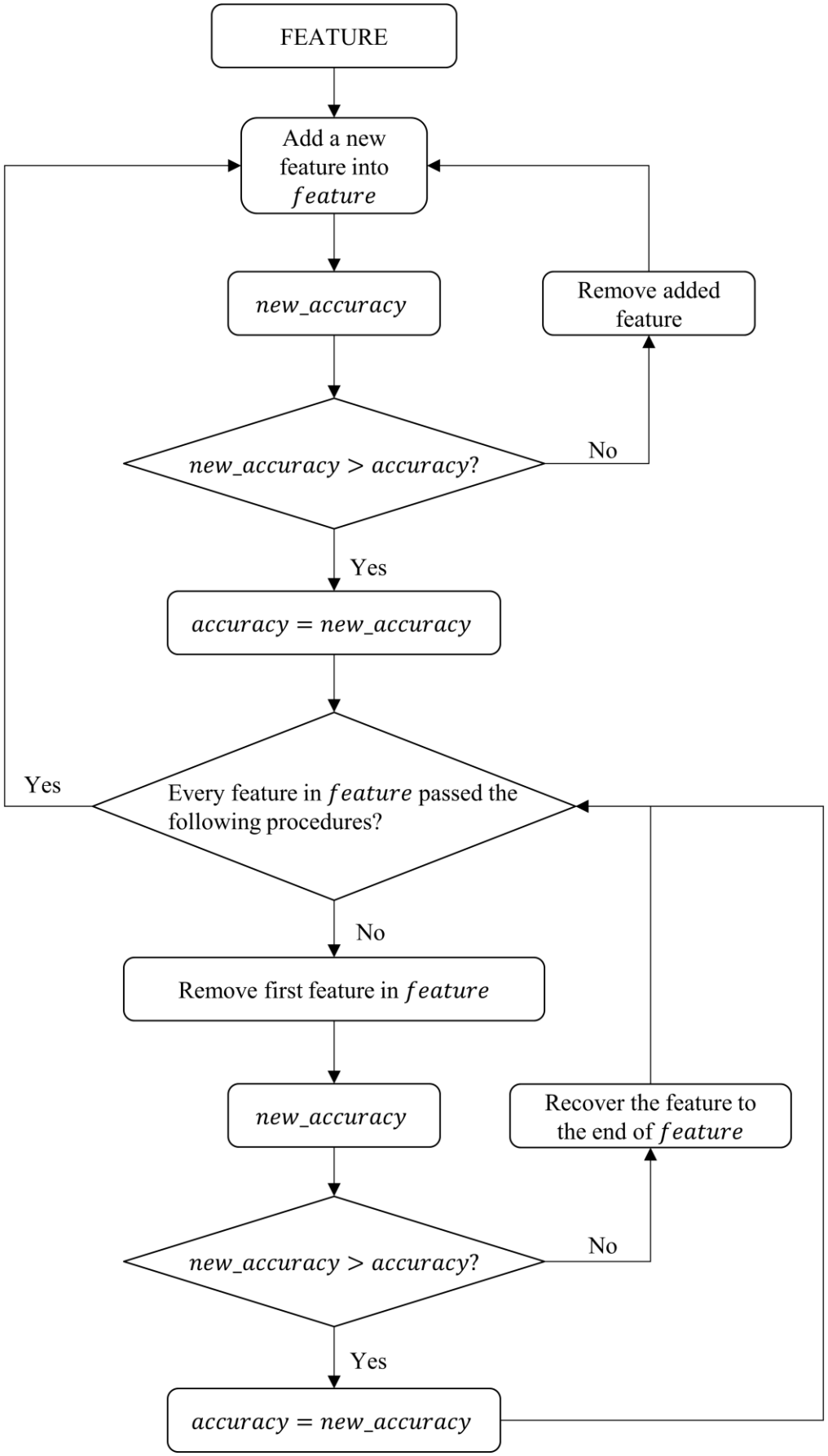
FEATURE
Add a new feature into $feature$
$new\_accuracy$
Remove added feature
$new\_accuracy > accuracy$?
No
Yes
$accuracy = new\_accuracy$
Yes
Every feature in $feature$ passed the following procedures?
No
Remove first feature in $feature$
$new\_accuracy$
Recover the feature to the end of $feature$
$new\_accuracy > accuracy$?
No
Yes
$accuracy = new\_accuracy$

Figure 3.6 Flow chart of SFFS. The $accuracy$ was initialized to zero before the algorithm began. This process would be terminated when all the features in FEATURE had been traversed.

Classification: We used the LIBSVM toolbox for classify the samples (Chang & Lin, 2011). During the feature selection procedure, the performance of selected feature subset was evaluated by calculate an n-fold cross validation function defined in the toolbox. We have to note that for the three-class classification problem, we constructed classifier groups based on the one-against-one strategy manually so that the features used for different classification task is also different (i.e. the input of each classifier is different) in order to reach the best performance. Thus, the training of the three classifiers was also finished respectively. Figure 3.7 is drawn for explaining the principles in an intuitional way.

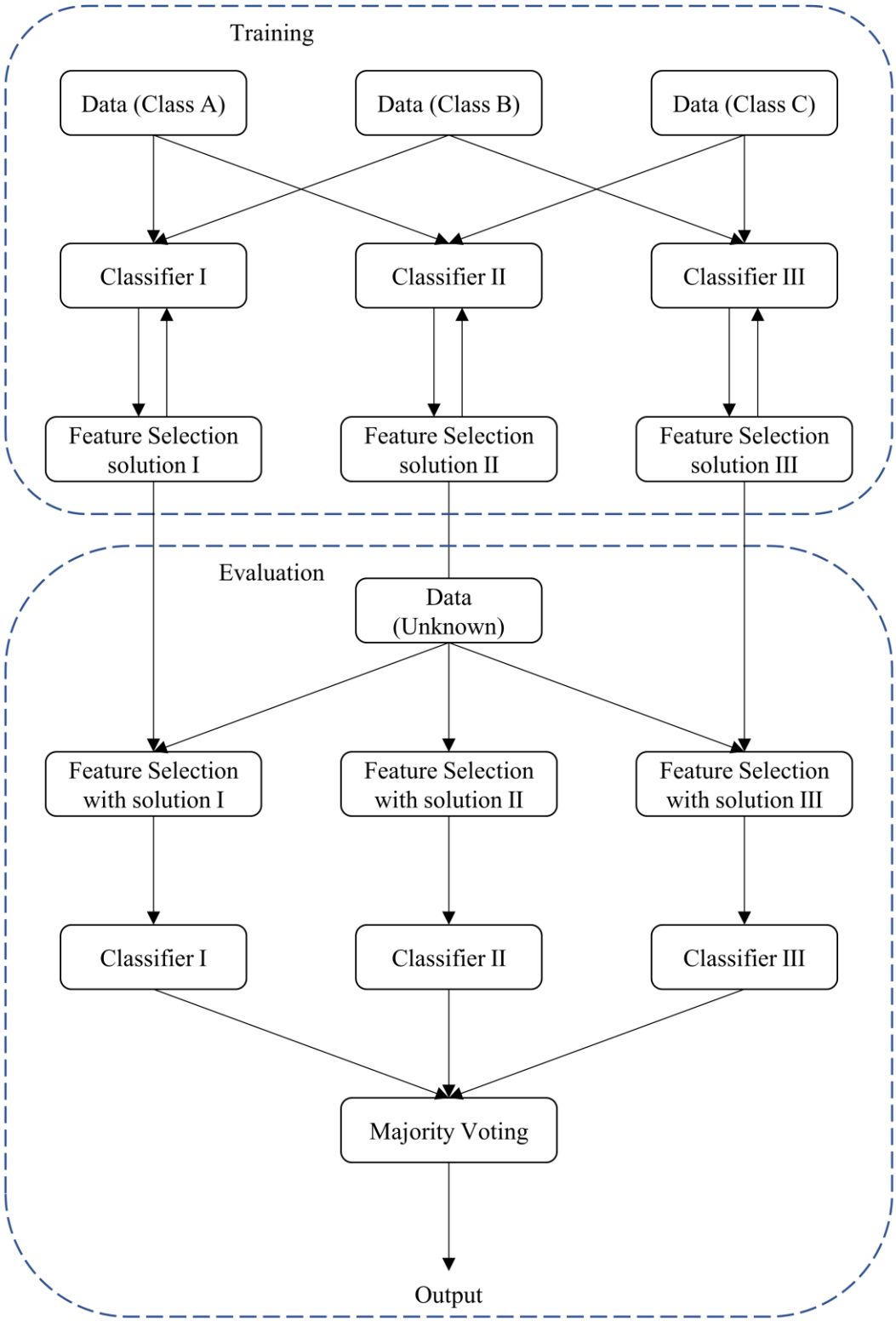

Figure 3.7 The conceptual diagram of combining the feature selection with different classifiers. This method customize the solution of selecting features for each classifier with different missions. In this way, all of these classifiers were able to work with the most appropriate input feature vectors in the meantime, so that they can show the best

performance without any burden from others.

3.3 Results

3.3.1 Training

In order to create a SVM model with both the spatial and temporal information, each epoch was divided into five isometric sections (i.e. 500 ms for each section) and sent for feature extraction independently after features from each entire epoch. Therefore, it resulted in that each feature vector had dimensions of 288 finally. A detailed description of features are stated in Table 3.1.

Table 3.1 Description of features

Feature	Description
F1	PLV of each channel calculated with EEG data from 0 ms to 2000 ms.
F2	PLV of each channel calculated with EEG data from 0 ms to 400 ms.
F3	PLV of each channel calculated with EEG data from 400 ms to 800 ms.
F4	PLV of each channel calculated with EEG data from 800 ms to 1200 ms.
F5	PLV of each channel calculated with EEG data from 1200 ms to 1600 ms.
F6	PLV of each channel calculated with EEG data from 1600 ms to 2000 ms.
F7	ERD/S of each channel calculated with EEG data from 0 ms to 2000 ms.
F8	ERD/S of each channel calculated with EEG data from 0 ms to 400 ms.
F9	ERD/S of each channel calculated with EEG data from 400 ms to 800 ms.
F10	ERD/S of each channel calculated with EEG data from 800 ms to 1200 ms.
F11	ERD/S of each channel calculated with EEG data from 1200 ms to 1600 ms.
F12	ERD/S of each channel calculated with EEG data from 1600 ms to 2000 ms.

Data from the first 8 participants was used during the training process, and they provided 188 samples in total. All these samples were sent to the feature selections procedure together to make sure the determined selection solution had minor influence from individual difference. Moreover, the parameter n of n-fold cross validation was set to equal to the number of participants so that the samples could be partitioned perfectly. The accuracy of each classifier is shown in the Table 3.2 below.

Table 3.2 Accuracy of each classifier

	Mission	Accuracy (%)
Classifier I	Observation vs. Execution	65.87
Classifier II	Observation vs. Imagination	72.22
Classifier II	Execution vs. Imagination	66.67

The features used to achieve the accuracies mentioned above is shown in Table 3.3.

Table 3.3 Result of feature selection

	F1	F2	F3	F4	F5	F6	F7	F8	F9	F10	F11	F12
FP1								□				
FP2								□				
F7												
F3										□		
Fz												
F4												
F8												
T3												
C3												
Cz	○	△										
C4											○	
T4												△
T5										△		
P3										△		
Pz												
P4												
T6									○			
O1											○	
O2							□				○	

△: Selected feature for Classifier I

□: Selected feature for Classifier II

○: Selected feature for Classifier III

3.3.2 Evaluation

Three classifiers were modified with the data from participant No. 1 to No. 8 according to those feature selection solutions respectively. Then the data from participant No. 9 to No. 17 (except for No. 11 which belongs to a left-handed participant) was processed to

obtain features for classification. Due to the application of one-against-one strategy, another majority voting procedures was necessary before output the final results of classes. Classification accuracy for each participant is shown in the Table 3.4 below.

Table 3.4 Classification accuracy in evaluation

Participant No.	Accuracy (%)
9	38.9
10	54.4
12	34.4
13	38.9
14	54.2
15	41.4
16	40.0
17	50.0
Average	44.0

In order to test whether these accuracies had a statistic meaning, the bootstrap resampling method which was mentioned in section 2.2.2 was applied again to obtain the distribution of these accuracies. As shown in Figure 3.8, the average of classification accuracy is significantly higher than the random probability (which is 33.3% in this case).

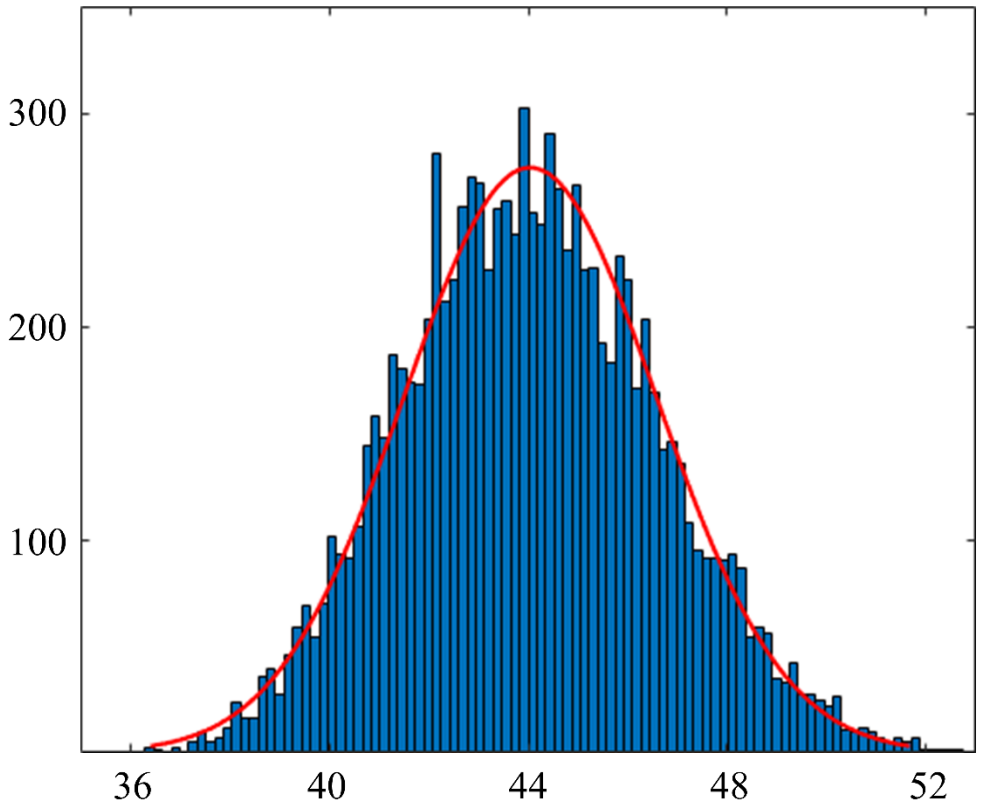

Figure 3.8 Estimated distribution of the classification accuracy ($\mu = 46.50, \sigma = 1.27$). Bootstrap resampling was run for ten thousand times.

3.4 Discussion

The first thing that need to be discussed is the selected features and their function in revealing the spatio-temporal feature of EEG signals recorded during different tasks. The result in Table 3.3 has been mapped to a topography (ignoring temporal axis) as shown in Figure 3.9 so that the electrodes which played important roles during classify the three different movement-related cognitive processes could be exposed intuitively. It is noticed that some classifiers shared the features from same electrode. The Classifier I (which is responsible for distinguish between observation and execution) and Classifier III (which classifies imagination and execution) both selected electrode Cz as a useful sensor, while Classifier II did not. This result suggested that the cerebral activity recorded by electrode Cz was a private one belonged to movement imagination process.

Similarly, the signal collected by electrode Oz was suggested to contain the information belonged to execution a movement. Cz's activation during movement imagination was expected since the very beginning (Beisteiner et al., 1995; Jankelowitz & Colebatch, 2002). However, the reason why the visual cortex participated in the execution process is still not clear. It might be due to the visual presentation of progress bar although there is no more evidence to support this conjecture.

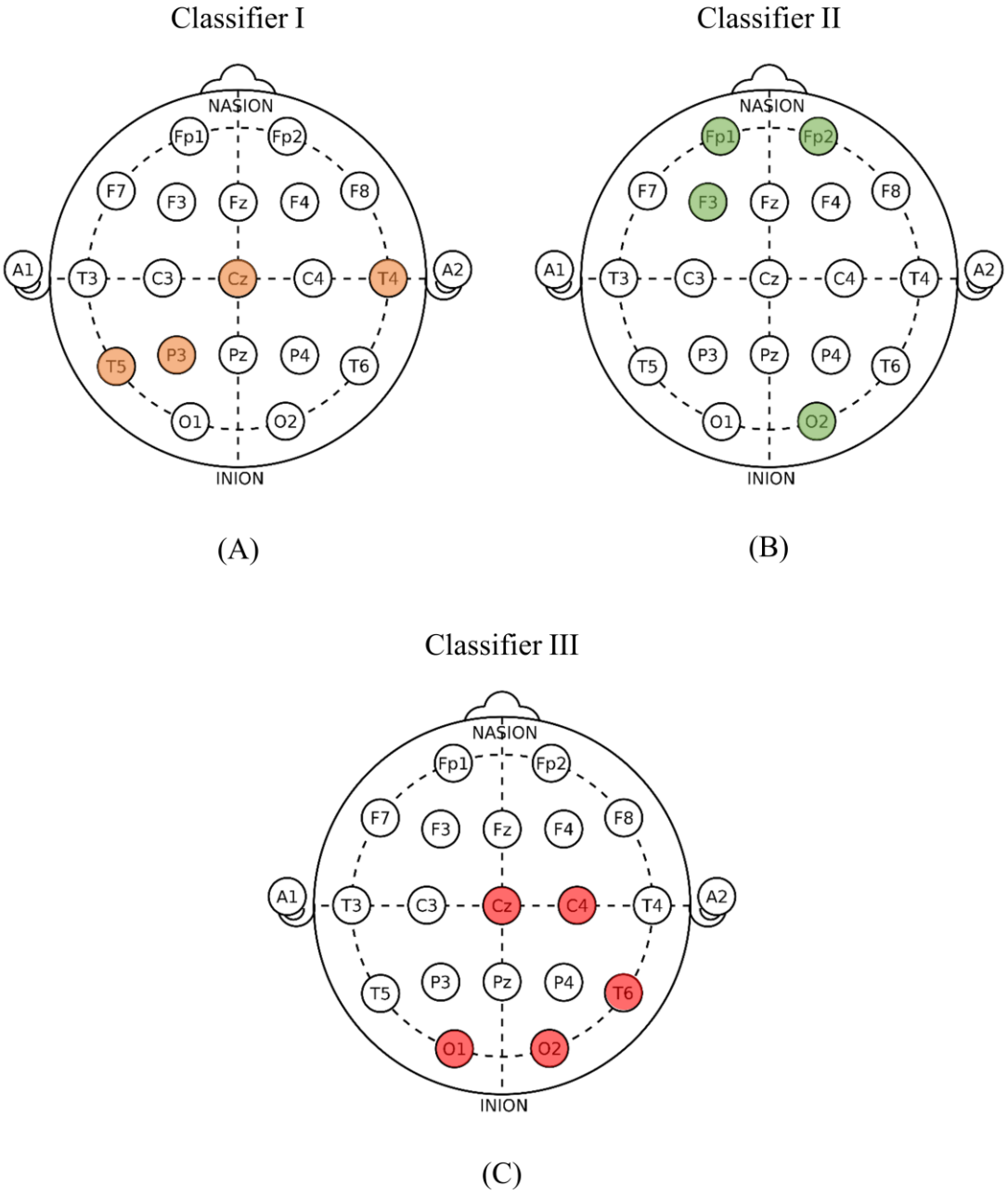

Figure 3.9 Electrodes that played a part in classification. (A) Features extracted from T5, P3, Cz, and T4 electrodes were used to classify EEG signals recorded from movement observation and execution. (B) Features extracted from FP1, FP2, F3, and O2 electrodes were used to classify EEG signals recorded from movement observation and imagination. (C) Features extracted from Cz, C4, T6, O1 and O2 electrodes were used to classify EEG signals recorded from movement observation and imagination.

Power variation at electrode T5 and P3 during period of 800 to 1200 ms were both selected to distinguish observation from execution. Comparisons were done as shown in Figure 3.10. In alpha band, the ERD phenomenon was more dramatic when observation movements. According to other studies, the area covered by electrode T5 and P3 is usually been considered as the Wernicke's area (Fiori et al., 2011; Harpaz et al., 2009; Hong et al., 1996; Jung et al., 2010). In consideration of the function of Wernicke's area, it is reasonable to speculate that participant were trying to encoding the gestures semantically during they saw them (Eulitz et al., 2000; Levelt et al., 1998; Proskovec et al., 2016).

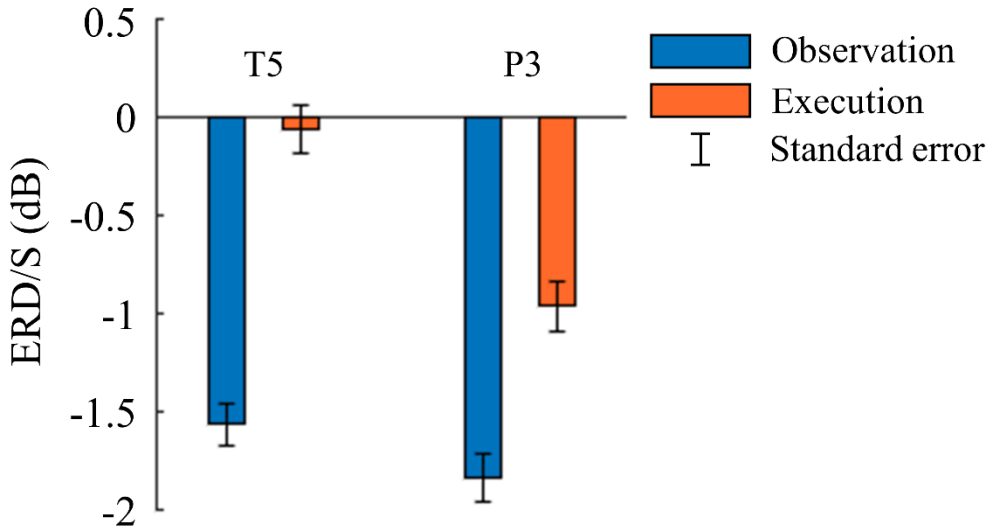

Figure 3.10 Power variation compared to baseline (ERD/S) in 8 to 13 Hz of EEG recorded at electrode T5 and P3, during the period of 800 to 1200 ms after stimulus onset. Both the comparison at electrode T5 and P3 showed significant difference between observation and execution ($p < 0.001, N = 404$ for each comparison).

When the Wernicke's area was activated, another region with similar function participant in the process as well—the Broca's area. Significant difference of alpha band power variation between observation and imagination were observed at F3 electrode (see Figure 3.11). This is pretty reasonable because many scientists have reported that the mirror neuron system is related to the neurons at Broca's area, although it is still controversial (Fazio et al., 2009; Heiser et al., 2003; Marshall et al., 2009). This result could be considered as a new evidence to prove that Broca's area participated in the neural circuit caused by hand movement observation.

Through the same approach, we particularly looked into the activity recorded by electrode C3 and C4 which have been usually considered as the indicator in motor imagination based BCI systems. In our result, alpha band power feature recorded at electrode C4 during 1200 to 1600 ms was taken into account for the classification between imagination and execution. Generally, imagining the movement of someone's right hand would lead to the alpha band ERD of motor cortex (which is known as mu rhythm) in left hemisphere; in the meantime, signal from C4 electrode is expected to perform a beta band ERS. Same tendency could be observed slightly in Figure 3.12. Moreover, this result suggested that right hemisphere seemed to be effective when distinguish whether someone was making a movement with their right hand or just imagining or preparing for it. It is hard to say if the process is a contralateral one due to the limits of our experiment design.

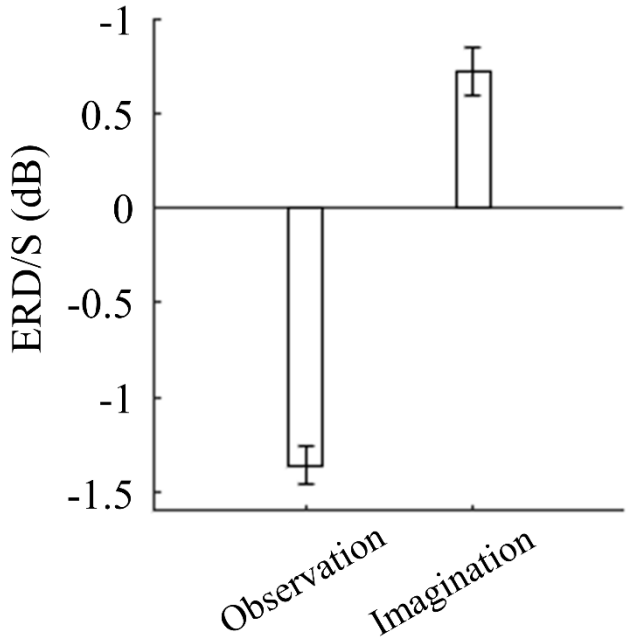

Figure 3.11 Clear alpha band desynchronization was observed during 800 to 1200 ms at the position of F3 during movement observation. Error bar shows the standard error, and the significance of the difference between observation and imagination was confirmed ($p < 0.001, N = 404$).

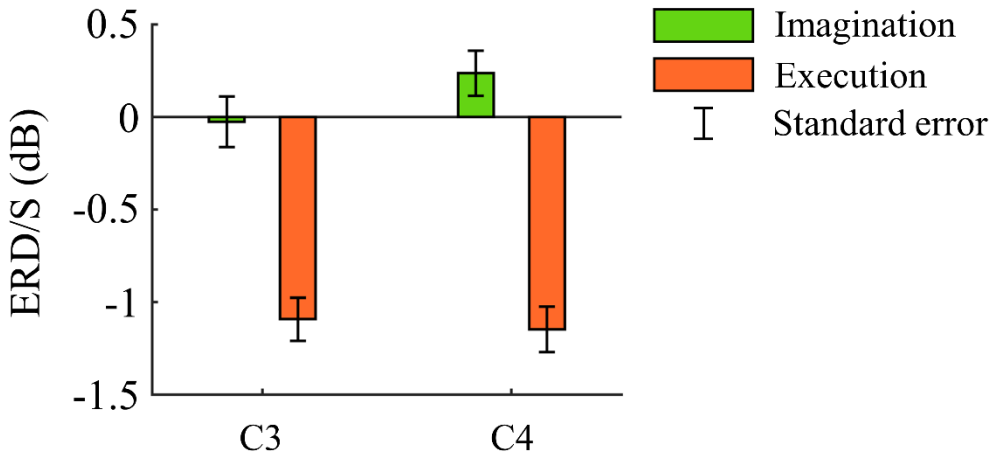

Figure 3.12 Alpha band power changes in electrode C3 and C4. EEG recorded from both the C3 and C4 position showed obvious ERD during reproduce the observed gestures. However, when imagine the gestures, ERS appeared at C4 while slight ERD at C3 electrode. In-electrode tests suggested significance for both ($p < 0.001, N = 404$).

Only two PLV features from same electrode were chosen by two of the three classifiers,

which suggested the three process shared similar pattern of functional connectivity. The whole brain functional network during movement observation, imagination, and execution are shown in Figure 3.13 below. As we mentioned above, the common-chosen electrode in both observation-execution and execution-imagination pairs, Cz, was expected to contain the information that represent the EEG activity related to movement execution. From Figure 3.14, it was found that PLV of Cz electrode had a lowest value in the first 400 ms when participants were actually pose the gestures. This phenomenon suggested that measuring how much the motor cortex took part in the functional network would be an effective method to recognize the EEG when users were making a movement.

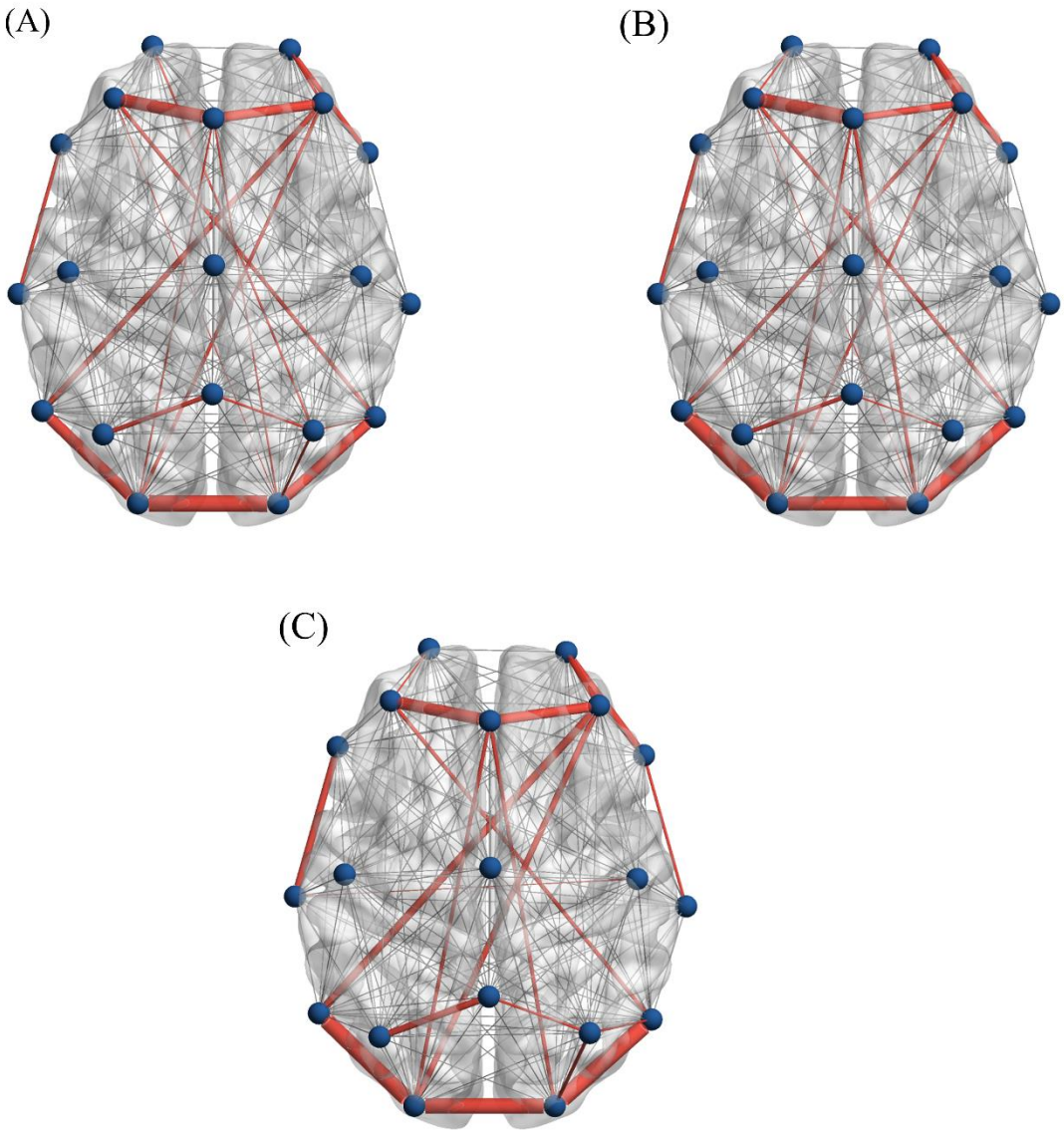

Figure 3.13 Grand average of theta band PLV during whole (A) observing movements, (B) imagining movements, and (C) executing movements. Colored lines indicate that the grand average PLV between the two electrodes at the end points is over 0.6.

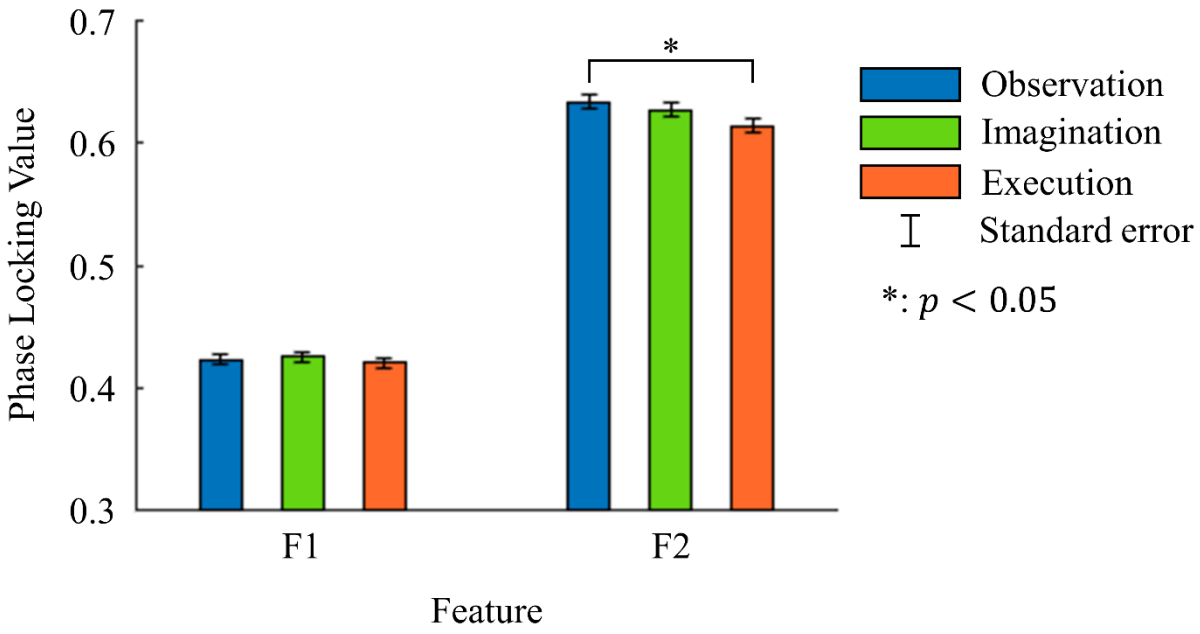

Figure 3.14 Average PLV between Cz and other electrodes. A bootstrap-resampling based statistic test indicated that the value of observation and execution were significantly different during 0 to 400 ms after stimulus onset. Additionally, the difference between imagination and execution was marginally significant ($p = 0.0610$) at the same period.

General EEG analysis focuses on the several hundred milliseconds after stimulus onset, since most responses happened in this narrow period. Nevertheless, as a result, half of the selected features were extracted from the EEG data recorded over 800 ms after the stimulus onset. This may be because that the first dynamic movement happened at 500 ms in the stimulus video in observation period, however, it cannot explain that the Classifier III also considered the latter features to be useful. Therefore, we think it is important to pay more attention to the late components of EEG signal in the future researches.

In summary, this research studied about the difference of normal human scalp electrophysiological activity among people are taking three different tasks: movement observation, imagination, and execution. We successfully found several representative features to distinguish them with each other, which included information collected from

the Broca's area, motor cortex, the Wernicke's area, and visual cortex. The procedure of searching those features was finished with a special methodology—wrapper based feature selection method, which was usually used in machine learning and pattern recognition in the past days. We think this methodology has the potential to be more helpful in studying other problems as well as cognitive neuroscience.

3.5 Summary

In this study, we demonstrated how to use those findings in Chapter 2 to solve problem in the field of neurorobotics. We successfully proposed a possible approach to make machines be able to know whether someone is making a movement or just imagining a movement, or even just saw a movement made by someone else, although its accuracy still have the space to be improved.

Chapter 4

General Conclusion & Future Plan

In the beginning of this thesis, our attention was firstly drawn to the phenomenon that an activation of the motor-sensation-related cerebral region was observed when normal healthy human participants were presented with images of tools. A further investigation suggested that this phenomenon might appear as long as there is a manipulable object in view, even it is not a tool. After a careful consideration, we decided to verify this inference with EEG, which has the highest temporal resolution in all of the mainstream neuroimaging technique.

Cognitive activity leads to variation of neurons' electrophysiological signs, and these signs are easily to be analyzed through the existing signal process methods and theory from modern information science. Therefore, the major methods for EEG analysis was firstly introduced in Chapter 1, and all the methods we used in further researches (in Chapter 2 and Chapter 3) were included in them or a development based on them. We emphasized on the wavelet transform for calculating ERSP and the estimation of functional connectivity via extracting phase information in EEG. Results from simulations were given to prove the validity of the methods we used.

The study about the hypothesis mentioned above was descripted in Chapter 2. We designed the experiment and ran it with 20 volunteered participants to collect necessary EEG data. Results from rigorous analysis indicated that seeing manipulable daily goods caused activity at a wide range of motor-sensory-related regions. But, seeing someone grasping a these object is different. Extra activity was observed. In the meantime, we found different performance of temporal-parietal connection between seeing objects

and seeing interaction, and between seeing hand. These finding revealed human's different understanding on objects, body part, and relationship (interaction).

Another question is, what the immediate reason was that seeing those grasping images led to the activation in a wide range of cerebral cortex. We suspected that it might be the result of a superposition of a series of cognitive processes, at least including movement observation, and might contained a movement imagination to imitate the seen stimulus as well. Therefore, another experiment aimed at distinguish which activations (cerebral regions) belonged to which cognitive process (movement observation, imagination, and execution) was done as descripted in Chapter 3. During analyzing the data we acquired from the experiments in Chapter 2, we noticed PLV's ability to indicate how much a cerebral region participated in current cognitive process. Traditionally, participation of a certain area could only by the approach of detecting the power or potential change near this area, but with the PLV we have been able to find more area that is concerned with the process in the domain of phase. Hereby, we applied a data driven method into our research (as descripted in Chapter 3), and found that the activation of the Broca's area and the Wernicke's area were related with the movement observation process; the right hemisphere of motor cortex (or somatosensory cortex which are close to each other) seemed to be a good indicator in distinguishing right hand movement imagination from making an actual movement; EEG recorded near electrode Cz was different between movement observation and execution, and had a potential to classify between imagination and execution. In brief, it is possible to distinguish human's brain activity when someone is seeing a movement, imagining a movement, or actually making a movement by analyzing cerebral activity of the Broca's area, the Wernicke's area, motor cortex, and visual cortex.

Additionally, we founded that the late EEG signal seemed to be more useful than what we thought before. Our results showed that the motor-related EEG signal was still

meaningful even after 800 ms since the beginning of visual stimulus or the onset cue of movement imagination and execution (Chapter 3). This was not expected before we ran the experiment because either the visual process or the movement execution process would be finished in a shorter time. It may suggest the existing of a post processing process, and could be observed at least at the Broca's area, the Wernicke's area, and visual cortex. Moreover, many EEG research have been focusing on the signal in the first second, but above results reminded us the late component need to be considered equally.

Furthermore, we noticed the participation of visual cortex during movement imagination; more evidence is needed to infer its purpose and function, but we thought it may suggested the dorsal pathway for visual information forwarding might be a bidirectional one. This topic is worthy to be studied in the future.

Finally, we want to summarize how this topic could be studied further in the future. Firstly, the purpose or function of the late activity during movement observation still need to be investigate. Secondly, whether there is a lateralization phenomenon at motor cortex when distinguishing motor imagination from motor execution is still not clear, and thirdly, what the role that visual cortex plays here. Additionally, a further think about using data-driven methods and machine learning to study normal cognitive neuroscience problems is recommended.

Bibliography

Asadzadeh, S., Yousefi Rezaii, T., Beheshti, S., Delpak, A., & Meshgini, S. (2020). A systematic review of EEG source localization techniques and their applications on diagnosis of brain abnormalities. *Journal of Neuroscience Methods*, *339*, 108740. https://doi.org/10.1016/J.JNEUMETH.2020.108740

Basti, A., Chella, F., Guidotti, R., Ermolova, M., D'Andrea, A., Stenroos, M., Romani, G. L., Pizzella, V., & Marzetti, L. (2022). Looking through the windows: a study about the dependency of phase-coupling estimates on the data length. *Journal of Neural Engineering*, *19*(1), 016039. https://doi.org/10.1088/1741-2552/AC542F

Beisteiner, R., Höllinger, P., Lindinger, G., Lang, W., & Berthoz, A. (1995). Mental representations of movements. Brain potentials associated with imagination of hand movements. *Electroencephalography and Clinical Neurophysiology/Evoked Potentials Section*, *96*(2), 183–193. https://doi.org/10.1016/0168-5597(94)00226-5

Buccino, G. (2014). Action observation treatment: a novel tool in neurorehabilitation. *Philosophical Transactions of the Royal Society B: Biological Sciences*, *369*(1644). https://doi.org/10.1098/RSTB.2013.0185

Caldara, R., Deiber, M. P., Andrey, C., Michel, C. M., Thut, G., & Hauert, C. A. (2004). Actual and mental motor preparation and execution: A spatiotemporal ERP study. *Experimental Brain Research*, *159*(3), 389–399. https://doi.org/10.1007/s00221-004-2101-0

Cardinali, L., Frassinetti, F., Brozzoli, C., Urquizar, C., Roy, A. C., & Farnè, A. (2009). Tool-use induces morphological updating of the body schema. *Current*

Biology, *19*(12), R478–R479. https://doi.org/10.1016/J.CUB.2009.05.009

Carvalhaes, C., & De Barros, J. A. (2015). The surface Laplacian technique in EEG: Theory and methods. *International Journal of Psychophysiology*, *97*(3), 174–188. https://doi.org/10.1016/J.IJPSYCHO.2015.04.023

Catrambone, V., Greco, A., Averta, G., Bianchi, M., Valenza, G., & Scilingo, E. P. (2019). Predicting Object-Mediated Gestures from Brain Activity: An EEG Study on Gender Differences. *IEEE Transactions on Neural Systems and Rehabilitation Engineering*, *27*(3), 411–418. https://doi.org/10.1109/TNSRE.2019.2898469

Cerri, G., Cabinio, M., Blasi, V., Borroni, P., Iadanza, A., Fava, E., Fornia, L., Ferpozzi, V., Riva, M., Casarotti, A., Martinelli Boneschi, F., Falini, A., & Bello, L. (2015). The mirror neuron system and the strange case of Broca's area. *Human Brain Mapping*, *36*(3), 1010–1027. https://doi.org/10.1002/HBM.22682

Chang, C. C., & Lin, C. J. (2011). LIBSVM: a library for support vector machines. *ACM transactions on intelligent systems and technology (TIST)*, 2(3), 1-27.

Chao, L. L., & Martin, A. (2000). Representation of Manipulable Man-Made Objects in the Dorsal Stream. *NeuroImage*, *12*(4), 478–484. https://doi.org/10.1006/NIMG.2000.0635

Chatrian, G. E., Lettich, E., & Nelson, P. L. (1985). Ten Percent Electrode System for Topographic Studies of Spontaneous and Evoked EEG Activities. *American Journal of EEG Technology*, *25*(2), 83–92. https://doi.org/10.1080/00029238.1985.11080163

Chen, X., Bin, G., Daly, I., & Gao, X. (2013). Event-related desynchronization (ERD) in the alpha band during a hand mental rotation task. *Neuroscience Letters*, *541*, 238–242. https://doi.org/10.1016/J.NEULET.2013.02.036

Creem-Regehr, S. H., & Lee, J. N. (2005). Neural representations of graspable objects: are tools special? *Cognitive Brain Research*, *22*(3), 457–469. https://doi.org/10.1016/J.COGBRAINRES.2004.10.006

Darvas, F., Pantazis, D., Kucukaltun-Yildirim, E., & Leahy, R. M. (2004). Mapping human brain function with MEG and EEG: methods and validation. *NeuroImage*, *23*(SUPPL. 1), S289–S299. https://doi.org/10.1016/J.NEUROIMAGE.2004.07.014

Delorme, A., & Makeig, S. (2004). EEGLAB: an open source toolbox for analysis of single-trial EEG dynamics including independent component analysis. *Journal of Neuroscience Methods*, *134*(1), 9–21. https://doi.org/10.1016/J.JNEUMETH.2003.10.009

Domingo Pascual-Marqui, R. (1999). *Review of Methods for Solving the EEG Inverse Problem*. *1*(1), 77–90.

Eulitz, C., Hauk, O., & Cohen, R. (2000). Electroencephalographic activity over temporal brain areas during phonological encoding in picture naming. *Clinical Neurophysiology*, *111*(11), 2088–2097. https://doi.org/10.1016/S1388-2457(00)00441-7

Fadiga, L., & Craighero, L. (2006). Hand Actions and Speech Representation in Broca's Area. *Cortex*, *42*(4), 486–490. https://doi.org/10.1016/S0010-9452(08)70383-6

Fadiga, L., Craighero, L., & D'Ausilio, A. (2009). Broca's Area in Language, Action, and Music. *Annals of the New York Academy of Sciences*, *1169*(1), 448–458. https://doi.org/10.1111/J.1749-6632.2009.04582.X

Fazio, P., Cantagallo, A., Craighero, L., D'ausilio, A., Roy, A. C., Pozzo, T., Calzolari, F., Granieri, E., & Fadiga, L. (2009). Encoding of human action in Broca's area. *Brain*, *132*(7), 1980–1988. https://doi.org/10.1093/BRAIN/AWP118

Fellrath, J., Mottaz, A., Schnider, A., Guggisberg, A. G., & Ptak, R. (2016). Theta-band functional connectivity in the dorsal fronto-parietal network predicts goal-directed attention. *Neuropsychologia*, *92*, 20–30. https://doi.org/10.1016/J.NEUROPSYCHOLOGIA.2016.07.012

Fiori, V., Coccia, M., Marinelli, C. V., Vecchi, V., Bonifazi, S., Gabriella Ceravolo, M., Provinciali, L., Tomaiuolo, F., & Marangolo, P. (2011). Transcranial Direct Current Stimulation Improves Word Retrieval in Healthy and Nonfluent Aphasic Subjects. *Journal of Cognitive Neuroscience*, *23*(9), 2309–2323. https://doi.org/10.1162/JOCN.2010.21579

Gallese, V., Fadiga, L., Fogassi, L., & Rizzolatti, G. (1996). Action recognition in the premotor cortex. *Brain*, *119*(2), 593–609. https://doi.org/10.1093/BRAIN/119.2.593

Garcea, F. E., Almeida, J., & Mahon, B. Z. (2012). A right visual field advantage for visual processing of manipulable objects. *Cognitive, Affective and Behavioral Neuroscience*, *12*(4), 813–825. https://doi.org/10.3758/S13415-012-0106-X/TABLES/3

Glomb, K., Ponce-Alvarez, A., Gilson, M., Ritter, P., & Deco, G. (2017). Resting state networks in empirical and simulated dynamic functional connectivity. *NeuroImage*, *159*, 388–402. https://doi.org/10.1016/J.NEUROIMAGE.2017.07.065

Graimann, B., Huggins, J. E., Levine, S. P., & Pfurtscheller, G. (2002). Visualization of significant ERD/ERS patterns in multichannel EEG and ECoG data. *Clinical Neurophysiology*, *113*(1), 43–47. https://doi.org/10.1016/S1388-2457(01)00697-6

Groeger, J. A. (2013). Understanding Driving : Applying Cognitive Psychology to a Complex Everyday Task. *Understanding Driving*. https://doi.org/10.4324/9780203769942

Groppe, D. M., Urbach, T. P., & Kutas, M. (2011). Mass univariate analysis of event-related brain potentials/fields I: A critical tutorial review. *Psychophysiology*, *48*(12), 1711–1725. https://doi.org/10.1111/J.1469-8986.2011.01273.X

Harpaz, Y., Levkovitz, Y., & Lavidor, M. (2009). Lexical ambiguity resolution in Wernicke's area and its right homologue. *Cortex*, *45*(9), 1097–1103.

https://doi.org/10.1016/J.CORTEX.2009.01.002

Heiser, M., Iacoboni, M., Maeda, F., Marcus, J., & Mazziotta, J. C. (2003). The essential role of Broca's area in imitation. *European Journal of Neuroscience*, *17*(5), 1123–1128. https://doi.org/10.1046/J.1460-9568.2003.02530.X

Hirsch, G. V., Bauer, C. M., & Merabet, L. B. (2015). Using structural and functional brain imaging to uncover how the brain adapts to blindness. *Annals of Neuroscience and Psychology*, *2*(1), 7. https://doi.org/10.7243/2055-3447-2-7

Hong, C. C. H., Jin, Y., Potkin, S. G., Buchsbaum, M. S., Wu, J., Callaghan, G. M., Nudleman, K. L., & Gillin, J. C. (1996). Language in Dreaming and Regional EEG Alpha Power. *Sleep*, *19*(3), 232–235. https://doi.org/10.1093/SLEEP/19.3.232

Jankelowitz, S. K., & Colebatch, J. G. (2002). Movement-related potentials associated with self-paced, cued and imagined arm movements. *Experimental Brain Research 2002 147:1*, *147*(1), 98–107. https://doi.org/10.1007/S00221-002-1220-8

Jeannerod, M. (1994). The representing brain: Neural correlates of motor intention and imagery. *Behavioral and Brain Sciences*, *17*(2), 187–202. https://doi.org/10.1017/S0140525X00034026

Jung, T. Du, Kim, J. Y., Lee, Y. S., Kim, D. H., Lee, J. J., Seo, J. H., Lee, H. J., & Chang, Y. (2010). Effect of repetitive transcranial magnetic stimulation in a patient with chronic crossed aphasia: Fmri study. *Journal of Rehabilitation Medicine*, *42*(10), 973–978. https://doi.org/10.2340/16501977-0637

Klem, G. H., Otto Lu Èders, H., Jasper, H., & Elger, C. (1958). The ten±twenty electrode system of the International Federation. *EElectroencephalography and Clinical Neurophysiology*, *10*(1), 371–375.

Lachaux, J.-P., Rodriguez, E., Martinerie, J., & Varela, F. J. (1999). Measuring Phase Synchrony in Brain Signals. *Hum Brain Mapping*, *8*, 194–208. https://doi.org/10.1002/(SICI)1097-0193(1999)8:4

Levelt, W. J. M., Praamstra, P., Meyer, A. S., Helenius, P., & Salmelin, R. (1998). An MEG Study of Picture Naming. *Journal of Cognitive Neuroscience*, *10*(5), 553–567. https://doi.org/10.1162/089892998562960

Makeig, S. (1993). Auditory event-related dynamics of the EEG spectrum and effects of exposure to tones. *Electroencephalography and Clinical Neurophysiology*, *86*(4), 283–293. https://doi.org/10.1016/0013-4694(93)90110-H

Maris, E., & Oostenveld, R. (2007). Nonparametric statistical testing of EEG- and MEG-data. *Journal of Neuroscience Methods*, *164*(1), 177–190. https://doi.org/10.1016/j.jneumeth.2007.03.024

Marshall, P. J., Bouquet, C. A., Shipley, T. F., & Young, T. (2009). Effects of brief imitative experience on EEG desynchronization during action observation. *Neuropsychologia*, *47*(10), 2100–2106. https://doi.org/10.1016/J.NEUROPSYCHOLOGIA.2009.03.022

Marty, B., Bourguignon, M., Jousmäki, V., Wens, V., Op de Beeck, M., Van Bogaert, P., Goldman, S., Hari, R., & De Tiège, X. (2015). Cortical kinematic processing of executed and observed goal-directed hand actions. *NeuroImage*, *119*, 221–228. https://doi.org/10.1016/J.NEUROIMAGE.2015.06.064

McNair, N. A., & Harris, I. M. (2012). Disentangling the contributions of grasp and action representations in the recognition of manipulable objects. *Experimental Brain Research*, *220*(1), 71–77. https://doi.org/10.1007/S00221-012-3116-6/FIGURES/3

Milner, D., & Goodale, M. (2006). The visual brain in action (Vol. 27). OUP Oxford.

Milner, A. D., & Goodale, M. A. (2008). Two visual systems re-viewed. Neuropsychologia, 46(3), 774-785.

Mishkin, M., Ungerleider, L. G., & Macko, K. A. (1983). Object vision and spatial vision: two cortical pathways. Trends in neurosciences, 6, 414-417.

Monti, R. P., Anagnostopoulos, C., & Montana, G. (2015). *Estimating and simulating multiple related functional connectivity networks via the MNS Package*.

Murias, M., Webb, S. J., Greenson, J., & Dawson, G. (2007). Resting State Cortical Connectivity Reflected in EEG Coherence in Individuals With Autism. *Biological Psychiatry*, *62*(3), 270–273. https://doi.org/10.1016/J.BIOPSYCH.2006.11.012

Neuper, C., & Pfurtscheller, G. (2001). Event-related dynamics of cortical rhythms: frequency-specific features and functional correlates. *International Journal of Psychophysiology*, *43*(1), 41–58. https://doi.org/10.1016/S0167-8760(01)00178-7

Ni, L., Liu, Y., & Yu, W. (2019). The dominant role of functional action representation in object recognition. *Experimental Brain Research*, *237*(2), 363–375. https://doi.org/10.1007/S00221-018-5426-9/FIGURES/6

Nicholls, J. G., & Nicholls, J. G. (2001). *From neuron to brain*.

Nunez, P. L., & Westdorp, A. F. (1994). The surface laplacian, high resolution EEG and controversies. *Brain Topography 1994 6:3*, *6*(3), 221–226. https://doi.org/10.1007/BF01187712

Oostenveld, R., Fries, P., Maris, E., & Schoffelen, J. M. (2011). FieldTrip: Open source software for advanced analysis of MEG, EEG, and invasive electrophysiological data. *Computational Intelligence and Neuroscience*, *2011*. https://doi.org/10.1155/2011/156869

Oostenveld, R., & Praamstra, P. (2001). The five percent electrode system for high-resolution EEG and ERP measurements. *Clinical Neurophysiology*, *112*(4), 713–719. https://doi.org/10.1016/S1388-2457(00)00527-7

Papitto, G., Friederici, A. D., & Zaccarella, E. (2020). The topographical organization of motor processing: An ALE meta-analysis on six action domains and the relevance of Broca's region. *NeuroImage*, *206*, 116321. https://doi.org/10.1016/J.NEUROIMAGE.2019.116321

Peirce, J., Gray, J. R., Simpson, S., MacAskill, M., Höchenberger, R., Sogo, H., ... & Lindeløv, J. K. (2019). PsychoPy2: Experiments in behavior made easy. *Behavior research methods*, 51(1), 195-203.

Pernier, J., Perrin, F., & Bertrand, O. (1988). Scalp current density fields: concept and properties. *Electroencephalography and Clinical Neurophysiology*, *69*(4), 385–389. https://doi.org/10.1016/0013-4694(88)90009-0

Pfurtscheller, G., & Neuper, C. (1997). Motor imagery activates primary sensorimotor area in humans. *Neuroscience Letters*, *239*(2–3), 65–68. https://doi.org/10.1016/S0304-3940(97)00889-6

Pockett, S., Bold, G. E. J., & Freeman, W. J. (2009). EEG synchrony during a perceptual-cognitive task: Widespread phase synchrony at all frequencies. *Clinical Neurophysiology*, *120*(4), 695–708. https://doi.org/10.1016/J.CLINPH.2008.12.044

Proskovec, A. L., Heinrichs-Graham, E., & Wilson, T. W. (2016). Aging modulates the oscillatory dynamics underlying successful working memory encoding and maintenance. *Human Brain Mapping*, *37*(6), 2348–2361. https://doi.org/10.1002/HBM.23178

Proverbio, A. M. (2012). Tool perception suppresses 10-12Hz μ rhythm of EEG over the somatosensory area. *Biological Psychology*, *91*(1), 1–7. https://doi.org/10.1016/j.biopsycho.2012.04.003

Proverbio, A. M., Adorni, R., & D'Aniello, G. E. (2011). 250 ms to code for action affordance during observation of manipulable objects. *Neuropsychologia*, *49*(9), 2711–2717. https://doi.org/10.1016/J.NEUROPSYCHOLOGIA.2011.05.019

Rizzolatti, G., & Craighero, L. (2004). THE MIRROR-NEURON SYSTEM. *Http://Dx.Doi.Org/10.1146/Annurev.Neuro.27.070203.144230*, *27*, 169–192. https://doi.org/10.1146/ANNUREV.NEURO.27.070203.144230

Rizzolatti, G., Fadiga, L., Gallese, V., & Fogassi, L. (1996). Premotor cortex and the recognition of motor actions. *Cognitive Brain Research*, *3*(2), 131–141. https://doi.org/10.1016/0926-6410(95)00038-0

Roach, B. J., & Mathalon, D. H. (2008). Event-related EEG time-frequency analysis: An overview of measures and an analysis of early gamma band phase locking in

schizophrenia. In *Schizophrenia Bulletin* (Vol. 34, Issue 5, pp. 907–926). Oxford University Press. https://doi.org/10.1093/schbul/sbn093

Rüther, N. N., Brown, E. C., Klepp, A., & Bellebaum, C. (2014). Observed manipulation of novel tools leads to mu rhythm suppression over sensory-motor cortices. *Behavioural Brain Research*, *261*, 328–335. https://doi.org/10.1016/J.BBR.2013.12.033

Rzepecki-Smith, C. I., Meda, S. A., Calhoun, V. D., Stevens, M. C., Jafri, M. J., Astur, R. S., & Pearlson, G. D. (2010). Disruptions in Functional Network Connectivity During Alcohol Intoxicated Driving. *Alcoholism: Clinical and Experimental Research*, *34*(3), 479–487. https://doi.org/10.1111/J.1530-0277.2009.01112.X

Sauseng, P., Klimesch, W., Schabus, M., & Doppelmayr, M. (2005). Fronto-parietal EEG coherence in theta and upper alpha reflect central executive functions of working memory. *International Journal of Psychophysiology*, *57*(2), 97–103. https://doi.org/10.1016/J.IJPSYCHO.2005.03.018

Stéphanie Cochin, S., Barthelemy, C., Roux, S., & Joëlle Martineau, J. (1999). Observation and execution of movement: similarities demonstrated by quantified electroencephalography. *European Journal of Neuroscience*, *11*(5), 1839–1842. https://doi.org/10.1046/J.1460-9568.1999.00598.X

Tong, L., Liu, R. wen, Soon, V. C., & Huang, Y. F. (1991). Indeterminacy and identifiability of blind identification. *IEEE Transactions on Circuits and Systems*, *38*(5), 499–509. https://doi.org/10.1109/31.76486

Verma, A., & Brysbaert, M. (2011). A right visual field advantage for tool-recognition in the visual half-field paradigm. *Neuropsychologia*, *49*(9), 2342–2348. https://doi.org/10.1016/J.NEUROPSYCHOLOGIA.2011.04.007

Vogt, S., Rienzo, F. Di, Collet, C., Collins, A., & Guillot, A. (2013). Multiple roles of motor imagery during action observation. *Frontiers in Human Neuroscience*, *0*(NOV), 807. https://doi.org/10.3389/FNHUM.2013.00807/BIBTEX

Weiler, J. M., Bloomfield, J. R., Woodworth, G. G., Grant, A. R., Layton, T. A., Brown, T. L., McKenzie, D. R., Baker, T. W., & Watson, G. S. (2000). Effects of fexofenadine, diphenhydramine, and alcohol on driving performance. A randomized, placebo-controlled trial in the Iowa driving simulator. *Annals of Internal Medicine*, *132*(5), 354–363. https://doi.org/10.7326/0003-4819-132-5-200003070-00004

List of Figures

List of Abbreviations

ANOVA	Analysis Of Variance
BA	Broca's Area
BOLD	Blood Oxygen Level Dependent
CF	Central Frontal lobe
Corr	Correlation
DFT	Discrete Fourier Transform
DTF	Directed Transfer Function
EEG	Electroencephalogram
EOG	Electrooculogram
ERD	Event-Related Desynchronization
ERP	Event-Related Potential
ERS	Event-Related Synchronization
ERSP	Event-Related Spectral Perturbation
ePLV	effective Phase Locking Value
FFT	Fast Fourier Transform
fMRI	functional Magnetic Resonance Imaging
fNIRS	functional Near-Infrared Spectroscopy
HbO	oxygenated hemoglobin
HbR	deoxygenated hemoglobin
HT	Hilbert Transform
ICA	Independent Component Analysis
LAG	Left Angular Gyrus
LCS	Left Central Sulcus

LS	Left Somatosensory Cortex
MI	Mutual Information
MI-BCI	Motor Imagining based Brain Computer Interface
MNS	Mirror Neuron System
PLV	Phase Locking Value
PLI	Phase Locking Index
PS	Phase Synchrony
RAG	Right Angular Gyrus
RCS	Right Central Sulcus
RF	Right Frontal Lobe
RS	Right Somatosensory Cortex
SFFS	Sequential Forward Floating Selection
SNR	Signal-to-Noise Ratio
STFT	Short-Time Fourier Transform
SVM	Support Vector Machine
TE	Transfer Entropy